Cervical weakness and preterm birth: The structure and function of the internal cervical os

James Peter Nott BSc (Hons) MSc

Submitted in accordance with the requirements for the degree of

Doctor of Philosophy

The University of Leeds

School of Medicine

September 2019

The candidate confirms that the work submitted is their own, except where work which has formed part of jointly authored publications has been included. The contribution of the candidate and the other authors to this work has been explicitly indicated below. The candidate confirms that appropriate credit has been given within the thesis where reference has been made to the work of others.

The work in Chapter one of the thesis has appeared in publication as follows:

Nott, J.P., Bonney, E.A., Pickering, J.D., and Simpson, N.A.B. 2016 The structure and function of the cervix during pregnancy. *Translational Research in Anatomy*. **2**, pp. 1–7.

I was first author on the review article. The other authors contributed through reviewing and editing the work prior to final submission.

The work in Chapter three of the thesis has appeared in publication as follows:

Nott, J.P., Pervolaraki, E., Benson, A.P., Bonney, E.A.,, Wilkinson, N., Simpson, N.A.B. 2017. Diffusion tensor imaging determines three-dimensional architecture of human cervix: a cross-sectional study. *BJOG: An International Journal of Obstetrics & Gynaecology*. **125**(7), pp. 812-818.

I was responsible for study design, sample collection, data collection and collation and analysis, as well as authoring the paper. The contribution of the other authors was study design, data collection and reviewing of the manuscript.

Candidate Achievements

Publications

Nott, J.P., Bonney, E.A., Pickering, J.D., and Simpson, N.A.B. 2016 The structure and function of the cervix during pregnancy. *Translational Research in Anatomy*. **2**, pp. 1–7.

Nott, J.P., Pervolaraki, E., Benson, A.P., Bonney, E.A.,, Wilkinson, N., Simpson, N.A.B. 2017. Diffusion tensor imaging determines three-dimensional architecture of human cervix: a cross-sectional study. *BJOG: An International Journal of Obstetrics & Gynaecology*. **125**(7), pp. 812-818.

Poster and Oral Presentations

Nott, J. *et al*. Modelling cervical microarchitecture: insights from diffusion-tensor imaging. 8th World Congress of Biomechanics, Dublin, July 2019

Nott, J. *et al*. Diffusion-tensor MRI analysis of cervical microarchitecture: a comparison between the pre and postmenopausal cervix. Blair Bell annual research meeting, RCOG, London, March 2017

Nott, J. *et al*. High field strength small bore magnetic resonance imaging identifies dense, organized, encircling fibres at the cervical internal os. Society

of Maternal and Fetal Medicine, Las Vegas, Nevada, United States, January 2017

Nott, J. *et al*. GVS conference, University of Leeds, Leeds, October 2016

Nott, J. *et al*. Determination of cervical microarchitecture using magnetic resonance imaging. 2nd Annual Preterm Birth Conference, Chelsea and Westminster Hospital, London, September 2016

Nott, J. *et al*. DTMRI derived tractography defines the structural architecture of the human cervix. Summer Meeting of the British Association of Clinical Anatomists, Brighton, July 2016

Awards

Awarded 1st prize from best poster presentation at Unversity of Leeds FMH conference, Leeds, July 2015

Acknowledgements

I would like to thank my primary supervisor, Mr. Nigel Simpson, for his guidance, expertise, encouragement and most of all patience throughout the last few years. I would also like to thank my co-supervisor, Prof. James Pickering, for his valuable feedback from the start, and for always finding the time to sit down with me. I'd also like to thank Dr. Eletheria Pervolaki, Dr. Al Benson, Dr. Nafisa Wilkinson, Dr. Elizabeth Bonney, Dr. Derek Maguee, Dr. Darren Treanor and Dr. Johnathan Dalton for their help and expertise throughout.

I'd like to thank the Faculty of Medicine and Health for funding me and giving me the opportunity to work and study at the University of Leeds, and the patients who kindly gave consent to participate in the research.

A big thank you goes out to the staff in the Histopathology department and the Leeds Centre for Women's Health at St James Hospital who were especially helpful in facilitating all of the research described in this thesis. I would also like to thank all of the members of the Women's Health group who guided me throughout my time in the lab.

Finally, I'd like to thank my family and friends for getting me through my education. Without their support and encouragement, this would not have been possible.

Abstract

The cervix is integral to the maintenance of pregnancy and timely delivery of the baby. Mechanical failure of the cervix resulting in spontaneous preterm birth presents with collapse of the internal os, yet little is known about why the cervix behaves in this way. This may in part be due to research being technically limited and/or limited to punch biopsies of the distal cervix that did not include tissue from the internal os. The aim of this thesis was to re-evaluate cervical anatomy using novel laboratory and imaging methods to gain further insight into the structure of the cervix and how this may influence function during pregnancy.

To achieve this, whole cervical samples were obtained from women undergoing hysterectomy for benign pathology. Uterine tissue was subsequently fixed and analysed using 2D and 3D histological methods. Cervical anatomy was characterised using markers for smooth muscle and collagen and analysed using computer-assisted quantification methods. Sequential tissue slices were then reconstructed to produce 3D models of the proximal, middle and distal cervix.

High-resolution diffusion-tensor imaging was used to determine whether complex cervical anatomy could be visualised using radiological methods. Tissue was assessed using quantitative and qualitative diffusion methods, and directly compared to immunohistochemically stained tissue. The results obtained demonstrated that diffusion-tensor imaging accurately assessed

cervical anatomy and provided further detail in terms of fibre volume, density and organisation. *Ex vivo* endoscopic ultrasound was used to assess whether current, established medical imaging technology could discern cervical smooth muscle and collagen fibres. Although this method could be used to identify gross anatomical structures, it was not an appropriate method to identify cervical microanatomy.

The results described in this thesis provide further insight into how the cervix resists intrauterine forces throughout pregnancy, and then dilates and effaces to allow for delivery of a fetus. Diffusion-tensor imaging accurately assessed cervical anatomy, which may have implications for *in vivo* characterisation of cervical remodelling during pregnancy and identifying those at risk of delivering early. Finally, observations in this thesis encourage continued re-examination of the cervix using high-resolution imaging to provide insight into function and to develop strategies to discern cervical insufficiency from other known causes of preterm birth.

Table of Contents

List of Figures

List of Tables

List of Equations

Abbreviations

Abbreviation	Definition
2D	Two-dimensional
3D	Three-dimensional
AD	Axial Diffusion
ADC	Apparent Diffusion Coefficient
APE	Aminopropyltriethoxysilane
CD	Caesarean Delivery
CE	Columnar Epithelium
CI	Confidence Interval
CIn	Cervical Insufficiency
CL	Circular Layer
CMP	Cervical Mucus Plug
Col1α-1	Collagen 1 alpha 1
CSMC	Cervical Smooth Muscle Cell
DAB	Diaminobenzidine
DT	Diffusion Tensor
ECM	Extracellular Matrix
EMG	Electromyography
FA	Fractional Anistropy
FOV	Field of View
GAG	Glycosaminoglycan
GnRH	Gonadotropin Releasing Hormone

H & E	Haematoxylin and Eosin
HN	Hypogastric Nerves
ICE	Intracardiac Echo
IHP	Inferior Hypogastric Plexus
IVUS	Intravascular Ultrasound
LIF	Light Induced Fluorescence
LL	Longitudinal Layer
MIM	Medical Imaging Manager
MP	Multiparous
MRC	Medical Research Council
MRI	Magnetic Resonance Imaging
MT	Masson's Trichrome
NP	Nulliparous
OCT	Optical Coherence Tomography
PBS	Phosphate Buffered Saline
POP	Pelvic Organ Prolapse
PTB	Preterm Birth
RCOG	Royal College of Obstetricians
RCT	Randomised Control Trial
RD	Radial Diffusion
ROI	Region of Interest
SE	Squamous Epithelium
sPTB	Spontaneous Preterm Birth
SHG	Second Harmonic Generation

SHN	Superior Hypogastric Nerve
SVD	Spontaneous Vaginal Delivery
TAH	Total Abdominal Hysterectomy
TGF-β	Transforming Growth Factor-β
TV	Tract Volume
TVUS	Transvaginal Ultrasound
VH	Vaginal Hysterectomy
α-SMA	α- smooth muscle actin

Chapter 1 Overview of cervical structure and function

1.1 Introduction

The uterus is a fibromuscular organ located within the pelvis that is responsible for protecting and nurturing the developing conceptus (Marieb, 2004). It is described as having two distinct parts: a muscular uterine corpus and a more fibrous uterine cervix. During pregnancy, the cervix provides a barrier to the ascent of vaginal microorganisms and retains the growing fetus *in utero* (Myers et al., 2015). Towards term the cervix undergoes extensive tissue remodelling to allow for delivery of the fetus. Inherited and acquired weakness of the cervix may compromise function and increase the risk of preterm birth (PTB; Gravett et al., 2010). However, little is known about the underlying cervical anatomy and how this relates to function during pregnancy.

1.2 Gross anatomy of the uterine cervix

1.2.1 Anatomical Description

The human cervix is a firm, cylindrical organ that is contiguous with the inferior pole of the uterine corpus. The non-gravid cervix is approximately 25mm in length along the longitudinal axis, with an anteroposterior diameter ranging between 20-25 mm and a transverse diameter of 25-30 mm, although considerable inter-individual variations occur due to age, parity and stage of menstrual cycle (Asplund, 1952; Anthony et al., 1982; Singer and Jordan, 2006). Two anatomical regions that lie above and below the vaginal reflection are described: the portio supravaginalis and portio vaginalis, respectively (Fig. 1.1). The portio vaginalis projects into the anterior aspect of the vagina forming

the vaginal fornices at the margin of the cervix. The central canal runs from the internal to the external os thereby allowing for communication between the cavity of the corpus and the lumen of the vagina (Fig. 1.1; Singer and Jordan, 2006).

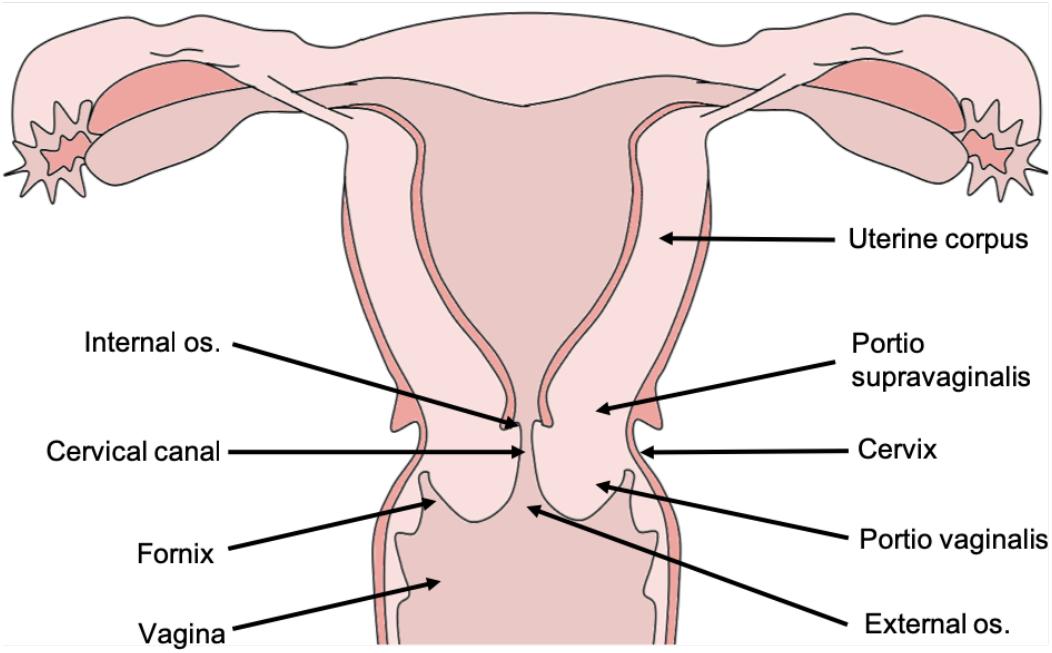

Figure 1.1 Diagrammatic representation of the gross anatomy of the uterus and cervix in the coronal plane.

The cervix forms the lower portion of the uterus and projects into the vagina to form vaginal fornices at the margin of the cervix. The internal and external cervical os allow for communication between the cavity of the uterine corpus, cervical canal and lumen of vagina.

The cervix is located within the ‘true pelvis’, posterior to the bladder base and directly anterior to the rectum. Typically, the uterine corpus arches forward over the superior surface of the bladder, creating an angle of anteflexion between the corpus and the internal os. Similarly, the projection of the portio vaginalis into the upper vagina creates an angle of anteversion between the two structures. Separating the bladder from the upper portion of the cervix is the perimetrium, which is reflected onto the base of the bladder forming the vesicouterine pouch. Lateral extensions of this tissue, the cardinal ligaments, pass towards the pelvic walls and contain a number of important structures including the uterine vessels and the ureter (Fig. 1.2). Posteriorly, the rectouterine pouch (of Douglas) is formed as a result of the peritoneal reflection from the cervix inferiorly to the posterior vaginal fornix and onto the rectum (Drake et al., 2010).

1.2.2 Supporting Structures

The cervix is supported by paired ligaments on either side: the uterosacral and cardinal (transverse cervical) ligaments (Fig. 1.2).

The uterosacral ligaments pass from the posterior and lateral supravaginal portions of the cervix to the middle three sacral vertebrae (Singer and Jordan, 2006), though other attachments include levator ani, coccygeus and obturator internus (Blaisdell, 1917). Descriptions of the ligament state that it has a poorly organised structure consisting of sparse collagen I and III fibres, smooth muscle, elastin and adipose tissue (Cole et al., 2006). A regional analysis demonstrated that at the cervical attachment the ligament is relatively well-developed and consists of closely packed smooth muscle fibres and vessels.

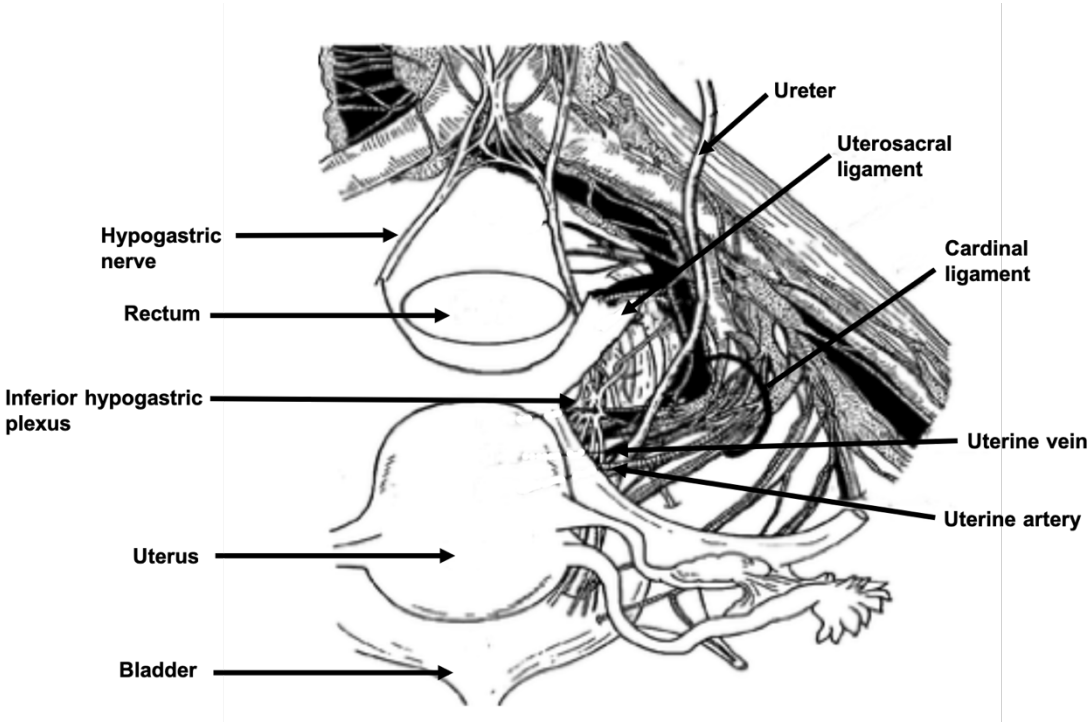

Figure 1.2 Diagrammatic representation of the uterosacral and cardinal ligaments with anatomical relations

Diagram demonstrates the relationship between the bladder, uterus, rectum and associated supporting structures. The cardinal ligament has been stripped of the associated adipose and connective tissue to demonstrate the vascular constituents: uterine artery and vein. The cut uterosacral ligament is closely related to the inferior hypogastric plexus, the hypogastric nerve, ureter and rectum.

Adapted with permission from Ramanah *et al.* (2012)

The sacral attachment is comparatively underdeveloped and consists of loose connective tissue, fat, lymphatics, and autonomic nerves and ganglia from the inferior hypogastric nerve (Campbell, 1950; Butler-Manuel et al., 2000, 2008). The ligament is thought to facilitate the passing of nerves to the pelvic viscera and therefore should be preserved during pelvic surgery. However, it is likely to have limited supportive value, other than to maintain the natural anteverted position of the uterus (Campbell, 1950; Ramanah et al., 2008).

The cardinal ligament is defined as a perivascular sheath, which passes from the cervix to the internal iliac artery, though alternative attachment sites at the iliac fossae, ischial spines and the broad ligament have been described (Ramanah et al., 2012). Histological analysis has demonstrated that the cardinal ligament is predominantly composed of blood vessels from the internal iliac system (Fig. 1.2), nerves arising from the inferior hypogastric plexus and preganglionic splanchnic nerves, surrounded by loose areolar connective tissue, collagen (I and III) and elastin fibres (Range and Woodburne, 1964; Kato et al., 2002). The cardinal ligament is thought to provide support to the pelvic viscera. This was demonstrated by histopathologic analysis of the cardinal ligaments of postmenopausal women with and without pelvic organ prolapse (POP). A higher expression of collagen III and a lower quantity of elastin were recorded in the POP group (Ewies et al., 2003), suggesting that changes in tissue composition may affect the mechanical function of the ligament.

1.2.3 Vasculature

The cervix receives blood via branches of the uterine artery, though vaginal arteries arising from the internal iliac arteries may also contribute (Palacios Jaraquemada et al., 2007). The vascular composition at the uterocervical junction is thought to comprise of four distinct regions: an outer region

containing larger vessels, an arteriole and venule region, an endocervical capillary region and an inner pericanalar zone of small veins and capillaries surrounding the canal (Bereza et al., 2012; Walocha et al., 2012). This arrangement is thought to exist throughout the cervix, although variations in vessel size and vessel course are noted between the portio supravaginalis and portio vaginalis (Bereza et al., 2012). This dense vascular network provides an extensive and rapid means of communication via immune cells, hormones and chemokines/cytokines, which may facilitate cervical remodelling during pregnancy (Section 1.5.1). The combination of pericanalar and middle/peripheral veins creates an efficient double venous drainage system of the dense mucosal capillary plexus (Bereza et al., 2012; Walocha et al., 2012). The inner pericanalar system of veins may contribute to the formation of cervical varices during pregnancy, occasionally resulting in bleeding and/or thrombosis (Hurton et al., 1998; Sammour et al., 2011).

1.2.4 Nervous control

The cervix is a densely innervated organ (Tommaso et al., 2016). A plexus of autonomic nerves (of Frankenhauser) is situated at the base of the organ, which is an extension of the inferior hypogastric plexus (Fig. 1.3)

There is disagreement on the visceral afferent pathways that convey painful stimuli. Classical descriptions indicate that these nerves pass within the pelvic splanchnic nerves to enter the spinal cord at levels S2 to S4, to ascend the spinal cord via the spinothalamic pathways. Recently, it has been suggested that the vagus nerve may convey visceral afferent signals from the cervix. Physiological and functional imaging studies in women who have complete spinal cord injury at T10 and above demonstrate an awareness of cervical stimulation (Komisaruk et al., 1997; Komisaruk et al., 2004). Such an

injury would block the previously mentioned ascending pathways, as they enter at spinal level S2 to S4. These observations are also supported by functional magnetic resonance imaging (MRI) investigations, whereby a region of sensory nuclei in the brainstem, collectively known as the nucleus solitarius, was activated following cervical stimulation (Komisaruk et al., 2004).

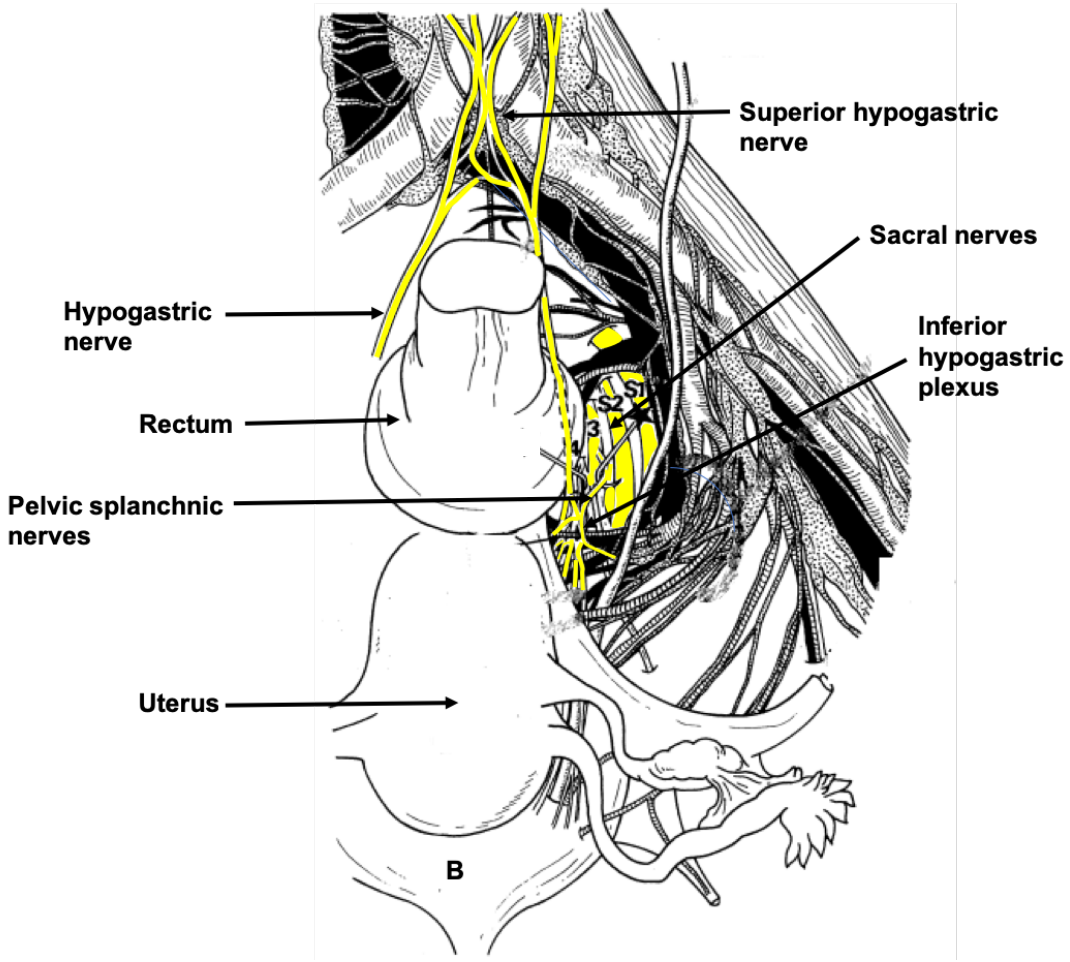

Figure 1.3 Diagrammatic representation of the location of the nerves within the pelvis

Diagram shows the postganglionic sympathetic nerves of spinal levels T_{10} – S_2. These nerves travel as the superior hypogastric nerve (SHN) on the anterior surface of the abdominal aorta. The SHN splits into left and right hypogastric nerves (HN) at the division of the aorta into left and right common iliac arteries. The HN circumnavigate the rectum to enter the inferior hypogastric plexus (IHP). The preganglionic parasympathetic nerves from spinal levels S_2-S_4 pass within the ventral rami of these nerves. Pelvic splanchnic nerves arise on the lateral surface of the pelvic floor. The hypogastric and pelvic splanchnic nerves converge to form the IHP on the pelvic floor. Some preganglionic parasympathetic nerves synapse at the IHP, but most synapse at intramural ganglia in the walls of the bladder, uterus or rectum (Marieb, 2004).

Adapted with permissions from: Kato *et al.,* 2002

1.3 Microanatomy of the cervix

1.3.1 Epithelium

The endocervical canal is lined by a single folded layer of mucus-secreting columnar cells, which serve as a protective barrier to ascending vaginal microorganisms. This layer extends towards the squamous epithelium of the vagina to form the squamocolumnar junction, an anatomical location susceptible to dysplastic change (Beckmann et al., 2010). Infoldings of the columnar epithelium create extensive crypt-like structures that secrete cervical mucus and act as storage sites for spermatozoa following intercourse (Fluhmann, 1957). Squamous metaplastic processes often occlude these clefts, manifesting clinically as Nabothian follicles (Fig. 1.4; Callahan and Caughey, 2013).

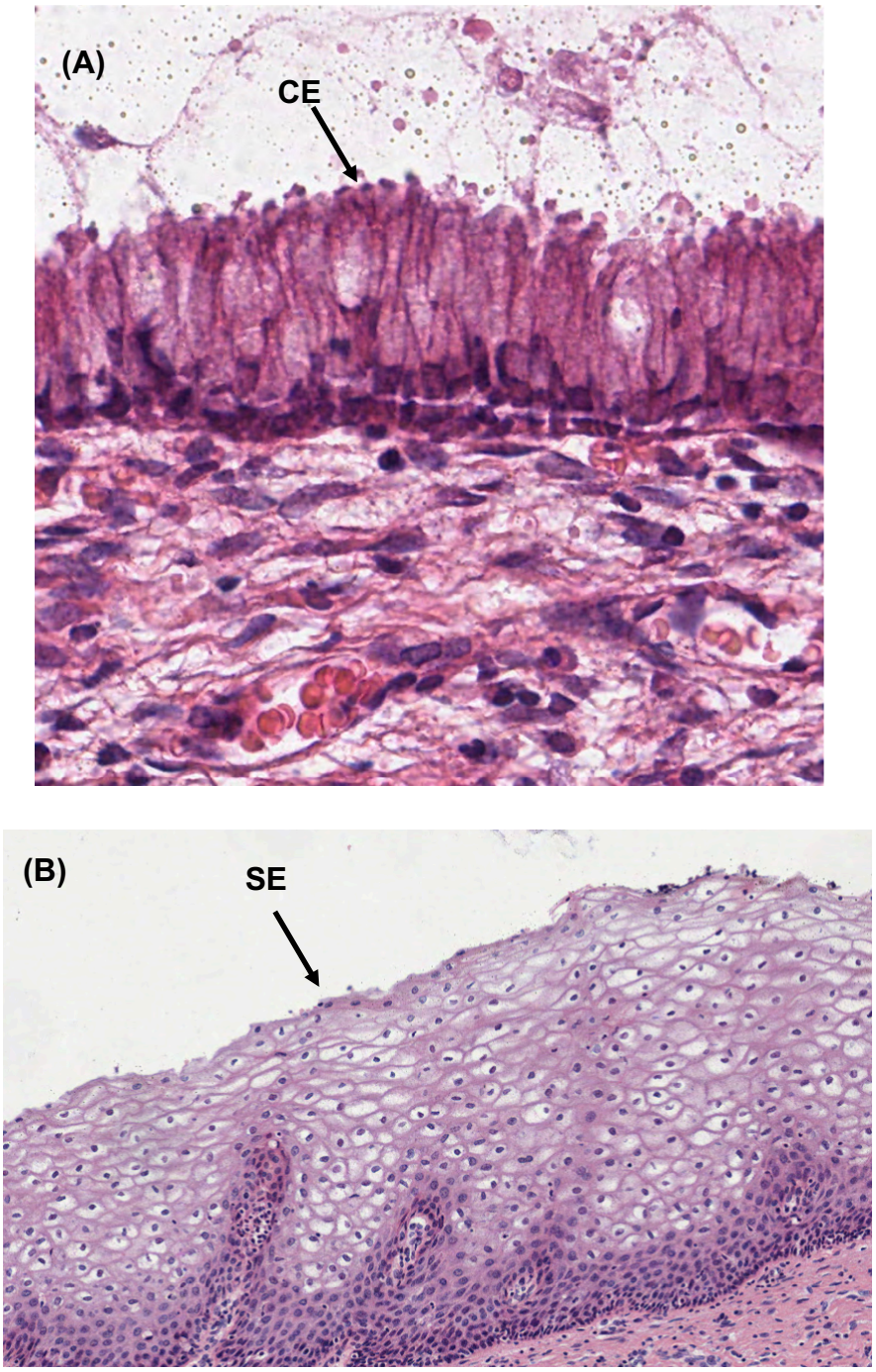

Figure 1.4 Representative haematoxylin and eosin stained sections of normal adult cervical tissue

A. Tall columnar epithelium (CE) within the endocervical canal*. B. Stratified squamous epithelium of the ectocervix.

*Image courtesy of Professor Andrew Hanby (University of Leeds)

1.3.2 Smooth muscle

The cervical stroma is typically described as having a small cellular component. Histological studies have consistently reported that smooth muscle accounts for 10-15% of the cervical stroma, though values ranging up to 45% have been documented (Danforth, 1947, 1954; Hughesdon, 1952). It is unclear why such varied measurements have been observed, yet an overly muscular cervix has been suggested as a cause of cervical weakness during gestation (Roddick et al., 1961). The distribution of smooth muscle was initially thought to be scattered at random throughout the stroma and unlikely to be functional (Danforth, 1947, 1954). However, further insight has been offered following improved immunohistochemical analysis and functional studies (Vink et al., 2016). Cervical smooth muscle cells were observed to be orientated circumferentially around the cervical canal and contracted in response to oxytocin stimulation. These findings are significant because they provide support for an occlusive muscular structure within the cervix that may determine cervical competence during pregnancy. This observation is discussed further in section 1.9.3.

1.3.3 Extracellular matrix

Cervical tissue is mainly composed of a dense, insoluble extracellular matrix (ECM). The ECM serves to provide strength and rigidity to resist mechanical loading encountered in pregnancy. It is primarily composed of a dense, three-dimensional collagen network embedded in a highly viscous ground substance of glycosaminoglycans (GAGs), proteoglycans and interstitial fluid.

1.3.3.1 Collagen

The predominant protein of the cervical ECM is collagen, which forms approximately 80% of its dry weight. The cervix contains 70-80% collagen I and

20-30% collagen III, with a small concentration of collagen IV in the basement membrane (Maillot and Zimmermann, 1976; Kao and Leslie, 1977). Collagen serves to provide structural integrity to tissues, though the proportion of collagen fibre types and the underlying fibre organisation are further determinants of tissue strength (Aspden, 1988; Gan et al., 2015). Homotypic collagen I fibres possess the greatest tensile strength outside of bone and cartilage. However, collagen I and III form heterotypic fibrils, which result in a decrease in collagen fibre size and tensile strength of the tissue (Keene et al., 1987; Moalli et al., 2004). This has been observed in the tendinous arch of levator ani and the cardinal ligaments, which resulted in an increased incidence of POP (Section 1.2.2; Ewies et al., 2003; Moalli et al., 2004). The exact proportion of collagen fibre types in the cervix is yet to be determined, yet it is likely to be a determinant of mechanical strength.

Ultrastructural studies have aimed to determine cervical collagen fibre directionality within the cervix using X-ray diffraction, optical coherence tomography (OCT) and diffusion-tensor (DT) MRI (Aspden, 1988; Weiss et al., 2006; Gan et al., 2015). The descriptions of the underlying structure are varied, yet two zones are consistently described: an inner longitudinal layer, which extends through the length of the cervix parallel to the cervical canal, and an outer layer of encircling fibres. As collagen provides tensile strength to resist stretching, it is thought that the longitudinal fibres resist cervical effacement (Aspden, 1988), whilst the encircling fibres resist forces that promote cervical dilation (Gan et al., 2015; Myers et al., 2015). Regional differences in the concentration of these encircling fibres remain to be described.

1.3.3.2 Elastin

Elastin has consistently been reported as comprising a small percentage of the

stromal substance (Danforth, 1983). The majority of elastic fibres are found in vessel walls, but a few are scattered throughout the cervical stroma (Danforth, 1947). In more recent studies, the proportion of elastin has been observed to be greater (0.9-1.6%) when specific staining or biochemical techniques were used (Leppert and Keller, 1982; Leppert et al., 1983). Elastin was seen to be oriented from the external os to the periphery, whereby fibres extended as a band towards the internal os. At the internal os the elastic fibres became sparse, corresponding to where the greatest amount of smooth muscle was found (Leppert et al.,1986). Elastin is presumed to be important in cervical remodelling during and after pregnancy, as it may allow for the cervix to return to its original shape following vaginal delivery.

1.3.3.3 Glycosaminogylcans and proteoglycans

Proteoglycans are extracellular proteins that are covalently attached to at least one GAG (Esko et al., 2009). Glycosaminoglycans are unbranched polysaccharides of repeating disaccharide units, which may exist independently from a core protein (Shimizu et al., 1980; Osmers et al., 1993). The mechanical function of the extracellular matrix is regulated by the interaction of proteoglycans, GAGs and collagen fibres, as they serve to resist compressive forces, maintain tissue hydration and to regulate collagen fibril formation and spacing (House et al., 2009). GAGs are hydrophilic and so increase the osmotic pressure of water within the cervical ECM (Myers et al., 2015). The tensile strength of collagen fibres counteracts subsequent tissue swelling, which limits an increase in tissue volume. Proteoglycans bind to collagen fibrils to regulate collagen spacing and cross-linking (Danielson et al., 1997). An imbalance of the interactions between proteoglycans and GAGs within the ECM will alter the properties of cervical tissue, possibly transforming the rigid cervix to a relatively

more pliable organ. This naturally occurs during pregnancy, via a process termed cervical remodelling, to alter the mechanical properties of the cervix and allow for the passage of the fetus during childbirth (section 1.5.3).

1.3.3.4 Water

Water is the main constituent of the cervix. Reported hydration levels vary between studies, with values ranging from 74.4% - 79.3% (Danforth et al., 1974; Roberts et al., 1988). Slight differences in protocols may account for these disparities, as increased water content was found at the squamocolumnar junction (Roberts et al., 1988), whereas Danforth et al. (1974) used 2cm punch biopsies at the external os. Roberts et al. (1988) also reported a significant difference in hydration levels between pre and postmenopausal samples (79.3% vs. 75.9%; $p<0.05$). The authors reported that this difference only became apparent following menopause and observed no relationship between age and hydration levels in the premenopausal samples. Slight differences in water content throughout the menstrual cycle have been reported. Shimizu et al. measured the proportion of water at 78.1% and 79.7% for the proliferative and secretory phases, respectively (Shimizu et al., 1980). During pregnancy water is drawn into the cervix due to changes in the concentration GAGs and proteoglycans, increasing water content from 74.4 to 78.4% (Danforth et al., 1974).

1.4 Function of the non-gravid cervix

1.4.1 Cyclical changes and the structure of the cervix

The cervix is a highly plastic organ that undergoes regular morphological change during the menstrual cycle, due to the fluctuations in the underlying circulation of hormones. The uterine and ovarian cycles are regular natural

changes that occur in the female reproductive organs from menarche (first occurrence of menstruation) to the final period (Ferin et al.,1993). The cycles allow for the maturation and release of oocytes, as well as for the preparation of the uterine corpus for implantation. The cycles consist of distinct phases, which are described in figure 1.5.

Few studies have sought to document variations in cervical anatomy during the menstrual cycle, as imaging studies focus on changes in the relative size of the uterine corpus and the thickness of the endometrial layer during each phase. Nevertheless, the cervix has been observed to demonstrate a considerable amount of anatomical (and physiological) variation throughout the cycles. This is required to either promote or prevent the passage of spermatozoa and to facilitate endometrial shedding.

Cyclical changes of the diameter of the internal cervical os have been characterised. In Asplund's classic series of radiographic studies (Asplund, 1952), it was reported that during the menstrual and proliferative phases the cervical canal was at its widest, and the cervical mucosa more serrated, when compared to the secretory phase (Fig. 1.6; Asplund 1952).

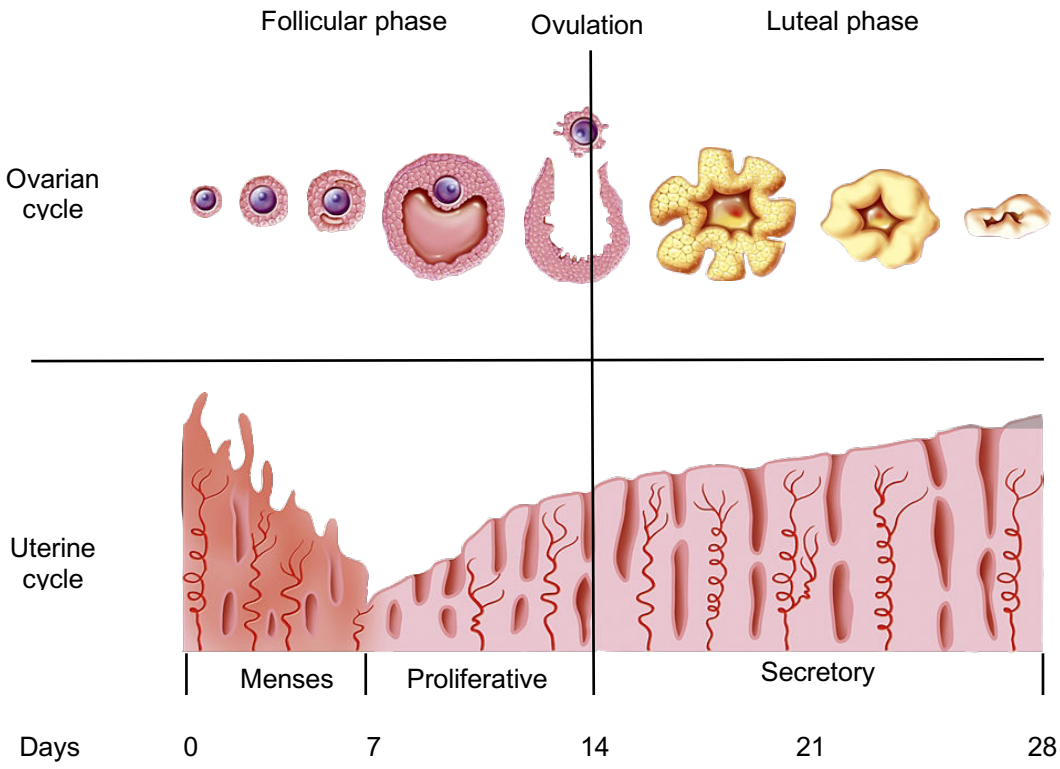

Figure 1.5 A schematic representation of the uterine and ovarian cycles

The uterine cycle is governed by changes in circulating hormones. Increasing levels of oestrogen are characteristic of the follicular phase of the ovarian cycle, as well as the discharging of menstrual blood (menses) and subsequent thickening of the endometrium (proliferative phase). At approximately day 14 of the cycle, a surge in associated hormones results in the dominant follicle releasing an ovocyte, in an event called ovulation. At this point the remnants of the primary follicle (corpus luteum) produces large amounts of progesterone, to further thicken the endometrium in preparation for potential implantation. If implantation does not occur within approximately two weeks of ovulation, the corpus luteum involutes, causing a sharp drop in oestrogen and progesterone levels. This drop in circulating hormones leads to menstruation and the restarting of the cycles.

Adapted from: https://www.gettyimages.co.uk/detail/illustration/menstrual-cycle-drawing-stock-graphic/594417528

This has been subsequently supported and further quantified in magnetic resonance imaging (MRI) studies in which the mean width of the cervical canal was 4.5mm in the follicular phase and 3.8mm in the luteal phase of the ovarian cycle (McCarthy et al., 1986). In a separate radiographic study, the internal os appeared tightly closed during the luteal phase of the ovarian cycle and appeared to relax before the onset of menstruation (Youssef, 1958). Contrast material injected into the uterine cavity was retained between one to three hours in the follicular phase, between four to eight hours in the luteal phase, and less than 30 minutes two days prior to menstruation (Youssef, 1958). These results indicate that the cervix can narrow and widen at the junction between the corpus and the cervix, which may be attributed to a muscular and/or collagenous occlusive mechanism at this level.

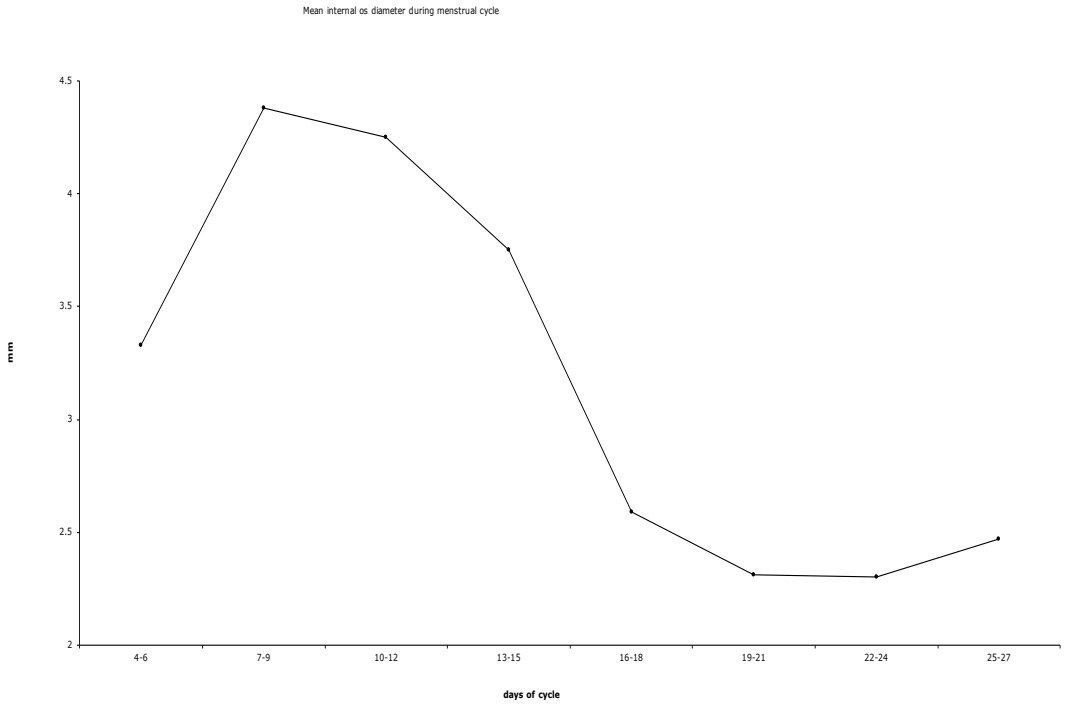

Figure 1.6 The changes in the mean diameter of the internal os throughout the menstrual cycle.

Adapted with permissions from: Asplund (1952)

1.4.2 Cervical mucus production and secretion

The production and secretion of cervical mucus by the cervical columnar cells throughout the menstrual cycle is regulated by oestrogen and progesterone (Martyn et al., 2014). During ovulation the mucus produced has a stretchy and stringy consistency, facilitating the migration of sperm by providing an environment that is optimal for ascent, storage and survival (Martyn et al., 2014). Furthermore, cervical mucus appears to select and exclude sperm cells with deficient locomotive mechanisms (Curlin and Bursac, 2013) The secretion of progesterone by the corpus luteum predominates the second half of the cycle (Fig. 1.5). The mucus reduces in fluidity and volume, becoming tacky and viscous, discouraging spermatozooal and microbial ascent into the uterus.

1.5 Changes during pregnancy

The function of the cervix from conception is to retain and protect the growing conceptus. An effective barrier is accomplished through retaining a sufficient length of closed cervix within which the cervical mucus plug (CMP) can deter ascent of microbes from the lower genital tract (Becher et al., 2009; Hansen et al., 2014). Cervical shortening is a consequence of increasing gestational forces and cervical remodelling, which leads to the opening of the internal os (cervical funnelling). Therefore, the structural integrity of the proximal cervix is integral to preventing the early descent of the fetal membranes and conceptus into the cervical canal.

1.5.1 Cervical remodelling and changes in the ECM

The cervix undergoes important biochemical changes throughout gestation that ultimately change the mechanical properties of the organ. This process is

termed cervical remodelling, and consists of four overlapping phases: softening, ripening, dilation and postpartum restoration.

1.5.2 Softening

Cervical 'softening' is a slow, incremental process that occurs in a progesterone-rich environment (Cunningham et al., 2010). In this extended phase of remodelling two significant changes occur: proliferation of cervical epithelial cells and a measurable change in collagen solubility. The rapid growth of epithelial cells allows for increased cervical mucus production (Timmons et al., 2010). The decline in tissue compliance is caused by the progressive disorganisation of the collagen network and increased collagen solubility (Uldbjerg et al., 1983; Granstrom et al., 1989). However, the cervix must maintain a degree of structural integrity to support the pregnancy until term, which is achieved by the maintenance of collagen content (House et al., 2005; Timmons et al., 2010).

1.5.3 Ripening and dilation

Towards term the disorganization of collagen accelerates, and the cervix 'ripens' and 'dilates' at the onset of labour. During this time, the ECM is disrupted, a consequence of a sharp increase in hyaluronan and a decrease in decorin. Hyaluronan is a GAG that serves to draw in water into the ECM of the cervix. The increase in water (74.4% non-pregnant vs. 78.4% immediately postpartum; Danforth et al. 1974) is thought to either disperse and/or prevent the aggregation of collagen fibrils (Osmers et al., 1993; El Maradny et al., 1997; Ludmir and Sehdev, 2000; Straach et al., 2005). The predominant proteoglycan in non-pregnant cervical tissue is decorin, which binds to collagen fibrils to regulate spacing and crosslinking. Term

pregnancy is associated with a 40-50% reduction of decorin (Norman et al., 1991; House et al., 2009), which decreases the stability of the collagen network. Changes in the material properties of the cervix coincide with increased cervical loading from the fetal membranes and/or the presenting part, uterine contractions and altered cervical anatomy, which ultimately results in dilation of the cervix.

1.5.4 Postpartum repair

In the days following a vaginal delivery, the cervix begins to regain its original shape, with little indication of pregnancy being identified one month postpartum (Danforth, 1983). Cervical elastic fibres may allow for the cervix to recoil following delivery (Leppert et al., 1986). Laceration (a linear separation or tear of the squamous or columnar epithelium which extends into the stroma) and erosion of the epithelium have been observed on colposcopic examinations 3-11 days following vaginal delivery. At six weeks postpartum these lesions have healed (Wilbanks and Richart, 1966, 1967). Cervical ectopy, as a consequence of vaginal birth, is seen to persist at six weeks postpartum (Wilbanks and Richart, 1967).

Cervical collagen concentration has been observed to decrease by 45-75% during the later stages of pregnancy, when compared with non-pregnant values (Uldbjerg et al., 1983; Granstrom et al., 1989; Westergren-Thorsson et al., 1998). Reduced collagen content is a requirement for vaginal birth, as a high concentration is associated with prolonged time to cervical effacement (Ekman et al., 1986). Wedge biopsies of cervical tissue taken immediately postpartum demonstrated substantial collagen degradation and an accumulation of GAGs when compared to a control group (Danforth et al., 1960; Danforth, 1983). In a separate study, collagen concentration changes were

quantified at three, six, twelve and fifteen months postpartum following uncomplicated pregnancies. Measurements steadily increased until 12 months following parturition, with increments to the ninth month being statistically significant. Collagen values did not increase after 12 months. The authors proposed that the association between a short inter-pregnancy interval and preterm birth maybe, in part, due to incomplete remodelling of the cervix (Sundtoft et al., 2011).

1.5.5 Imaging studies during pregnancy

The appearances of the cervix throughout pregnancy have been well documented using transvaginal ultrasound (TVUS). The majority of women maintain a cervical length between 30-40mm throughout pregnancy (Fig. 1.7A; Royal College of Obstetricans and Gynaecologists. 2011). Pregnancies in which the cervical length is less than 20mm are more likely to result in preterm delivery (i.e. before 37 completed weeks of pregnancy; Fig.1.7b). Strategies used to prevent this include reinforcement of the short or weak cervix by inserting an encircling suture (cerclage; Royal College of Obstetricans and Gynaecologists, 2011).

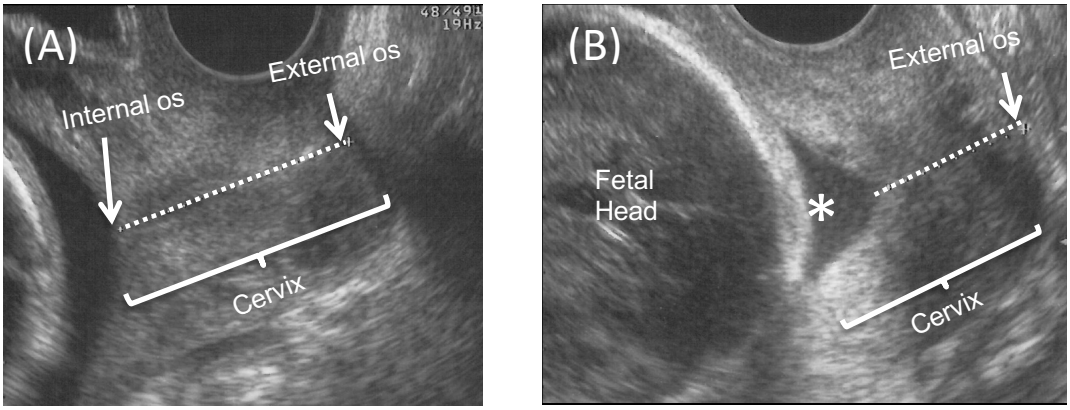

Figure 1.7 Transvaginal ultrasound scan images displaying changes in the appearance of the cervix in the mid-trimester of pregnancy.

(A) A scan at 19 weeks gestation demonstrating normal views of a closed internal os and cervical length of 37 mm. The dotted line indicates the course of the cervical canal. The mother was receiving progesterone injections due to previous midtrimester loss at 19 weeks. The baby was delivered at term.

(B) Scan at 23 weeks gestation showing collapse of internal os (asterisk) with fetal membranes protruding into the upper cervical canal and consequent shortening of the cervical barrier to 19mm. The mother had had previous deliveries at 33 and 35 weeks.

Maintenance of length may be assisted in normal pregnancy by displacement of the internal cervical os. In a study looking at singleton and twin pregnancies, two transperineal scans were performed 12 weeks apart (20 and 32 weeks). Similar displacement of the internal os was observed in both groups (21mm vs. 20mm), however anterior and inferior displacement was observed in singleton and twin pregnancies respectively (Fig. 1.8). Cervical shortening was only associated with inferior displacement (Parikh et al., 2011). It was speculated that the increased inferior displacement seen in twin pregnancies was caused by increased uterine weight, leading to the stretching of the cervical support structures and accelerated cervical change. The use of physician-inserted cervical pessaries in pregnancies at risk of preterm birth is hypothesised to accentuate anterior displacement and may explain their efficacy (Section 1.11.2 Goya et al., 2012).

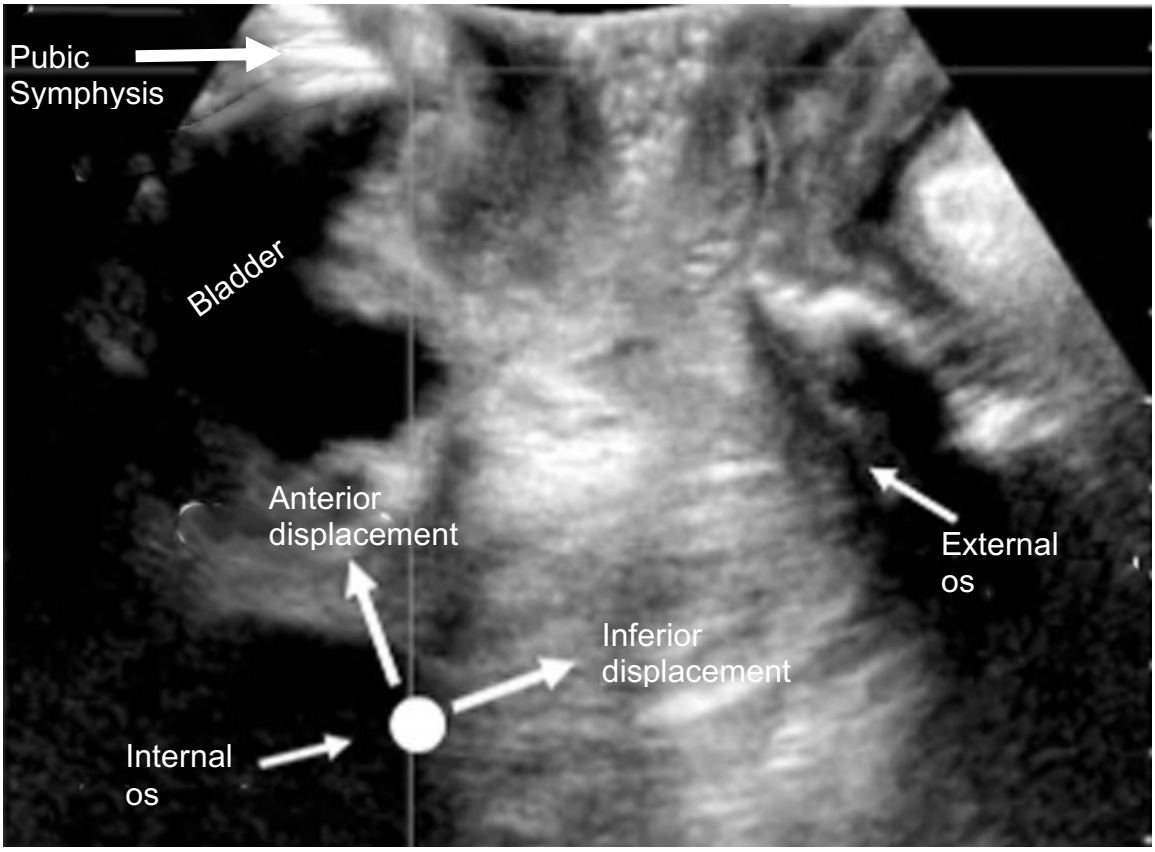

Figure 1.8 Transperineal ultrasound scan of the cervix

Transperineal ultrasound demonstrates the observed displacement of the internal os during pregnancy relative to the pubic symphysis. Inferior displacement of the internal os is associated with accelerated cervical change.

Adapted with permissions from: Parikh *et al.* 2011

The three-dimensional (3D) anatomy of the cervix during pregnancy is poorly understood (House et al., 2013). The preferred methods of investigation include MRI (House et al., 2005; House et al., 2009) and 3D ultrasonography (Parikh et al., 2004; Lang et al., 2010). MRI data collected between 17-36 gestational weeks from women with suspected fetal abnormalities have demonstrated uterine structural changes. As gestational age increased, both the cross-sectional area of the cervical canal and cervical stroma increased by one-third. Morphologic changes were thought to result from a decrease in the tensile strength of the stroma due to collagenolysis, with increased collagen network relaxation and water content leading to an increased stromal area (Section 1.5.2; House et al., 2005). This increase in tissue volume may help keep the cervix closed during normal pregnancy whilst its mechanical properties change (Timmons et al., 2010).

In a later study, a comparison was made in a sample of 14 pregnant women between the three-dimensional anatomy of the uterus and cervix in the second and third trimesters. Changes in cervical anatomy between the two-time periods were a result of an increase in the volume of the lower amniotic cavity, leading to a shorter cervix as pregnancy progressed into the third trimester (House et al., 2009).

1.6 Preterm birth

1.6.1 Definitions and statistics

Preterm birth affects 15 million pregnancies annually worldwide and is the leading cause of neonatal morbidity, as well as the second leading cause of death in children under five years (March of Dimes, 2012). In the United Kingdom, approximately 8% of babies are born preterm, which equates to

approximately 60,000 children being born preterm each year (ONS, 2011). A baby is considered to have been born preterm if he/she is delivered before 37 completed weeks, and this can be further subdivided depending on gestational age (Table 1.1).

Preterm birth may be *indicated* if mother or baby are felt to be at risk of further prolongation of the pregnancy, or *spontaneous* when delivery occurs without initiation. The latter can be linked to one of several pathways: variations in the size and/or shape of the uterus (as seen in Müllerian variants; Chan et al. 2011), deficient placentation (Vahanian et al., 2015), altered microbial flora within the lower genital tract (Smith and Ravel, 2017), systemic infection/inflammation (Cappelletti et al., 2016), and reduction in length and/or strength of the cervix. The first four are beyond the scope of this thesis and the reader is referred to the cited review articles for further insights into these associations. However, the cervix shall be considered.

Table 1.1 Subcategories of prematurity

Classification	Time period (weeks)
Extremely preterm	<28
Very preterm	28 – 32
Moderate to late preterm	32- 37

1.7 The cervix and preterm birth

Cervical dilation and effacement before term is part of the final common pathway leading to the delivery of a preterm fetus. In most cases, the process of premature cervical remodelling is activated by other pathologic processes, such as an infection-mediated response or decidual haemorrhage (Timmons et al., 2010). However, in a proportion of women, early cervical dilation in recurrent

pregnancies occurs independently of other drivers of parturition, leading to progressive cervical shortening in the first or second trimester, herniation of the amniotic sac down the cervical canal (Fig 1.9) and subsequent spontaneous preterm birth (sPTB). Women at risk may have inherited or acquired a short cervix (for example, following the removal of precancerous epithelial cells at the external os). Additionally, women who have undergone forceful dilatation of the cervix to facilitate, for example, surgical termination of pregnancy, are also known to have an increased risk of preterm birth.

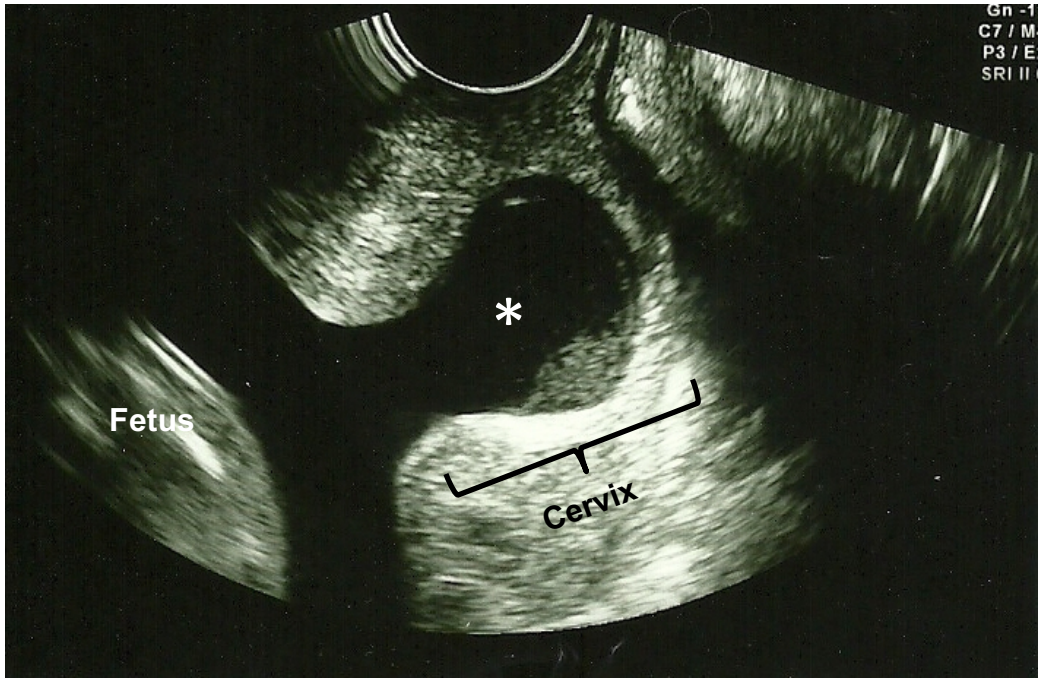

Figure 1.9 Transvaginal ultrasound scan at 22 weeks gestation demonstrating weakness and collapse of the internal os and subsequent protrusion of fetal membranes into the upper cervical canal (asterisk). The mother had had pervious excisional cervical surgery for precancerous change. The length of the closed cervix was 9 mm at the time of the scan and consequently a cervical stitch (cerclage) was inserted in order to extend gestation. The membranes ruptured and delivery of a live baby subsequently occurred at 31 weeks of pregnancy.

1.8 Cervical insufficiency

'Cervical insufficiency' (CIn) is a term commonly used to describe the pathway whereby reduction in strength or length of the cervix leads to early delivery, especially when this has occurred within the mid-trimester. It lacks a consistent definition, but is classically described as the inability of the uterine cervix to retain the growing fetus, often presenting with spontaneous and painless cervical dilation, protrusion (hourglassing) of the fetal membranes into the upper vagina, membrane rupture, and/or spontaneous labour and delivery. Making an accurate diagnosis presents the obstetrician with several problems. Firstly, there is no reliable diagnostic preconceptual test to estimate whether a cervix is able to retain a pregnancy (Hassan et al. 2011). Secondly, CIn may present with an array of symptoms that are common to conditions such as preterm labour and preterm premature rupture of membranes (Farquharson, 2006; Iams, 2009). A working definition of CIn is therefore *post hoc,* 'in which a cervical cerclage (inserting a stitch) is likely to improve pregnancy outcome' (Iams, 2009). However, this needs to be used with caution, as cerclage incurs potentially hazardous surgery and may not be necessary or the most appropriate intervention (RCOG, 2011).

1.9 The pathophysiology of cervical insufficiency

Cervical insufficiency is not a dichotomous condition (i.e. where it is either present or absent), but should rather be seen as an extended biological continuum with degrees of cervical competence (Iams et al., 1995). It may occur as a result of surgical trauma, traumatic damage of the anatomy of the cervix, or uterine/developmental abnormalities, all of which may impair mechanical

function. At a microscopic level, constitutional anatomical defects of the cervical stroma also have the potential to impair mechanical function.

Any deviations from the 'normal' cervical structure (see gross anatomy 1.3) may render the cervix mechanically insufficient to carry the pregnancy until term. This defect would be present in both the non-pregnant and pregnant states and would fall into the categories of either a localised cervical defect or a general connective tissue defect.

1.9.1 A high proportion of cervical smooth muscle in the cervical stroma

Although the cervix is predominantly a fibrous organ, the volume of smooth muscle varies, with observed proportions ranging from 0 – 45% (section 1.3.2; Danforth, 1947, 1954). A muscular cervix may compromise the strength derived from the dense collagen network. Abnormal smooth muscle/collagen ratios have been reported in small groups of women with suspected CIn (Roddick et al., 1961; Buckingham et al., 1965). In these investigations, tissue was obtained from the posterior portion of the distal cervix after the delivery of the placenta and analysed using standard histological practices. Specifically, tissues were marked with a trichrome stain that characterised collagen and smooth muscle. A greater proportion of smooth muscle was observed in women suspected of having a clinically weak cervix. However, caution must be observed before definitive conclusions can be drawn. The consequence of cervical remodelling is that the concentration of mature collagen fibrils decreases to allow for parturition and it may be normal for there to be a greater proportion of smooth muscle at delivery (Timmons et al., 2010). Further observations of the same sample in the non-pregnant condition would have provided further insight into whether this difference persists. Moreover, an up-to-date immunohistochemical

analysis of smooth muscle in non-pregnant women found no difference between CIn and control groups (Oxlund et al., 2010).

1.9.2 A low proportion of collagen in the cervical stroma

An inherently low concentration of collagen is thought to predispose women to CIn. Analysis of studies that sought to compare collagen concentrations between a CIn group and a control is challenging due to differences in sampling and analysis techniques (Rechberger et al., 1988; Petersen and Uldbjerg, 1996; Oxlund et al., 2010; Sundtoft et al., 2017). For example, in three of the four published reports experimental tissue was sampled from women in the non-pregnant condition (Petersen and Uldbjerg, 1996; Oxlund et al., 2010; Sundtoft et al., 2017). In the remaining study, samples were obtained from women identified as having CIn at the time of cerclage in the 15th gestational week. Control samples were either taken immediately postpartum or from normal non-pregnant women who were admitted for benign uterine disease (Rechberger et al., 1988). The non-pregnant studies determined that women with a history of CIn had a significantly lower cervical collagen concentration compared to the control group. However, Oxlund et al. (2010) adjusted data for age, parity and mid-trimester abortions and observed no differences between groups ($p<0.41$). Two-thirds of the sample used by Oxlund et al. (2010) were treated with cervical cerclage, which may have increased mean collagen concentration due to the presence of local scar tissue. Recently, Sundtoft et al. (2017) observed lower mean collagen concentration in women with cervical weakness without a history of the intervention compared to those who received cerclage in a previous pregnancy. However, collagen concentration values in these subgroups were significantly lower when compared to a control group following adjustments for age and parity (Sundtoft et al., 2017). In contrast, Rechberger et al. (1988)

found that collagen levels between a CIn group at the time of cerclage and non-pregnant women were comparable. It is clear that further research is needed to determine the relationship of collagen concentration and CIn.

The volume of mature crosslinked collagen fibrils may be of importance in CIn. Collagen extractability measurements reflect the amount of immature collagen fibrils present in biological tissue. Collagen extractability was demonstrated to be significantly higher in CIn groups when compared to controls, which may have altered the mechanical properties of the cervix (Rechberger et al., 1988; Petersen and Uldbjerg, 1996). This has been observed *in vivo* where mature, cross-linked collagen was measured using light-induced fluorescence (LIF). LIF values were found to be significantly lower in pregnant women at the time of cerclage compared to non-labouring women at term ($p=0.001$; Schlembach et al., 2003). Therefore, an increased volume of immature collagen fibrils in early pregnancy may decrease the tensile strength of the cervix.

1.9.3 A weak internal cervical os

The internal os contains the largest proportion of smooth muscle (Rorie and Newton, 1967). The significance of this has largely been overlooked, as previous authors established that smooth muscle cells appeared immature when examined histologically (Danforth, 1947, 1954). Due to the lack of in-depth research over many decades, there remains a paucity of accurate information regarding the internal os. It has previously been hypothesised that an occlusive mechanism exists in this region (FitzGerald, 1949). This mechanism would be integral to the maintenance of pregnancy, as intrauterine forces are centred at the internal os (House et al. 2013; Myers et al. 2015).

Therefore, cervical funnelling, which often precedes cervical shortening, may be a consequence of sphincter failure.

The cervix exhibits sphincteric behaviour in the non-pregnant condition. For example, at varying stages of the menstrual cycle the diameter of the internal os regularly changes (Section 1.4.1; Asplund, 1952; Youssef, 1958). Recent immunohistochemical studies have demonstrated that smooth muscle cells at the internal os are organised circumferentially around the canal and contract in response to oxytocin stimulation (Vink et al., 2016). However, measurements of smooth muscle were made independently of collagen content, and so the distributions of these two components at the proximal cervix are not known. Therefore, further structural investigations are paramount to understanding how a closed cervix is maintained until term and how an underlying weakness may contribute to pathologic cervical shortening.

1.9.4 Congenital connective tissue defect

Abnormalities in genes related to cervical connective tissue may, in part, play a role in the pathophysiology of CIn. Two candidate genes include collagen 1 α-1 (Col1α-1*)* and transforming growth factor-β (TGF-β). In a limited genetic association study, Warren et al. (2007) studied 130 Caucasian and Hispanic women with a history suggestive of CIn. Results indicated that 27.2% of the cohort had a first-degree relative with CIn. Women with CIn also had significantly higher frequencies in polymorphisms in Col1a1 and TGF-β genes when compared to a control matched by age and race, which may suggest that some women may be predisposed to CIn (Warren et al., 2007).

1.10 Diagnosis of cervical insufficiency

The diagnosis of CIn is clinically determined by cervical presentation on TVUS and a history of recurrent mid-trimester losses. Cervical funnelling may indicate cervical weakness, whereby the cervix progressively dilates and sequentially adopts a “T”, “Y”, “V”, “U” presentation (Fig. 1.10). Gestational age at delivery has been shown to differ significantly ($p< 0.0001$) between high risk women (i.e. previous sPTB and short cervix) who present with a “U” shaped funnel compared to a “V” shaped funnel and a no funnel group, following scans prior to 23 weeks of gestation. No differences were observed between a “V” funnel and no funnel. Similarly, time to delivery differed significantly between funnel groups ($p = 0.0004$); a “U” shape presentation demonstrated a significantly shorter time compared to a “V” funnel and no funnel ($P < 0.0001$). Comparisons between a “V” funnel and no funnel were not significant. Therefore, although cervical funnelling is associated with an increased risk of PTB, funnelling does not necessarily lead to this outcome.

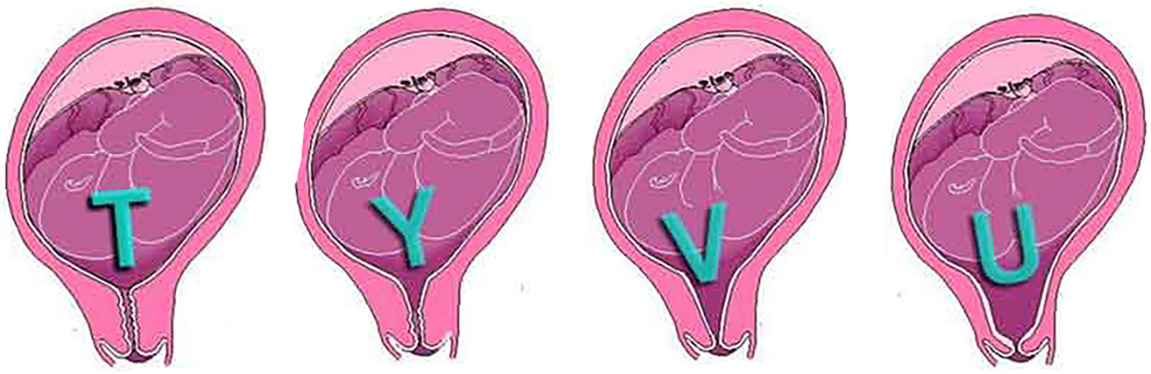

Figure 1.10 T, Y, V, U pattern in response to cervical loading

Diagram represents the sequential changes that occur in the cervix towards term.

An alternative presentation is progressive cervical shortening, yet this is also inconclusive. A short cervix is related to an increased risk of PTB (Iams et al., 1996), and this relationship is further strengthened if there is a history of PTB (Iams et al., 1995; Guzman et al., 1998) or if progressive shortening is noted during pregnancy. Like cervical funnelling, progressive cervical shortening is typical of normal cervical remodelling; most women who present with a clinically identified short cervix (<25mm) will deliver at term. This was previously highlighted in a preterm prediction study, where only 27% of women identified as having a short cervix delivered before 37 weeks (Iams et al., 1996). Furthermore, in a later study, women identified as having a very short cervix (<15mm) still had a 50% chance of delivering beyond 33 weeks (Hassan et al., 2000). Cervical shortening may also occur due to other pathways leading to the generation of inflammatory mediators (such as placental bleeding), and therefore is not unique to CIn (Gravett et al., 2010). In turn, TVUS is used as a predictor of PTB based on cervical length over time, but alone it is not suitable to distinguish CIn from other causes of PTB (Iams, 2009).

At present, there is no widely accepted objective test to clinically evaluate the mechanical properties of cervical tissue in either the pregnant or non-pregnant condition. The efficacy of methods, such as those that distend the cervical canal (Anthony et al., 1982; Kiwi et al., 1988; Cabrol et al., 1991; Hee et al., 2014), compress the cervix (Parra-Saavedra et al., 2011; Fuchs et al., 2013; Hee et al., 2013), measure electrical impedance (Gandhi et al., 2006; Jokhi et al., 2009; Jokhi et al., 2009; Wang et al., 2017) or indirectly assess its biomechanical properties (Hricak et al., 1990; Chan et al., 1998; Tekesin et al., 2003; House et al., 2005; Kuwata et al., 2010; McFarlin et al., 2010), remains to be determined as each possess limitations that are difficult to overcome.

Specifically, as these methods primarily assess the biomechanical properties of the cervix during pregnancy, it is not clear as to whether they can be used to discern primary cervical disease from other known causes of PTB.

1.11 Cervical weakness interventions

The following section will describe the three primary interventions used to prevent/delay a PTB: cervical cerclage, cervical pessaries and progesterone supplementation, with comparisons being made with expectant management. The literature discussed will pertain to singleton pregnancies in women at moderate to high risk of PTB, using randomised control trials (RCT) when possible. Women at risk of delivering early are those who have a history of spontaneous PTB and/or the presence of a short cervix on TVUS.

1.11.1 Cervical cerclage

Cervical cerclage involves the insertion of a stitch around the cervix to provide mechanical support. The original purpose of cervical cerclage, as proposed by Lash & Lash, was to repair a weakened internal os and to offer further structural support to this region (Lash & Lash, 1950). Presently, variations in surgical technique frequently involve the placement of a stitch at the midpoint of the cervix, which offers no biomechanical support to the region of the cervix for where uterine forces are centred (House and Socrate, 2006). Cervical cerclage is an invasive and potentially hazardous surgical intervention, commonly causing vaginal discharge, bleeding and pyrexia (Alfirevic et al., 2012). However, the clinician to help, coupled with the perceived need of the woman to receive an intervention, may lead to non-evidence-based practice.

1.11.1.1 History-indicated cerclage

Women with a history of PTB are 3-4 times more likely to deliver early, yet most will still deliver at term. Of those women with one previous PTB, 80% will deliver at term in the subsequent pregnancy; in women with two previous early births, 70% will deliver at term in the subsequent pregnancy (Rush et al., 1984). Early RCTs have highlighted the efficacy of cerclage in women at moderate and high risk of delivering before 37 weeks (Lazar et al., 1984; Rush et al., 1984). This is emphasised further in a larger multicentre trial conducted by the MRC/RCOG. The primary outcome was gestational length (before 33 weeks and before 37 completed weeks). Thirty-three weeks was considered a principal outcome because it was deemed that the greatest clinical complications precede this gestational age. There was a significant reduction in birth before 33 weeks in the cerclage group ($p<0.05$), yet more pregnancies reached term in the non-cerclage group (31% vs. 26%). Stratification of groups demonstrated a significant reduction of PTB before 33 weeks in women who had had three or more second trimester miscarriages/PTD (MRC/RCOG, 1993).

The results of the MRC/RCOG trial suggest that history-indicated cerclage may be of benefit in a minority of women. Cerclage was associated with increased intervention during pregnancy, yet its use should be considered if there is a likelihood of benefit (MRC/RCOG, 1993). However, the challenge of identifying high-risk women before the third PTB remains, as offering expectant management up until this point is unrealistic. Therefore, there is an urgent need to design tests that identify women who may have a weak cervix.

1.11.1.2 Ultrasound-indicated cervical cerclage

Monitoring cervical changes on TVUS was proposed to identify those women

who might truly benefit from surgical intervention. A suture is placed as a therapeutic measure in asymptomatic women in the presence of cervical shortening (<25mm) before 24 weeks. However, this criterion may not be sufficient as most women with a clinically short cervix will deliver at term (section 1.10). Berghella et al. (2004) identified that inserting a stitch based on a short cervix alone had no significant effect on delivery before 37 weeks. Subsequent trials have identified that women with a history of PTB and an extremely short cervix on ultrasound (<15 mm) may be better candidates for the procedure (Owen et al., 2009). A meta-analysis that was limited to asymptomatic women with a history of spontaneous preterm birth and a cervical length of <15mm demonstrated that cerclage significantly reduced the incidence of a PTB compared to the control. Significant reductions in births before 37, 32, 28 and 24 weeks were observed (Berghella et al., 2011).

1.11.2 Pessaries

During normal pregnancy, the cervix stays tightly closed with a CMP sealing the cervical canal. Impairment of the CMP, for example, by cervical effacement, can lead to ascending infection and subsequent preterm delivery. The cervical pessary is a silicon ‘doughnut-like’ structure that encircles the cervix and compresses the cervical canal, and so may prevent displacement of the CMP and premature dilation of the cervix. Additionally, the pessary alters the uterocervical angle by anteriorly displacing the internal cervical os. This may reduce the pressure on the internal os by distributing it onto the pelvic floor, associated ligaments and rectouterine pouch. A cervical pessary is a relatively non-invasive intervention, which can be easily placed in an outpatient clinic, without need for anaesthesia (Liem et al., 2013).

Investigations that have aimed to assess pessaries are difficult to

compare, as mixed results have been observed. For example, Goya et al. performed a prospective, open-label, randomized trial. Three-hundred and eighty women were randomized following routine mid-trimester ultrasonography between 18-22 weeks. Women were invited to participate if cervical length was <25mm. Birth before 34 weeks was significantly higher in the expectant management group (27% vs. 6%, $p<0.001$) and significant differences in favour of the experimental group were reported before 37 (59% vs. 22%, $p<0.0001$) and 28 weeks (2% vs. 8%, $p=0.0058$; Goya et al. 2012). Other authors have questioned the high percentage of women that delivered early in the control group and it is thought that the benefits of the intervention may have been over-emphasised. Subsequent studies by Hui et al, (2013) and Nicolaides et al. (2016), however, have found no difference between pessary placement and expectant management groups, despite being similar in design.

1.11.3 Progesterone

Progesterone has a significant role in the maintenance of early pregnancy. Initially, it is produced by the corpus luteum up until the ninth gestational week, whereby the placenta being the primary source thereafter (Csapo and Pulkkinen, 1978; Peyron et al., 1993). However, the role of progesterone in later pregnancy is less clear, despite progesterone supplementation being regularly used in the management of women who are deemed to be at moderate to high risk of a PTB Progesterone may attenuate an immune response, maintain uterine quiescence by limiting the stimulatory effects of prostaglandins and contraction-associated proteins, and regulate cervical remodelling (Loudon et al., 2003; Meis et al., 2003; Norwitz and Caughey, 2011). Towards parturition there is a functional withdrawal of progesterone activity at the level of the myometrium, which possibly provides a rationale for progesterone

supplementation. RCTs and meta-analyses determining efficacy have produced contradictory results, which likely stem from differences in the populations studied, the type and dosages administered, the gestational age at which progesterone is administered and the primary outcome of the study (Keirse, 1990; Meis et al., 2003; De Franco et al., 2007; O'Brien et al., 2007; Durnwald et al., 2009; Hassan et al., 2011; Grobman et al., 2012; Norman et al., 2016). Despite concerns on efficacy, progesterone does not appear to negatively impact childhood development (up until two years), which will provide comfort to both physicians and parents when discussing supplementation (Norman et al., 2016).

In those studies where a benefit was demonstrated, a high percentage of women still delivered preterm, indicating that progesterone may not be effective in all cases of PTB. In the instance of pregnancies threatened by CIn, it is not known whether progesterone is effective in prolonging time to delivery. Progesterone may play a significant role in controlling cervical remodelling, as the initial phase occurs in a progesterone-rich environment (Timmons et al.,2010). Progesterone administration in women with a short cervix at the time of randomization has shown to significantly reduce the rate of PTB (De Franco et al., 2007; Fonseca et al., 2007; Hassan et al., 2011), yet it is not clear whether progesterone acts to attenuate cervical change. Two retrospective cohort studies examined changes in cervical shortening in women with a history of prior PTB. In these cohorts, progesterone supplementation was not protective against cervical shortening (Durnwald et al., 2009; Pessel et al., 2013).

1.11.4 Summary of interventions

Given the heterogeneous nature of PTB, the discussed interventions are unlikely to be effective in all genotypic and phenotypic subgroups of women

who are at risk of delivering early. Comparisons of these three management protocols in high-risk women with a singleton pregnancy demonstrated no differences in terms of spontaneous delivery before 37, 34 and 28 weeks. However, irrespective of intervention, high proportions of women still delivered preterm at the designated outcome measures (Alfirevic et al., 2013). This study, however, was not a randomized trial, and therefore relied on limited data from arms of previous randomised trials and hospital databases, and so analyses may have been confounded by variables such as race and lifestyle habits. Nevertheless, it is still a concern that large proportions of women within these groups still delivered preterm.

The problem is further complicated if primary cervical disease is the underlying cause of PTB. Inconsistencies in both the definition and identification of CIn mean that it is challenging to identify subgroups of women that may have it. However, even if it was possible, these numbers would likely be small and so previous studies would not be appropriately powered to determine the effectiveness of the interventions in this subgroup. Furthermore, CIn is likely to be heterogeneous in nature and it may be too simplistic to think that a universal treatment exists.

1.12 The significance of a weak internal os and cervical insufficiency

Cervical insufficiency is a condition that is poorly understood and consequently remains a diagnosis of exclusion. It is likely that there are several mechanisms that lead to CIn and understanding the nature of each will assist in the identification of appropriate interventions. Presently, however, it is common to adopt a ‘one size fits all’ policy when selecting a screening/treatment pathway.

Progress must be made towards identifying individual causes of CIn, in an attempt to move away from this umbrella term. An area that could be pursued is weakness of the internal os. Despite this region of the cervix being overlooked in the past 50 years, it is interesting that two of the three previously described interventions aim to either reinforce the internal os or displace the internal os anteriorly so that cervical forces are not directed at this region.

It is thought that an occlusive muscular structure is located at the internal os that resists cervical forces associated with gestation (FitzGerald, 1949), yet this has not been identified histologically (Danforth, 1947; Hughesdon, 1952). However, histomorphometric measurements have shown that the proportion of smooth muscle within the cervical stroma progressively increases towards the internal os and contracts when stimulated with oxytocin (Rorie & Newton 1967; Oxlund et al. 2010; Vink et al. 2016).

Observations within a clinical setting suggest that an occlusive mechanism does exist at the proximal cervix. When a dilator is inserted into the cervical canal, resistance is encountered approximately 2-3cm past the external cervical os. Furthermore, radiographic studies have also provided evidence of an area within the proximal portion of the cervical canal that shows cyclical changes in its diameter (Asplund, 1952; Youssef, 1958; section 1.4).

MRI and ultrasound studies suggest that the proximal portion of the cervix is essential to cervical function during pregnancy (Myers et al., 2015). Sonographic studies show that cervical effacement begins here and proceeds distally (Williams and Iams, 2004), and in cases of premature cervical effacement, a weakened internal os may be responsible for the protrusion of fetal membranes into the cervical canal (funnelling) within the second trimester.

1.13 Aims of the thesis

The aim of this thesis is to re-examine the anatomy the cervix, with a focus on the internal os and its occlusive nature. Previous anatomical studies were technically limited by staining methodology and the analysis of two-dimensional (2D) microscopic tissue. The experiments conducted in chapter three aimed to determine the composition of the cervical stroma using immunohistochemical and 3D histological methods. Specifically, the chapter examined regional differences in cervical stroma to further understanding of how the cervix functions during pregnancy. In chapter four, *ex vivo* diffusion-tensor imaging aimed to examine whether the complex cervical anatomy identified in chapter three could be identified using advanced imaging strategies. The aim of chapter five was to determine whether *in vitro* endoscopic ultrasound could identify anatomy at the internal os that would allow it to remain closed during pregnancy.

Chapter 2 General Material and Methods

This chapter describes tissue preparation and histological methods common to much of the experimental work contained within the experimental chapters. Additional methods are provided within the relevant chapters that focus on specific imaging techniques.

2.1 Tissue preparation

Cervical tissue was obtained from women undergoing hysterectomy for benign gynaecological disease. Specific details of permissions and sample sizes are described in each experimental chapter. Following hysterectomy, a longitudinal incision was made through the uterine corpus and then each sample was immersed in a formal-saline solution (Fig. 2.1; 10% formalin, 0.9% sodium chloride, 4% formaldehyde) for a minimum of 24 hours. This time frame was determined by the histopathology department within the Leeds Teaching Hospitals Trust. The cervix was removed from the corpus via a transverse incision and then was hemisected in the midsagittal plane. The right hemisection was used throughout this research (Fig. 2.1). Each research sample was stored in a formal-saline solution for one week to ensure adequate tissue fixation. The length of each cervix sample was measured and recorded.

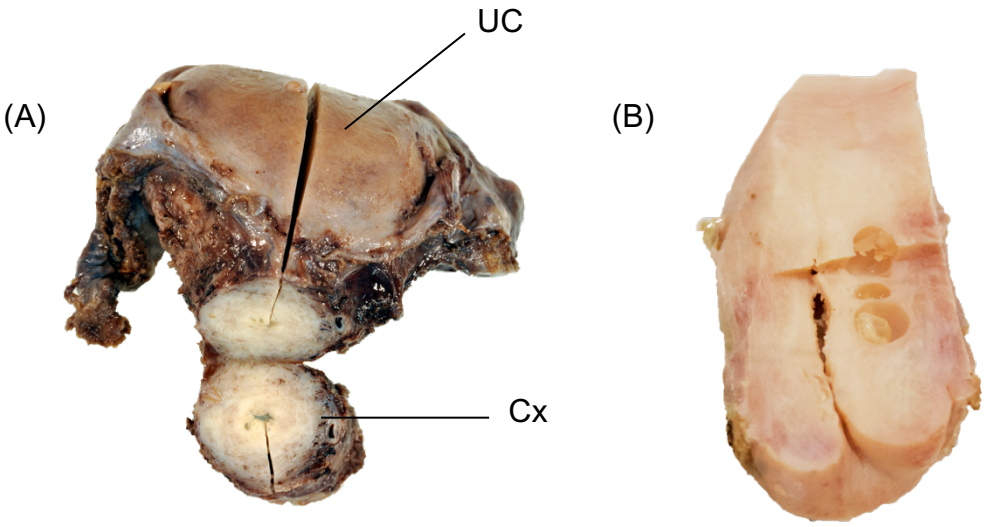

Figure 2.1 Images demonstrate the preparation of cervical tissue prior to imaging.

A: Amputation of the cervix (Cx) from the uterine corpus (UC) via a transverse incision. B: Image of right cervix hemisection segment taken prior to diffusion-tensor imaging (Chapter 4).

2.2 Tissue preparation for general histology staining

Each sample was divided into three portions portions along the length of the cervix to create whole transverse blocks from the proximal, middle and distal regions. Measurements of the size of each transverse block were made along the longitudinal axis (i.e. parallel to the canal). All blocks were embedded with paraffin wax.

Proximal, middle and distal tissue blocks were sectioned at 5μm using a Leica rotary microtome RM2235 (Biosystems, Switzerland). Sections were floated on a water bath (Thermo scientific, UK) at 45 degrees Celsius and mounted on to Aminopropyltriethoxysilane (APEs; protocol; Appendix) charged superfrost coated slides (Solmedia; United Kingdom). Slides were covered, dried for 24 hours at room temperature and placed on a hot plate (Thermo scientific hotplate 3120061, UK) for 60 minutes at 70 degrees Celsius prior to staining. Slides were dewaxed and dehydrated via a xylene and alcohol series, and stained with Haematoxylin and Eosin (H & E) and Masson's Trichrome (MT;

protocol in Appendix). Slides were placed through another alcohol and xylene series and cover slipped.

2.3 Tissue preparation for Immunohistochemistry staining

Five micrometer sections from the proximal, middle and distal cervix blocks were mounted onto APEs coated slides. Sections were covered, dried for 24 hours at room temperature and for a further 24 hours in an incubator set at 37 degrees Celsius. Slides were placed on a hot plate (Thermo scientific hotplate 3120061, UK) for 60 minutes at 70 degrees Celsius and dewaxed and dehydrated via a xylene and alcohol series.

Heat-mediated antigen retrieval was performed using an automated pressure cooker (Menapath, A. Menarini diagnostics, UK) using a citrate buffer antigen unmasking solution (Vector Laboraties, dilution). Slides were heated to a maximum temperature of 125 degrees Celsius. Sections were washed and cooled in deionised water. Tissue sections were incubated in 10% hydrogen peroxidase (Sigma-Aldrich, US) for 20 minutes at room temperature to block endogenous peroxidase. Slides were then mounted onto coverplates and placed in a sequenza. Sections were blocked in casein (1:10 diluent per section) for 20 minutes at room temperature. Primary antibodies for α-smooth Muscle Actin (α-SMA) markers and Col1α-1 were incubated for one hour. The primary antibody information is listed in table 2.1. Sections were incubated in a post primary block (Novolink, Leica, Germany) for 30 minutes, followed by incubation with a polymer (Novolink, Leica, Germany). Sections were removed from the sequenza and placed on a flat surface. Colour reaction was performed using diaminobenzidine (DAB) and a perioxidase substrate (Vector Laboratories, UK) for 5 minutes. Tissues were counterstained with

haematoxylin, washed with deionised water and dried for 12 hours at room temperature. Slides were then placed through an alcohol and xylene series and cover slipped.

Table 2.1 Primary antibody information

Antibody	Vendor/catalogue no.	Dilution	Description	Control tissue
α-SMA	DAKO/M085101-2	1:100	Monoclonal	Human uterine
Col 1α1	ABCAM/ab90395	1 : 100	Monoclonal	Human kidney

2.4 Image analysis

All slides were scanned and digitized with an Aperio AT2 scanner using a x20 objective (Leica, UK) and analysed using Medical Imaging Manager (MIM; http://www.heterogenius.co.uk). The image resolution was 0.5μm^2. Gross morphology was examined and recorded, with the researcher blinded from the region of cervix whilst examining each slide to avoid bias. Details of slide quantification are described in Chapter three.

Chapter 3 Histological Investigation of the Human Uterine Cervix

3.1 Introduction

During normal gestation the cervix is a load-bearing organ, resisting forces from uterine activity, tension from the uterine walls and hydrostatic and intrauterine pressure from the amniotic sac (House et al., 2013; Myers et al., 2015). Biomechanical modelling demonstrates that cervical forces are concentrated at the internal os and stromal deformation is a result of pressure reaching a critical level (House et al., 2013). This is observed clinically on TVUS, where pathologic cervical shortening starts with funnelling of the internal os (Fig 1.7 & 1.9). The internal os is clearly central to resisting forces associated with pregnancy, yet it is not known as to why this region weakens in some women.

The biomechanical properties of the cervix are thought to be partly determined by the underlying fibre composition and directionality within the cervical stroma (Aspden, 1988; Gan et al., 2015). The cervix is composed predominantly of fibrous tissue with a small proportion of smooth muscle and elastin (Danforth, 1947, 1954; Leppert and Keller, 1982) However, the cervix is not a homogenous structure, as variations in composition and fibre orientation vary between the internal and external os (Section 1.3). This is especially true of cervical smooth muscle cell (CSMC) content, with early studies noting an increase from 6.4 – 28.8% between the distal and proximal cervix respectively (Danforth, 1947, 1954; Hughesdon, 1952; Rorie and Newton, 1967). This variation was further confirmed by improved immunohistochemical and computer-assisted quantitative assessment. Researchers noted that smooth

muscle content increased by 50% towards the internal os, with the proximal cervix containing approximately 60% smooth muscle cells (Vink et al., 2016). Furthermore, the smooth muscle cells encircled the cervical canal and were observed to contract in organ bath studies. Authors proposed that these cells could form a muscular sphincter, which supported other clinical and non-clinical observations (FitzGerald, 1949; Asplund, 1952; Youssef, 1958; Williams and Iams, 2004)

However, large discrepancies between reported values may mislead clinicians and researchers as to the significance of smooth muscle cells within the cervix. These variations are likely a consequence of tissue evaluation methodologies, each of which have inherent limitations unique to the analysis technique (Ruifrok and Johnston, 2001; Gurcan et al., 2009). Secondly, although researchers agree that smooth muscle increases towards the proximal cervix, measurements were taken independently of collagen content. Consequently, little is known about the arrangement of muscle and fibrous tissue in this region and how this impacts function during pregnancy.

Fibrillar collagens are the main structural proteins of the cervix and are thought to be the principle determinant of cervical competency (70% collagen I vs. 30% collagen III; Maillot and Zimmermann, 1976; Kao and Leslie, 1977). To date, few studies have noted a relationship between alterations in the collagen network and CIn. However, little is known about regional differences in the ratio of collagen I/III throughout the cervix. Studies indicate that collagen III is essential for normal collagen I fibrillogenesis, yet a decrease in the collagen I/III ratio can alter the mechanical properties of tissue (Section 1.3; Liu et al., 1997; Lui et al., 2010). The collagen I/III ratio within the cervix has been investigated in animal and human studies during pregnancy, each producing conflicting

results (Iwahashi et al., 2003; Akins et al., 2011). Though clear sampling differences exist between the studies, which may explain differences in results obtained, these studies did not investigate the heterogeneity of fibrillar collagen within the cervix. If regional differences exist, it may indicate that specific regions of the cervix are more suited to dealing with an increasing load.

Given it is the internal os which typically funnels in cases of early cervical dilation, few studies have sought to describe the microarchitecture in this region. In this study, cervical anatomy is assessed using conventional and advanced histological practices to determine whether regional differences in CSMC and collagen morphology provide insight into function of the internal cervical os during pregnancy.

3.2 Methods

Ethical approval was granted by the Yorkshire and Humber Regional Ethical Committee (reference number 15/YH/0111). Thirteen non-pregnant, premenopausal women undergoing total abdominal hysterectomy (TAH) or vaginal hysterectomy (VH) for benign pathology were consented. No participants had a history of PTB, CIn, or cervical excisional surgery. (Table 3.1). Tissue preparation and histological and immunohistochemical processes are described in chapter 2.

Table 3.1 Patient demographics for cervical samples

Patient no.	Age (years)	Parity	Obstetric History	Diagnosis	Pre-hysterectomy interventions/investigations
27	46	3	3 x NVD	Stage III cystocele	Progestin
				Stage III uterovaginal descent	Physiotherapy management
28	42	2	2 x NVD	Endometriosis	Hysteroscopy
				Fibroid uterus	Endometrial ablation
					GnRH analogue
37	33	0	N/A	Fibroid Uterus	Esmya
38	49	3	3 x CD	Fibroid	hysteroscopy
				Irregular bleeding	
39	35	0	N/A	Pelvic pain secondary to endometriosis	Mirena
					Prostap
40	45	3	3 x SVD	Fibroid Uterus	Tranexamic acid
				Menorrhagia	
42	46	2	2 x SVD	Fibroid Uterus	Prostap
43	47	1	1 x CD	Fibroids	Mirena
				Menorrhagia	
45	48	0	N/A	Fibroids	Mirena
				Menorrhagia	Endometrial ablasion
46	42	2	2 x SVD	Endometriosis	Tranexamic acid
				Menorraghia	
47	44	2	2 x SVD	Endometriosis	Mirena
				Chronic pelvic pain	Prostap
48	41	1	1 x CD	Fibroid	Nothing described
				Dysmenorrhea	

SVD - Spontaneous vaginal delivery CD – Caesarean delivery

3.2.1 Image analysis and quantification

All slides were examined to determine general morphology at the proximal, middle and distal regions of the cervix. Stained tissue was quantified using bespoke probabilistic colour models, with a colour normalization method to account for stain intensity differences within an image stack. The colour models determined the probability of a pixel belonging to a particular class (colour/stain). The output of the model was a binary image of which the foreground (pixels of interest) and background were denoted as white and black respectively. For example, on DAB stained tissue sections, multiple regions of brown stained tissue were annotated (Fig. 3.1).

Initial models were estimated by selecting five regions of interest to specify for each class, which was repeated on 10 slides within an image stack (Fig. 3.1). A threshold value was assigned by the user (range 0 -1) to determine the probability that a pixel belongs to a particular class. In this instance, the threshold was set to 0.75, so there was a 75% chance that a pixel belonged to a particular class. Each bespoke model calculated the number of foreground pixels and divided it by the total number of pixels in each selected image to obtain a proportion.

The models were subsequently quantitatively and qualitatively validated on two reference slides. Quantitative assessment involved determining the proportion of foreground in a region of interest, whereas visual assessment involved a visual comparison of the original and binary images (Fig. 3.1). Multiple regions of interest were examined to determine whether each model was performing correctly. If the model misclassified areas of tissue, further annotations were added to specify the correct class and new models were built. This continued in an iterative fashion until models classified tissue correctly

(Fig. 3.2; Table. 3.2). Tissue sections were then defined using automatic methods and manually edited if tissue was misclassified. Once defined, tissue was quantified using the probabilistic models.

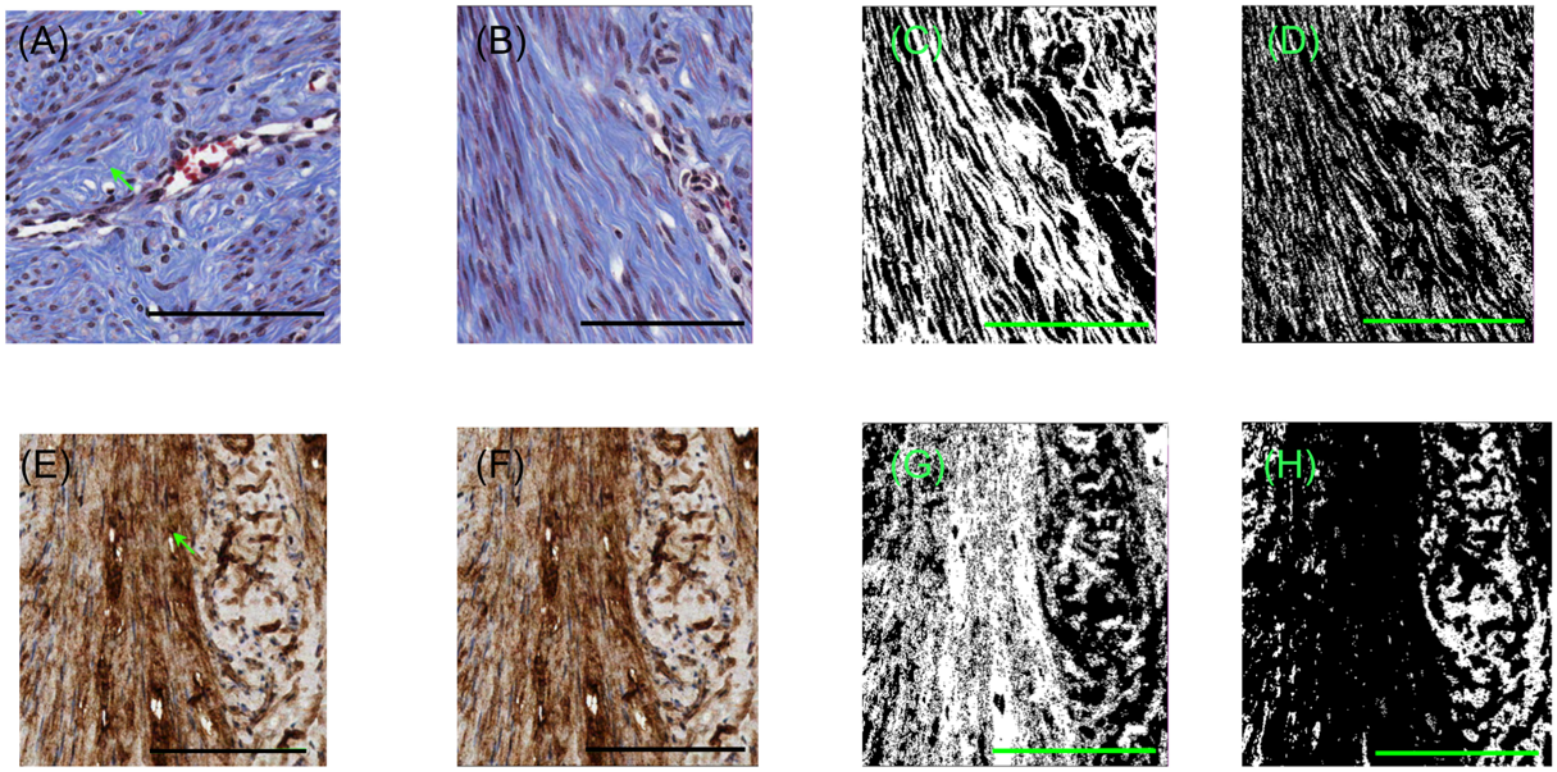

Figure 3.1 Building the probabilistic colour models

Sections of MT and DAB stained tissue sections respectively. A,E: the arrow represents a region of interest (ROI) to specify the selected colour for class one i.e. blue and brown. B, F: selected regions for the model to be tested. C, D, G, H: binary outputs of tested model; C, G: output for class one of model; the white foreground represents blue and brown (DAB) respectively; D, H: binary output for class two of model; the white foreground demonstrates red/black and beige respectively (scale bar in all images 1mm)

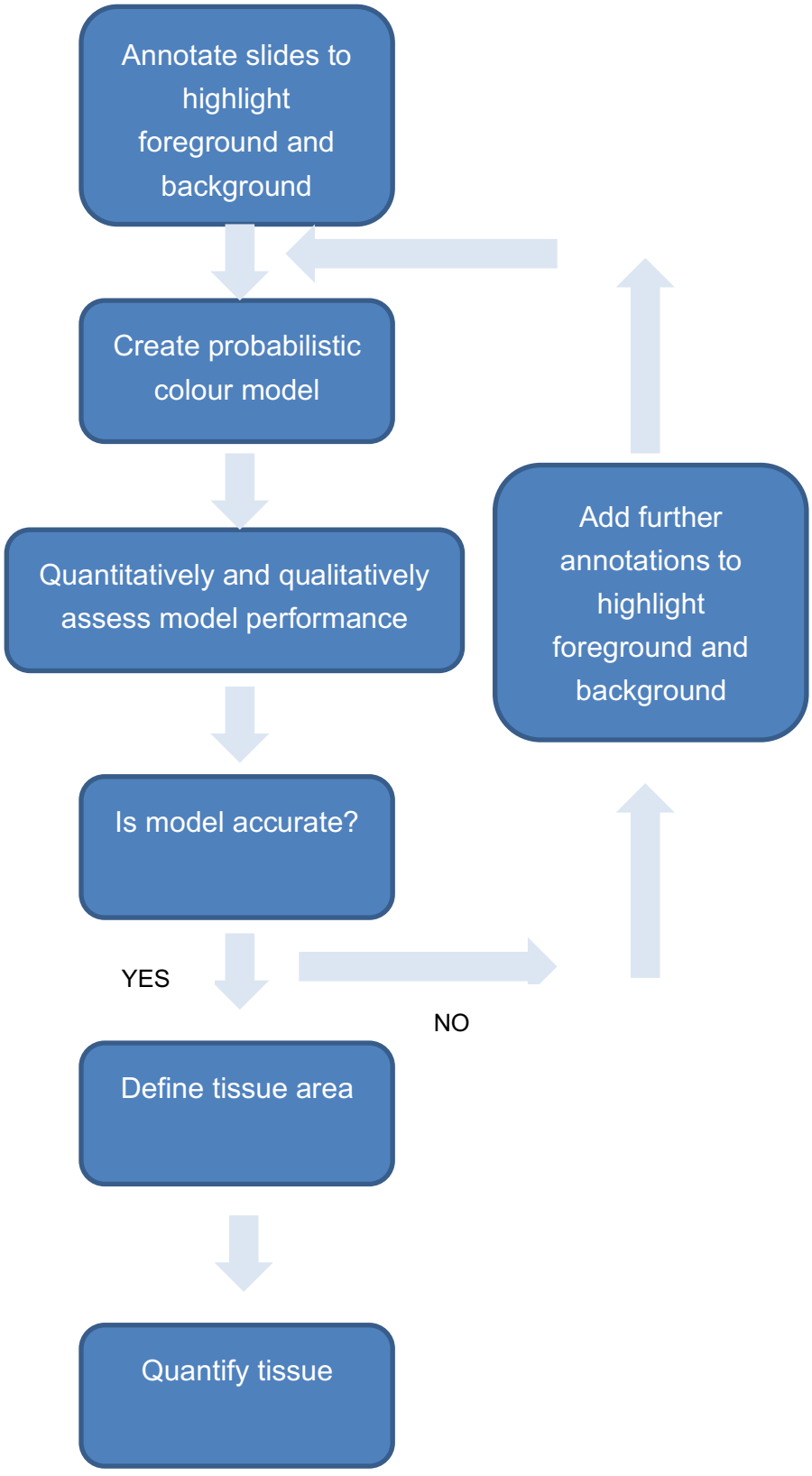

Figure 3.2 Flowchart describing the steps involved in creating probabilistic colour models

Table 3.2 Validation steps for probabilistic colour models

Stain	Classes	Iterations
α-SMA	DAB	2
	Haematoxylin	
Col1α-1	DAB	2
	Haematoxylin	
MT	Blue	6
	Red	

3.2.2 Three-dimensional histopathology

Multiple serial sections were produced from 2 cervical samples at the proximal, middle and distal regions, and stained with MT. Details of tissue preparation and staining methods are described in chapter 2. All slides were scanned and analysed using MIM and ordered sequentially in an imaging stack. Virtual slides were aligned using the section closest to the centre of the tissue as a reference point (Roberts et al., 2012; Fig. 3.2). The slide in the middle of the image stack was selected for all lists, as this slide generally contains the most tissue and provides details of the volume size prior to image registration. Virtual slides directly next to the reference slide were aligned to their neighbours. The aligned slides were then concatenated to produce a 3D volumetric dataset (Roberts et al., 2012; Fig. 3.3).

The performance of each dataset was qualitatively assessed by reviewing coronal and sagittal views. Inaccuracies occurring during alignment and registration would result in discontinuity between anatomical landmarks within the dataset. In this instance, landmarks such as nabothian follicles and the cervical canal were used to assess the model (Fig. 3.3). Minimal misalignment errors were observed in all datasets.

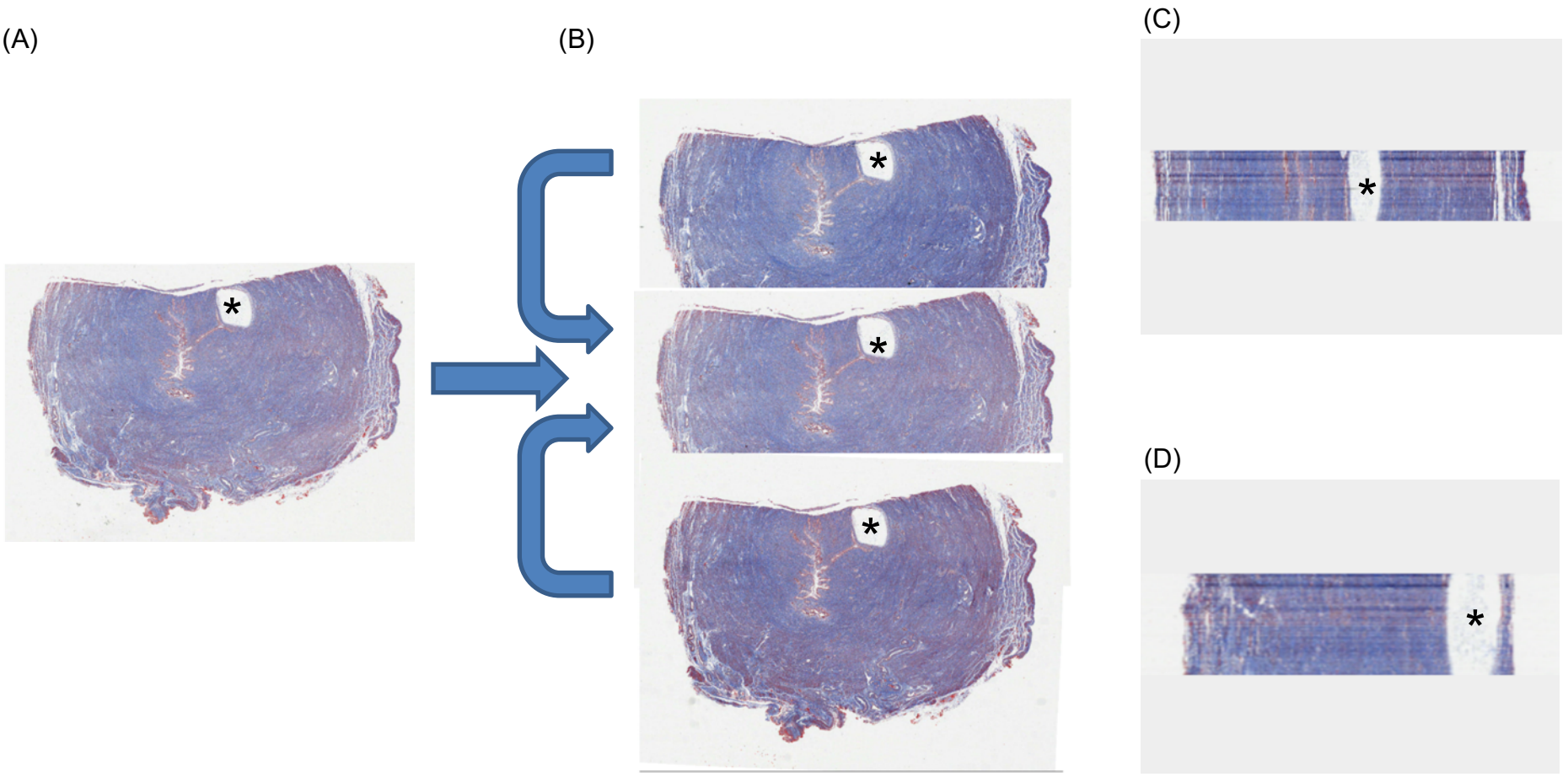

Figure 3.3 Diagrammatic representation of the alignment process

Selected tissue section (A) from the middle of the image list. Asterisk indicates Nabothian follicle. B. Alignment of neighbouring tissue sections to the middle slide. Alignment is continued to the periphery of the dataset. C. 3D volume produced from aligned slides in the sagittal plane. Note alignment of slides with reference to Nabothian follicle*. D. 3D volume produced from aligned slides in the coronal plane. Note alignment of slides with reference to Nabothian follicle*.

3.2.3 Statistics

Quantitative data were assessed for normality using the Shapiro-Wilk test and boxplots were examined to identify outliers. Data for MT and α-SMA were normally distributed with no outliers observed, and there was homogeneity of variances for both stains. One-way ANOVAs were performed to determine differences in positive staining in the proximal, middle and distal sections, with subsequent pairwise comparisons. Kruskal-Wallis tests were conducted on Col1α-1 stained sections.

Data were presented as mean ± standard deviation with a statistical significance accepted at $p < 0.05$. Differences were reported alongside confidence intervals (CI). All statistical analyses were performed using SPSS software v.23.0 (SPSS, Inc., Chicago, IL). Graphs were produced using GraphPad Prism 7 (GraphPad Software Inc., US).

3.3 Results

3.3.1 Evaluation of cervical architecture

Transverse cervical tissue was collected from the proximal, middle and distal regions from 10 non-pregnant women. Of these women, seven were multiparous and three were nulliparous. The mean age of the group was 43 ± 5 years.

3.3.1.1 Smooth Muscle

Analysis of transverse cervical sections from the proximal, middle and distal regions of the cervix demonstrated a gradient of smooth muscle content. The cervix contained approximately 30% smooth muscle at the proximal region (Figs. 3.4, 3.5 & 3.7), the majority of which was found at the radial edges of the

stroma. Smooth muscle was circumferentially organised towards the periphery, with inner longitudinal regions close to the endocervical canal (Figs. 3.4 & 3.5). This arrangement extended into the middle regions of the cervix, though less dense staining was observed (~25% content). Analysis of the distal region demonstrated significantly less positive staining compared to the middle and proximal regions ($p < 0.05$), as identified by positive staining for α-SMA, though a significant difference was only found when compared to the proximal region with MT stain. Positive staining in the distal cervix was largely reserved for vessels and some randomly scattered transverse and longitudinal fibres. Smooth muscle content at the distal cervix was found to be between 15-20%. CSMC morphology was consistent throughout samples.

3.3.1.2 Collagen

Collagen fibre morphology was mostly consistent throughout the cervical samples, though some variation was seen in the distal regions. Immunostained sections from the proximal and middle regions demonstrated organised bands of encircling collagen I fibres in the inner and mid-stroma, with some fibres extending towards the radial edges (Figs 3.4 & 3.6). These encircling fibres extended to the distal region in 50% of the sample, with no obvious pattern observed in the remaining sections. Quantitative analysis of Col1α-1 stained sections demonstrated a slight decrease in positive staining between distal and proximal regions (proximal = 30% ± 3%, middle = 30% ± 4%, distal = 33% ± 5%; Fig. 3.7). A gradient was observed in MT-stained sections (proximal 33% ± 8%, middle = 40% ± 5%, distal = 46% ± 9%; $F(2, 23) = 7.19$, $p = 0.006$), with a significant increase from the distal to the proximal regions (13%, 95% CI 5% to 22%, $P = 0.003$; Fig. 3.7).

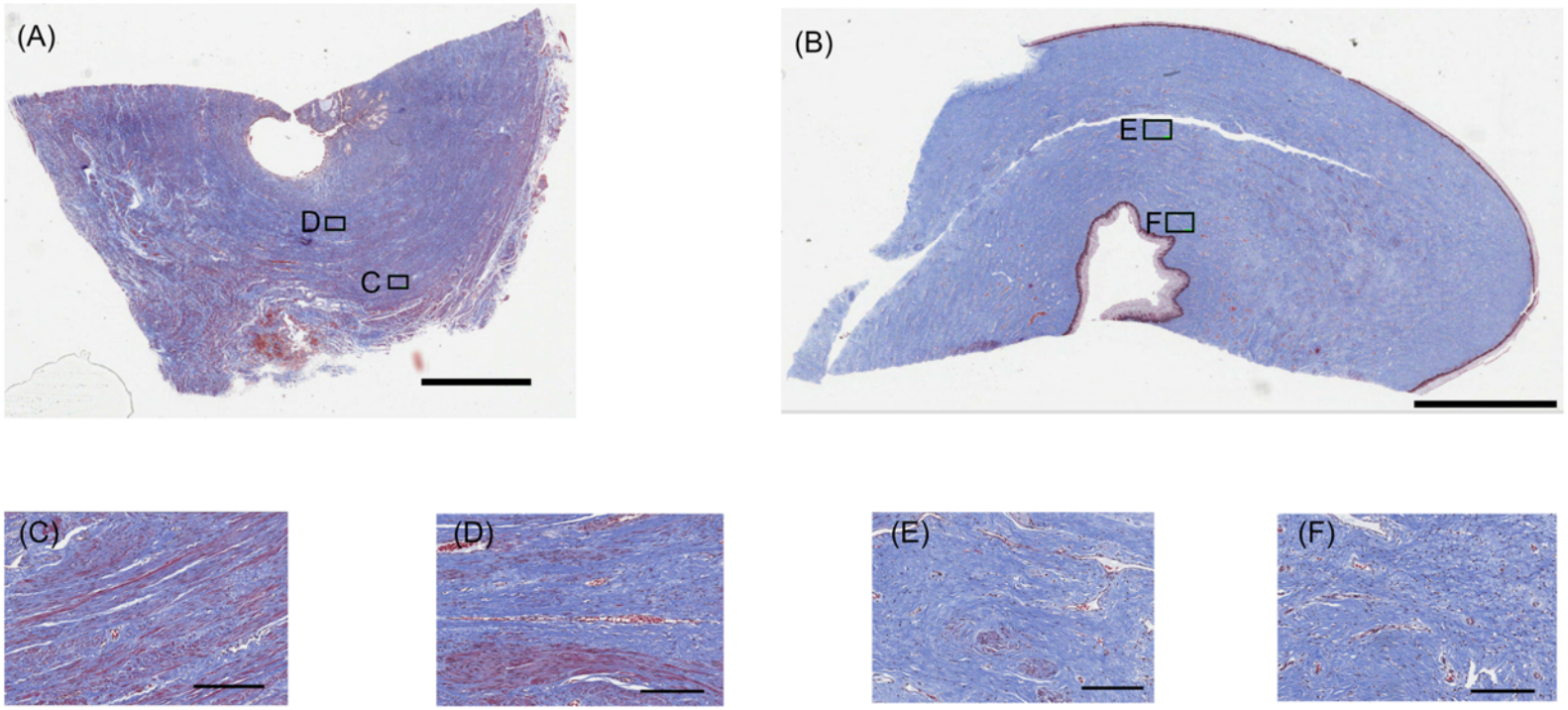

Figure 3.4 MT stained cervical tissue.

Transverse sections from the proximal (A) and distal (B) regions respectively. Boxes represent ROIs at the periphery and mid-stroma that were inspected at greater magnification. Scale bar 5mm. C-F. Selected ROIs at the periphery (C, E) and mid-stroma (D, F) at x5 magnification. Blue = collagen and red = smooth muscle, scale bar 0.2mm. C, D. Positive smooth muscle and collagen staining at the proximal cervix, with encircling smooth muscle regions at the periphery. E, F. Predominantly positive collagen staining observed at the distal cervix with scatterings of smooth muscle cells at vessel walls

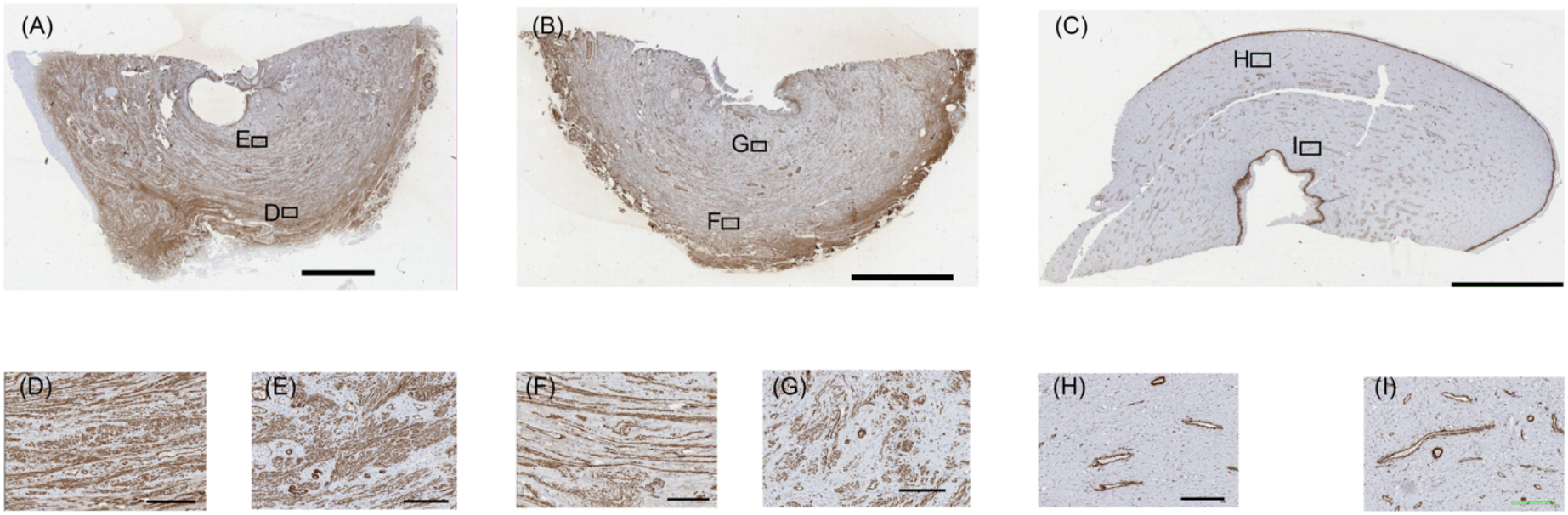

Figure 3.5 α-SMA stained cervical tissue

Transverse sections from the proximal (A), middle (B) and distal (C) regions respectively. A gradient of positive smooth muscle staining is observed, with an increase towards the proximal cervix. Boxes represent ROIs at the periphery and towards the canal that were inspected at greater magnification. Scale bar 5mm. D-I. Selected ROIs at the periphery (D, F, H) and towards the canal (E, G, I) at x5 magnification. Scale bar 0.2mm. D, E. Encircling and longitudinal smooth muscle cells at the periphery and central regions of the proximal cervix. F, G. Encircling and longitudinal fibres are demonstrated. H, I. Positive smooth muscle staining reserved for vessels.

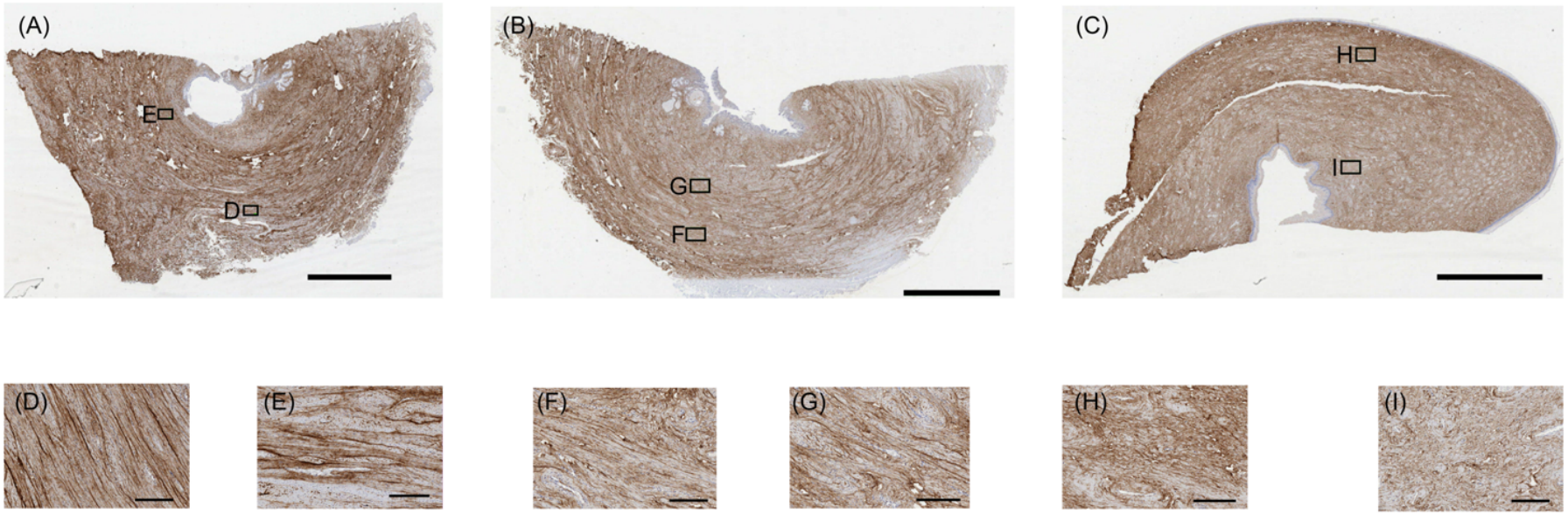

Figure 3.6 Col1α-1 stained cervical tissue

Transverse sections from the proximal (A), middle (B) and distal (C) regions respectively. Positive Col1α-1 staining is consistent throughout the cervix. Boxes represent ROIs at the periphery and mid-stromal region that were inspected at greater magnification. Scale bar 5mm. D-I. Selected ROIs at the periphery (D, F, H) and mid-stroma (E, G, I) at x5 magnification. Scale bar 0.2mm. D-G. Encircling collagen I fibres consistently observed at periphery and mid-stroma in proximal and middle regions of cervix. I, G. Collagen fibres I are randomly scattered at distal cervix.

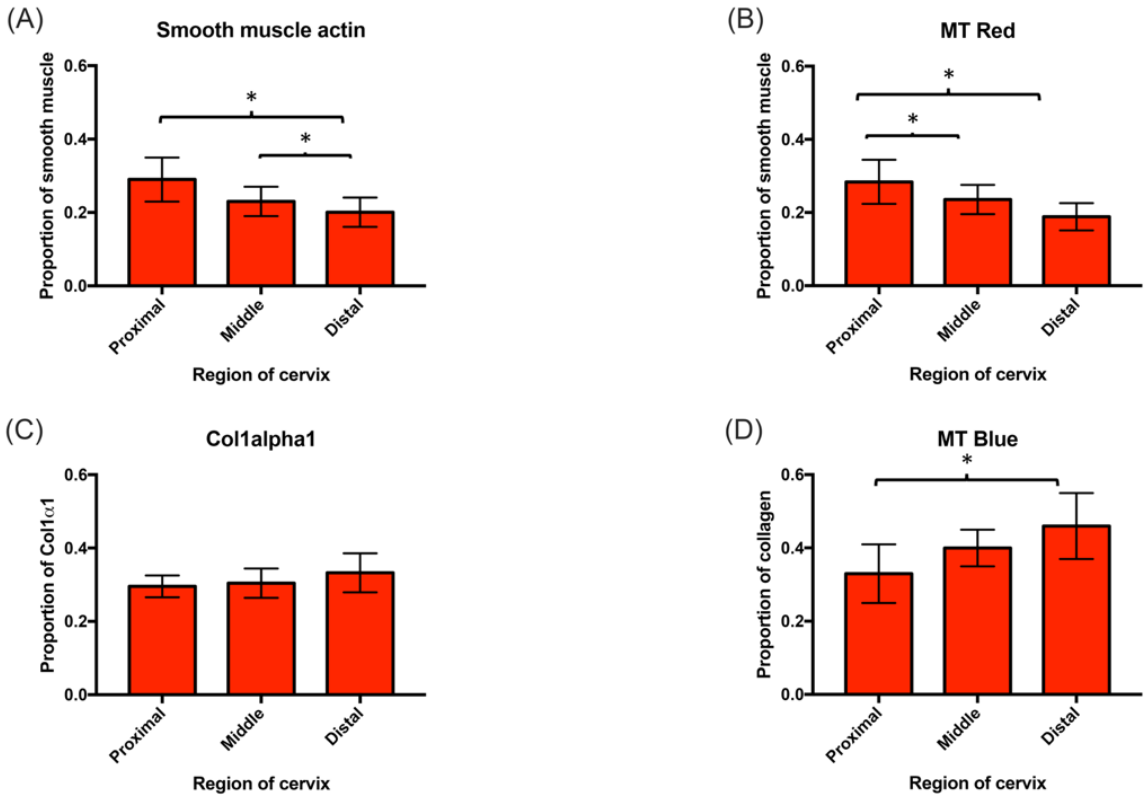

Figure 3.7 Characterisation of smooth muscle and collagen volumes in the proximal, middle and distal regions of the cervix.

Smooth muscle volume as detected using α-SMA (A) and MT (Red; B). Smooth muscle increased towards the proximal cervix, with significant differences between the proximal and distal cervix observed on both of the stains. C, D. Collagen I and total collagen volumes as detected using Col1α-1 (C) and MT (Blue; D). C. Collagen I increased towards the distal cervix, with no significant differences observed. D. The proportion of collagen increased significantly towards the distal cervix.

3.3.1.3 The effect of parity on cervical morphology

The effect of parity was evaluated on both the immunostained and MT-stained samples. Greater CSMC content was demonstrated in all regions in nulliparous women when compared to all parous women in α-SMA-stained sections, and in the proximal and middle regions in MT sections (Fig. 3.8). Further stratification of groups by parity demonstrated the greatest differences were between the nulliparous and para 3 subgroups, with greater CSMC concentration observed in the nulliparous group (Fig. 3.9). Agreement between stains was exhibited in the proximal and middle regions.

Evaluation of Col1α-1-stained sections demonstrated slight differences between nulliparous and parous subgroups. However, pronounced differences were observed in MT sections, particularly at the proximal region. Analysis of stratified groups showed that the greatest differences were between nulliparous and para 3 subgroups, which was most pronounced in proximal and middle regions in MT-stained tissue (Fig, 3.9).

3.3.1.4 The effect of previous caesarean delivery vs. spontaneous vaginal delivery on cervical morphology

The effect of previous caesarean delivery (CD) vs spontaneous vaginal delivery (SVD) was evaluated (Fig. 3.10). CSMC content was demonstrated to be similar across all regions of the cervix. Further, collagen I concentration was similar in the proximal and middle regions of the cervix, with differences only observed in the distal region. Overall collagen content was consistently higher in the CD group across all regions.

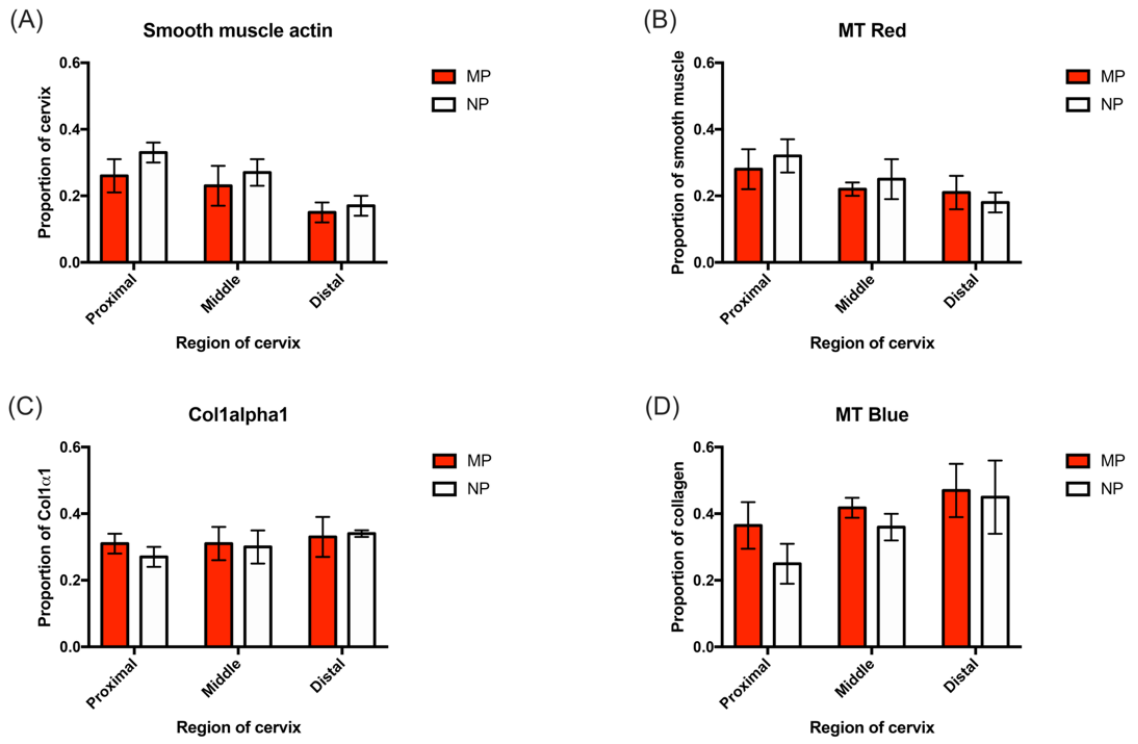

Figure 3.8 Characterisation of smooth muscle and collagen volumes in multiparous (MP) and nulliparous (NP) women in the proximal, middle and distal of the cervix.

Smooth muscle volume as detected using α-SMA (A) and MT (Red; B) A, B. Both markers demonstrated greater smooth muscle concentrations in the proximal and middle cervix in nulliparous samples. C, D. Collagen I and total collagen volumes as detected using Col1α-1 (C) and MT (Blue; D). C. Collagen I concentrations were similar between groups. D. General collagen concentrations increased at the proximal cervix in multiparous samples.

N = 9 (MP); 3 (NP)

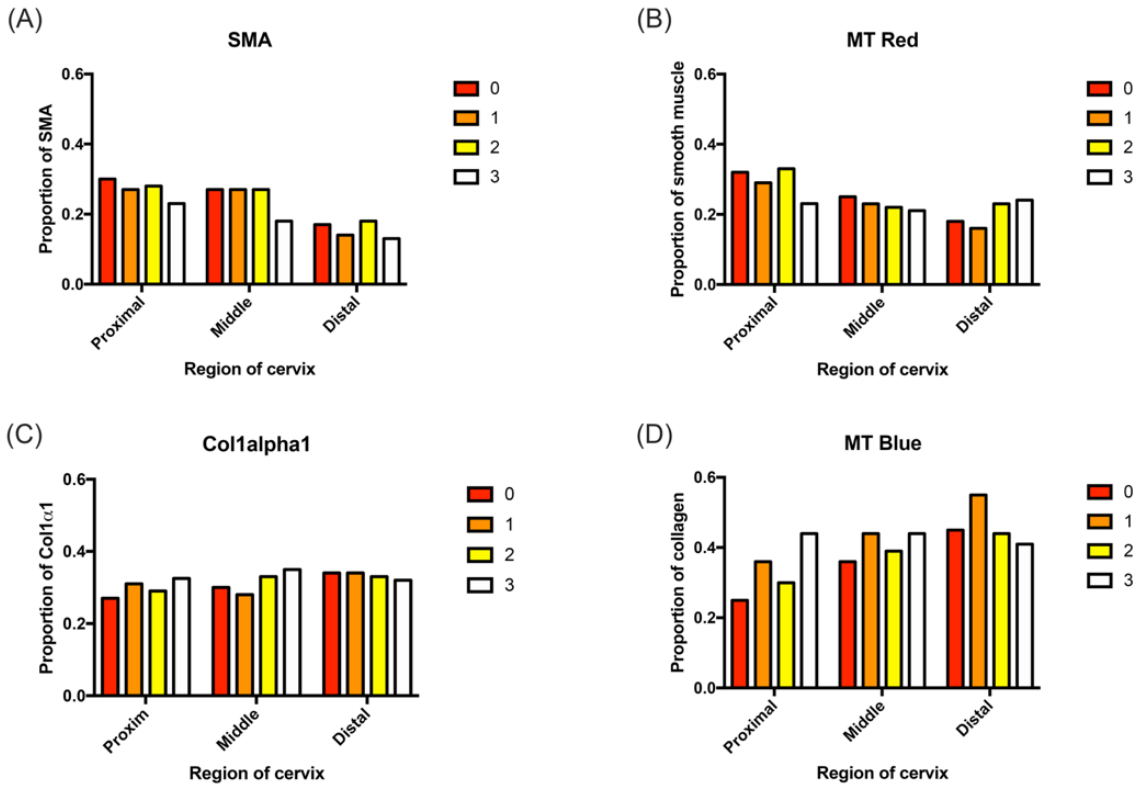

Figure 3.9 Characterisation of smooth muscle and collagen volumes at different grades of parity in the proximal, middle and distal regions of the cervix.

Smooth muscle volume as detected α-SMA (A) and MT (Red; B) A, B. A gradient in smooth muscle concentration is observed at the proximal cervix, with concentrations greatest in the para 0 subgroup. This gradient continued in the middle cervix. C, D. Collagen I and total collagen volumes as detected using Col1α-1 (C) and MT (Blue; D). C. A slight increase in collagen I with increasing parity is observed in proximal and middle regions. D. There is an increase in general collagen concentration between para 0 and para 3 in the proximal cervix.

N = 3 (nulliparous); 2 (para 1); 4 (para 2); 3 (para 3)

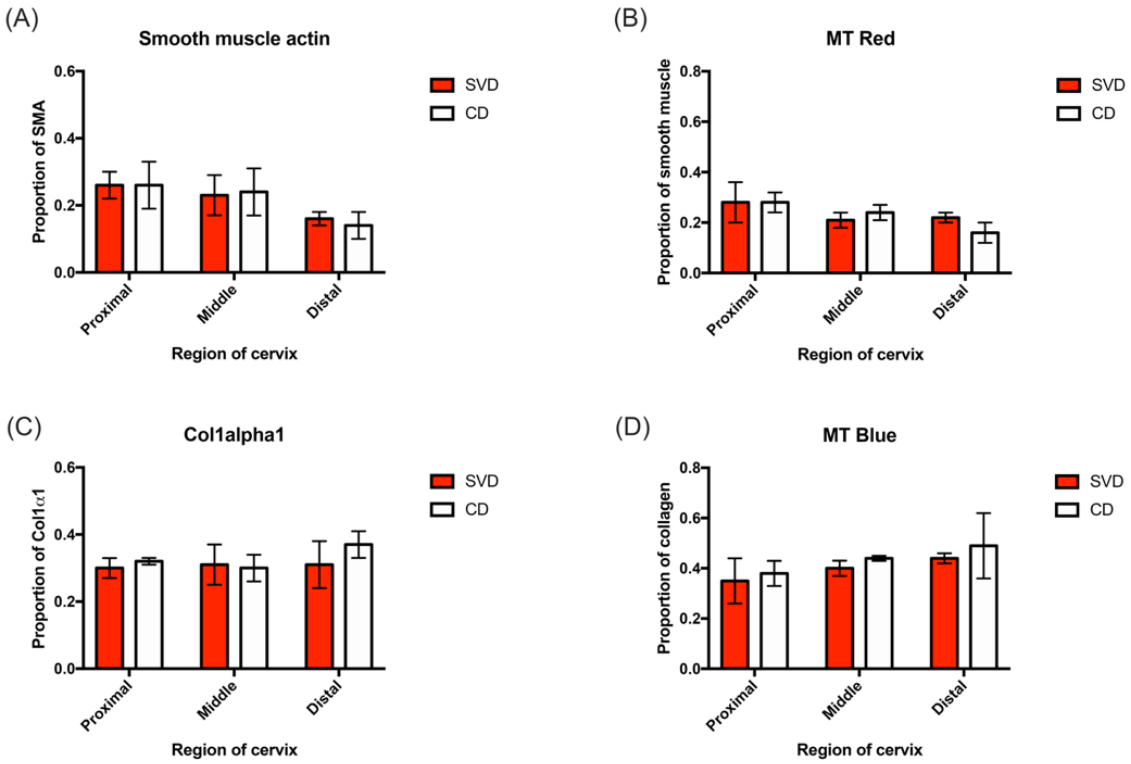

Figure 3.10 Characterisation of smooth muscle content and collagen content in response to SVD vs. CD in the proximal, middle and distal regions of the cervix.

Smooth muscle volume as detected using α-SMA (A) and MT (Red; B) A, B. Smooth muscle content is similar between SVD and CD groups in the proximal and middle regions. At the distal cervix, a greater smooth muscle concentration is demonstrated in the SVD group with MT marker. C, D. Collagen I and total collagen volumes as detected using Col1α-1 (C) and MT (Blue; D). Collagen I content is similar in the proximal and middle regions. A greater collagen I content is observed in the CD group in the distal cervix. D. Greater collagen content is observed in the CD group in all regions of the cervix.

N = 6 (SVD); 3 (CD)

3.3.2 3D histopathological reconstruction of cervical tissue

3.3.2.1 Gross morphology of cervical volumes

Analysis of 3D volumes indicated that clusters of CSMCs were concentrated at the periphery of cervical volumes in the proximal and middle regions of the cervix (Fig. 3.11 A, C). These clusters became less apparent towards the distal cervix, where collagen staining was mainly observed (Fig. 3.11 E). Subsequent clipping of volumes in the sagittal and coronal planes demonstrated that the peripheral cluster of CSMCs progressively decreased towards the mid-stroma, being replaced by dense collagenous regions. These collagenous areas extended towards the cervical canal. Analysis of the cut region of the hemisected samples in the sagittal plane demonstrated a relative paucity of smooth muscle cells in the mid-stroma and regions associated with the canal (Figs 3.11 B, D, F).

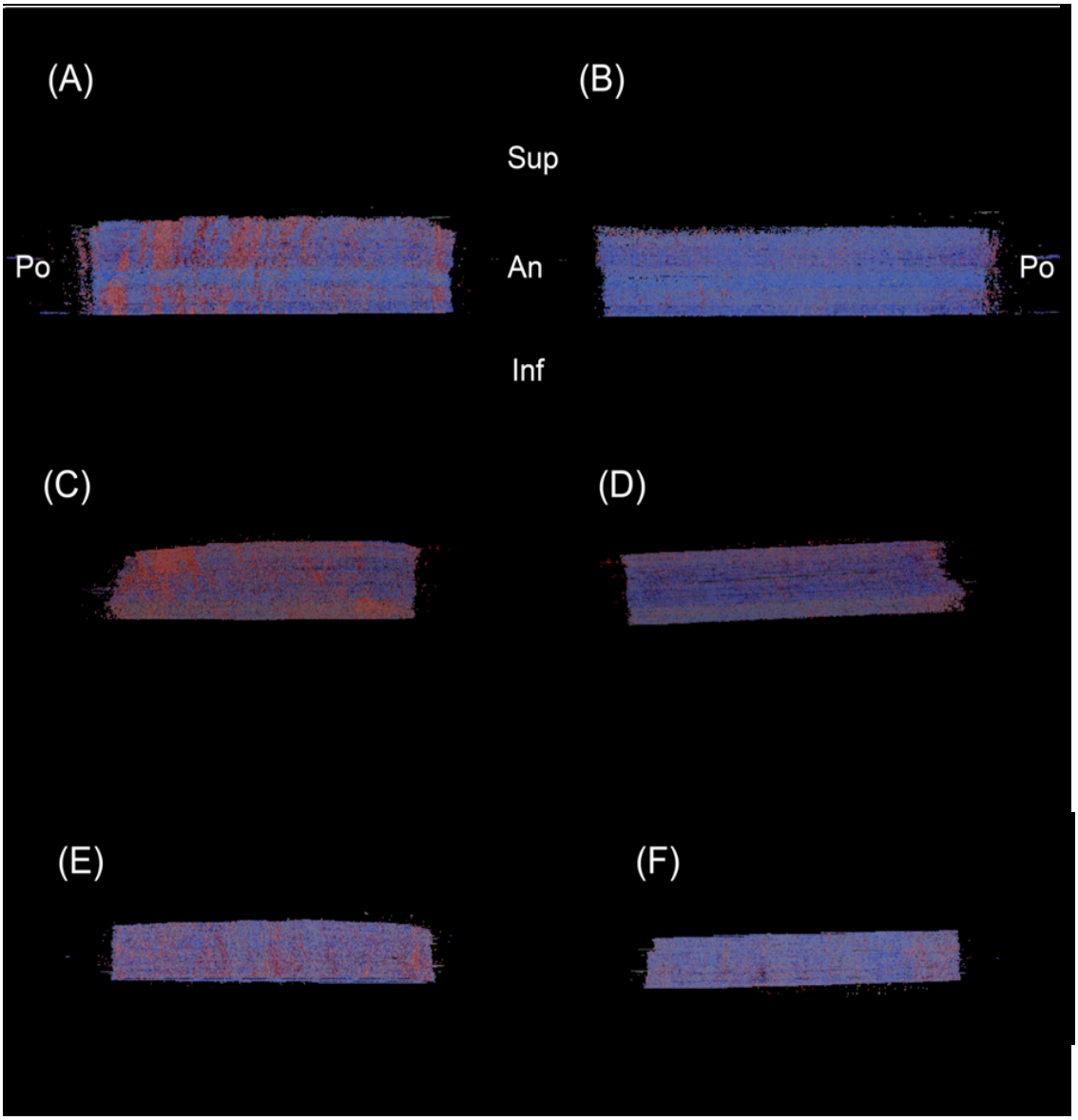

Figure 3.11 3D reconstruction of serial sections from the proximal, middle and distal regions of the cervix.

Peripheral surfaces of the proximal (A), middle (C), and distal (E) regions of the cervix. Prominent collections of smooth muscle cells (red) are present on the peripheral surfaces of the proximal and middle regions. B, D, F. Images demonstrate cut surfaces of cervical hemisections at the proximal (B), middle (D) and distal regions. Comparatively less smooth muscle cells are present at the middle and inner cervical stroma. High concentrations of collagen (blue) fibres are present.

3.4 Discussion

This study used conventional histology and immunostaining methods to investigate CSMC and collagen morphology. Qualitative and quantitative measurements demonstrated regional differences throughout the cervix. Three-dimensional histopathology provided greater insight into the distribution of smooth muscle and collagen in the proximal, middle and distal regions of the cervix.

3.4.1 General morphology

The progressive increase in smooth muscle content towards the internal os is in line with previous histomorphometric measurements (Rorie and Newton, 1967; Oxlund et al., 2010; Vink et al., 2016). Collections of encircling CSMCs were primarily observed at the periphery of the cervix, as confirmed by both 2D and 3D analysis, and progressively decreased towards the middle and inner stromal regions. Longitudinal regions of smooth muscle were observed towards the canal, which is consistent with previous investigations (Vink et al., 2016). The smooth muscle content at the proximal cervix measured in the current study is similar to earlier descriptions of the cervix, but is considerably less than in more recent reports (30% vs. 60%; Danforth, 1947, 1954; Rorie and Newton, 1967; Vink et al., 2016).

These observed differences may have arisen from differences in staining methodologies and quantitative analysis. Specifically, this study used a monoclonal antibody for α-SMA, compared to polyclonal used by Vink et al. (2016). Polyclonal antibodies bind to multiple epitopes on the target protein and may cross react with other proteins. Secondly, images were scanned at a greater magnification (x20 vs. x10). Image resolution will not have a great impact on the quantification of homogenous tissue, but may affect quantification

of detailed tissue regions (e.g. fibres or cells separated by non-stained tissue). Lower image resolution could therefore overestimate the proportion of stained tissue. Finally, the present study used alternative quantification software and analysis tools to examine sections, which may account for the difference in values obtained. We used bespoke probabilistic models with colour normalisation algorithms that were trained on multiple slides. Therefore quantitative evaluation is more robust to staining variation. In contrast, previous methods use colour threshold values for each individual slide, which are subject to greater user bias.

Nevertheless, a relatively large proportion of encircling smooth muscle was seen between the mid-stromal and radial regions of the proximal cervix, which previous authors have proposed to form a sphincter similar to other pelvic smooth muscle sphincters (Vink et al., 2016). However, comparisons of corresponding smooth muscle and collagen-stained sections suggest that CSMCs are interspersed within collagen fibres and do not form well-defined muscular bands like other pelvic sphincters. Other imaging investigations are needed to confirm this observation (Chapter 5).

It is unknown whether the encircling CSMCs possess basal tone in order to resist pressure. *In vivo* and *in vitro* physiological experiments have shown the ability of CSMCs to contract in response to oxytocin (Vink et al., 2016). This observation may be significant during labour where studies have demonstrated electromyographic activity in the latent phase, yet it is not known whether this has a bearing on the ability of the cervix to remain occluded during pregnancy (Pajntar et al., 1998; Rudel and Pajntar, 1999; Vink et al., 2016). Recent evidence suggests that progesterone decreases CSMC contractility, which would suggest either: 1) these cells do not offer structural support during

pregnancy, 2) increasing circulating progesterone acts to progressively relax cervical smooth muscle cells towards term or 3) a different mechanism influences the contraction of these cells (Mourad et al., 2017). It is clear that further discussion and enquiry is needed to determine whether cervical smooth muscle is a contributes to the maintenance of cervical competency.

Encircling collagen I fibres in the proximal and middle cervix were consistently observed throughout the sample. The tensile strength of the cervix is derived from this component of the ECM (Oxlund et al., 2010). Interestingly, although values of collagen I appear to remain constant throughout the cervix (~30%), there is a discrepancy when compared to MT-stained sections, where a progressive decrease in collagen staining is seen towards the proximal cervix. MT marks all collagen fibre types and the disagreement in measurements between markers may provide evidence of increased collagen III in the middle and distal portions. This is significant because collagen III copolymerises with collagen I to form heterotypic fibrils, which decreases the mechanical strength of tissues (Section 1.3; Klinge et al., 2001; Klosterhalfen et al., 2004). This may cause the distal cervix to be a relatively more pliable and may partly account for the accelerated rate of cervical change observed in some women from around 30 weeks of pregnancy (Bergelin and Valentin, 2001). Furthermore, the relative increase of the collagen I/III ratio towards the proximal cervix may provide further support for underlying anatomical architecture to resist the cervical forces concentrated at the internal os (House et al., 2013; Myers et al., 2015).

3.4.2 Parity

Cervical change in response to parity was observed. Smooth muscle content decreased between nulliparous and parous groups, with greatest differences observed between nulliparous and parity three subgroups. Furthermore,

although the proportion of collagen I does not appear to change in response to parity, analysis of MT-stained slides indicates an increase in another collagen subtype following pregnancy. A change in smooth muscle content after gestation has not been reported within the literature and warrants further investigation in a larger cohort. The present report contradicts previous investigations of overall collagen content in response to parity. Previous histomorphometric measurements in a large sample demonstrate a decrease by 1.7% after each successive pregnancy, but an increase 0.5% per year of age (Oxlund et al., 2010). Consequently, the increase in overall collagen content in the present study may be in response to age. However, a change in collagen I/III ratio in response to parity, particularly at the internal os, is not described in the literature and should be investigated in a larger sample.

A decrease in CSMC content and a decrease in the collagen I/III ratio may result in the cervix becoming a more compliant organ following vaginal birth. This may be reflected in early cervical resistance studies, where less force was required to dilate the cervical canal to 8mm in non-pregnant, parous women compared to a nulliparous group (Anthony et al., 1982). Furthermore, altered cervical anatomy may account in part for the shorter duration of labour in different grades of parity (Bergsjø et al., 1979). Changes in cervical morphology in response to parity may have significant implications in subsequent pregnancies in women suspected of having CIn. For example, if a congenital collagen/smooth muscle defect or deficit is responsible for a weak cervix, it may worsen with successive pregnancies in response to changes in the collagen I/III ratio and/or a decrease in CSMC content. This may be the cause of the high incidence of recurrent miscarriages and early PTBs in cases

of suspected CIn, and shorter gestational lengths in successive pregnancies (Sneider et al., 2016).

3.4.3 Mode of delivery

Smooth muscle content was observed to be similar in the SVD and CD subgroups. Collagen I did not change, but analysis of MT-stained slides shows possible increase in collagen III in the CD group. No evidence of scarring was evident. Cervical change in the present study may be more likely a response to age, rather than mode of delivery.

3.4.4 Limitations

The data were obtained from a small sample who received conservative management and subsequent hysterectomy for benign gynaecologic pathology. The effect of gonadotropin releasing hormone (GnRH) analogues on cervical microarchitecture is not known, as clinicians primarily focus on their effects on leiomyomas and the uterine endometrium in the diagnostic process. It is possible that treatment with GnRH analogues may alter the microanatomical structure of the cervix. However, as a common microarchitecture was observed between women who received GnRH analogues and those who received other treatment, it is likely that the effects of disrupting the hypothalamic-pituitary axis in this way had minimal effect on cervical microarchitecture. Secondly, disparities between obtained and previously reported values demonstrate the challenges of stain quantification. The present study used two smooth muscle stains that produced similar results, which may provide some validation for the quantification method used. Nevertheless, similar patterns of CSMC morphology were found, and so similar conclusions could be drawn.

3.4.5 Conclusion

This work has identified that the cervix possesses a system of encircling smooth muscle and collagen I fibres that become prominent towards the internal os, which may provide the proximal cervix the mechanical strength to resist gestation forces. Furthermore, this study has identified changes in cervical morphology in response to parity. Specifically, a decrease in smooth muscle content and an increase in the collagen I/III ratio at the internal os was observed, though further study in a larger sample and analysis using markers specific to collagen III is needed to confirm. Yet, this may provide an account for the shorter duration of labour in successive pregnancies, and more importantly, the shorter gestational lengths in multigravid women with a suspected cervical defect. These observations encourage the re-examination of the role of the internal os during pregnancy and prompt the development of high resolution clinical imaging to examine this region in clinical practice.

Chapter 4 Diffusion-tensor Imaging of the Human Uterine Cervix

4.1 Introduction

The composition of the cervical stroma is the principle determinant of the biomechanical strength of the tissue. During pregnancy, alterations in the extracellular matrix impact cervical architecture, causing the cervix to progressively remodel in preparation for a vaginal delivery (Granström et al., 1991; Osmers et al., 1993; El Maradny et al., 1997; Ludmir and Sehdev, 2000; Straach et al., 2005; House, Kaplan et al., 2009). As described in chapter 3, the cervical microanatomy is composed of prominent encircling CSMC and collagen I fibres, which likely gives this region structural integrity to resist intrauterine forces centred at the internal os. Abnormal anatomy may result in funnelling of the internal os and early cervical shortening, as observed on TVUS (Fig. 1.7 & 1.9). However, changes in the microanatomy, as a consequence of cervical remodelling, likely occur long before cervical funnelling. Methods to accurately study the microanatomy of the proximal cervix are typically invasive and are therefore not suitable in a clinical setting. Characterising cervical ultrastructure using high-resolution imaging techniques has the potential to identify cervical change caused by alterations in microanatomy.

Fibre ultrastructure has been studied using X-ray diffraction (Aspden, 1988), DT MRI (Weiss et al., 2006; Fujimoto et al., 2013), second harmonic generation (SHG; Reusch et al., 2013) and OCT (Gan et al., 2015; Yao et al., 2016). Overall, the fibre network is reported to be anisotropic (i.e., directional), with clearly defined radial regions extending along the length of the cervix. The

number and arrangement of the reported regions are varied, yet each imaging modality has highlighted a circumferential band of fibres that encircle the cervical canal, as observed in Chapter 3. These bands of encircling fibres likely resist forces associated with cervical dilation.

However, analysing the cervix using non-invasive imaging strategies is challenging. Previous accounts have been mostly derived from small volumes of tissue, as optical imaging and x-ray diffraction is limited by tissue penetration and the field of view (FOV). In contrast, DT MRI provides the opportunity to image large tissue volumes. The technique measures the relative diffusion coefficient of hydrogen protons at an intravoxel level when diffusion-sensitising gradients are applied, with diffusion occurring more easily parallel to underlying directional structures (Basser et al., 1994; Le Bihan et al., 2001; Mori, 2007). Subsequent fibre-tracking offers insight into tissue ultrastructure by predicting fibre directionality based on the direction of greatest diffusion, enabling identification and visualisation of whole-sample tracts (Bammer et al., 2003; Mori, 2007; Yeh et al., 2013). Diffusion-tensor MRI has been extensively used to visualise tracts in human models, including neuronal pathways in the human brainstem, the developing human fetal heart, and the human uterus, with qualitative agreement confirmed by subsequent histological investigation (Weiss et al., 2006; Aggarwal et al., 2013; Mekkaoui et al., 2013).

This study used DT MRI and associated fibre tracking methods to further characterise cervical structure. The aim was to determine whether regional differences existed as indicated by measurements of diffusion, tract orientation and tract volume.

4.2 Methods

Ethical approval was granted by the Yorkshire and Humber Regional Ethical Committee (reference number 15/YH/0111). Eight non-pregnant, premenopausal women undergoing TAH or VH for benign pathology were consented. No participants had a history of PTB, CIn, or cervical excisional surgery (Table 4.1).

4.2.1 Image Acquisition

Cervix samples were placed into a polytetrafluorethylene cylindrical tube (Cole-Palmer, Illinois, USA) and immersed in Fomblin (Sigma-Aldrich, Missouri, USA). Diffusion images were acquired on a Bruker Biospin (Ettlingen, Germany) 9.4 T vertical NMR/S scanner with a 22 mm diameter imaging coil. A 3D diffusion-weighted spin-echo sequence was applied at 20°C with the following parameters: echo-time = 15-60 ms, repetition time = 500-1000 ms, b = 1148 s/mm^2, averages 3-8, a matrix size = 256 × 256 × 256, slice thickness = 0.2 – 0.25 mm and an in-plane resolution = 0.2 – 0.25 mm. In each scan diffusion-weighted images were obtained in six directions, with an average scan time of 55 hours 24 minutes. All data were analysed in DSI Studio (http://dsi-studio.labsolver.org; Yeh et al., 2013).

Table 4.1 Patient demographics for cervical samples

Patient number	Age (years)	Parity	Obstetric History	Diagnosis	Pre-hysterectomy interventions/investigations
1	49	3	3 x NVD	Fibroid uterus	Hysteroscopy
					GnRH analogue
					Progestin
2	43	1	1 x CD	Fibroid uterus	GnRH analogue
3	46	3	3 x NVD	Stage III cystocele	Progestin
				Stage III uterovaginal descent	Physiotherapy management
4	42	2	2 x NVD	Endometriosis	Hysteroscopy
				Fibroid uterus	Endometrial ablation
					GnRH analogue
5	47	2	2 x NVD	Uterine prolapse	Physiotherapy management
6	36	0	N/A	Endometriosis	GnRH analogue
7	45	3	3 x NVD	Fibroid uterus	Tranexamic acid
8	44	0	N/A	Fibroid uterus	GnRH analogue

NVD- Normal vaginal delivery GnRH- Gonadotropin releasing hormone CD- Caesarian delivery N/A- Not applicable

4.2.2 Diffusion Measurements

Diffusion-tensor MRI yields values that infer tissue architecture by measuring the intrinsic properties of the diffusion of water. In unstructured space, diffusion occurs randomly in all directions, which is described as isotropic diffusion. Anisotropic diffusion is a consequence of diffusion being restricted by ordered structures, which include cellular membranes and extracellular components in biological tissue. Fractional anisotropy (FA) quantifies the deviation from isotropic diffusion on a continuum from 0 (isotropic/equal in all directions) to 1 (anisotropic/directionally dependent; Pfefferbaum et al., 2000; Fig. 4.1), and so provides a quantitative measurement that infers tissue organisation. FA was calculated as follows:

Equation 4.1 Calculation of FA

$$FA = \sqrt{\frac{3}{2} \cdot \frac{(\lambda_1 - \langle\lambda\rangle)^2 + (\lambda_2 - \langle\lambda\rangle)^2 + (\lambda_3 - \langle\lambda\rangle)^2}{{\lambda_1}^2 + {\lambda_2}^2 + {\lambda_3}^2}}$$

$$\langle\lambda\rangle = \frac{\lambda_1 + \lambda_2 + \lambda_3}{3}$$

where λ_1, λ_2, λ_3 correspond to the primary, secondary and tertiary eigenvalues (i.e., direction of diffusion) of the diffusion tensor, respectively (Pervolaraki et al., 2013).

Figure 4.1 A schematic representation of fractional anisotropy

Fractional anisotropy is a value that reflects the deviation from isotropic diffusion from 0 (equal in all directions) to 1 (directionally dependent).

FA, however, does not provide information for why anisotropy changes in biological tissues. Specifically, an increase in the primary diffusion direction or a decrease in either the secondary or tertiary diffusion directions will result in greater anisotropy. Therefore, the primary, secondary and tertiary diffusion directions were extracted and calculated to determine whether changes in FA were being driven predominantly by diffusion in the axial or radial directions. Axial diffusion (AD) was represented by the primary eigenvalue and radial diffusion (RD) was calculated as follows:

Equation 4.2 Calculation of RD

$$RD = \frac{(\lambda_2 + \lambda_3)}{2}$$

The magnitude of diffusion, expressed as the apparent diffusion coefficient (ADC), is a directionally independent measure. ADC measurements provide an indication of the complexity of biological tissue, as cellular components hinder

the diffusion process (Fig. 4.2). Consequently, the magnitude of diffusion reflects tract density and was calculated as follows:

Equation 4.3 Calculation of ADC

$$S(b) = S(0) * \exp(-b * ADC)$$

where $S(0)$ and $S(b)$ are the signal intensities of each voxel obtained with the b-values 0 and 1148 s/mm^2 respectively (Pervolaraki et al., 2017). Larger ADC values correspond to decreased tract density.

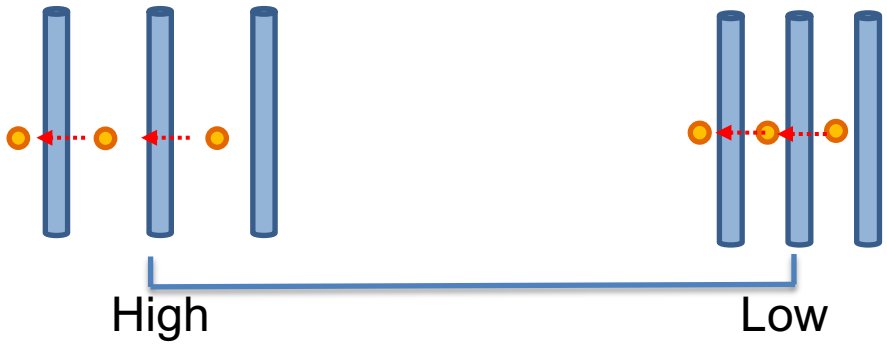

Figure 4.2 A schematic representation of ADC

Diffusion is restricted by the complexity of the underlying tissue structure. Dense cellular or extracellular structures hinder the diffusion process resulting in a low ADC output. ADC will progressively increase as tissues become less dense.

In this study, each image of the cervix was divided into five portions with respect to the length of each sample and the upper (proximal), middle and lower (distal) portions were selected for analysis. Intra-sample differences of quantitative values were determined for proximal, middle and distal transverse ROI. Relationships between ROI and axial and radial diffusion were sought to

determine whether changes in FA were being driven by diffusion in the axial or radial directions.

4.2.3 Fibre-tracking methods

Fibre tracking is a 3D modelling technique used to represent fibres in biological tissues following DT-MRI. Two techniques can be employed to visualise fibres: probabilistic and deterministic methods. Probabilistic fibre-tracking serves to explore all possible connections between regions of a tissue sample. The method allows the user to determine the distribution of all connections, yet provides a low percentage of valid connections, as all potential fibres are computed. By comparison, deterministic fibre tracking estimates the most likely route of a fibre pathway by identifying the principal diffusion direction and filtering out noisy fibres based on preselected criteria.

In this instance, a deterministic fibre tracking algorithm was applied to identify, visualise, and quantify whole-sample tracts within each cervix (Yeh et al., 2013), as fibres identified in this way are the most likely to be anatomically linked. Fibres were visualised if FA was greater than 0.2, if the principal diffusion direction diverged by less than 35° compared to that of the previous voxel, and if the length of the fibre was greater than 10mm (Fujimoto et al., 2013).

Circumferential tracts in the proximal, middle and distal regions of each cervix were determined by segmenting a ROI in the mid-sagittal plane in each of the regions. Tracts were visualised if they passed through this ROI. Total tract volume (TV; mm^3) was calculated in DSI Studio for each of the three regions.

4.2.4 Histological validation methods

Three DTI volumes were compared with corresponding immunostained sections from the proximal, middle and distal regions of each cervix. Transverse cervical blocks were prepared using the method described in Chapter three. Five micrometre sections were obtained using a Leica rotary microtome RM2235 (Biosystems, Switzerland) that provided a real-time sectioning count. Every fifth section was mounted, which created a 25μm gap between each obtained section. Sections were stained with H & E and MT stains, as well as primary antibodies for α-SMA and Col1α-1 (Chapter 2).

The three primary eigenvector files (i.e. x, y and z directions) were extracted from the DTI raw data file and combined into one data file (see appendix for a an account of procedures and C code). The code transforms the coordinates into RGB colour channels and prints the new values in raster scan order (i.e x, y, z, x, y, z). The new data file was uploaded to MIM for analysis. Two-dimensional histological sections were manually aligned to the corresponding plane in the DTI volumetric data. This was achieved as the approximate location of each tissue section was recorded in the z axis in the slide preparation process. Two-dimensional in-plane registration was then performed to compensate for deformations in the slide preparation process i.e. shrinkage as a consequence of the fixative process (Fig. 4.3).

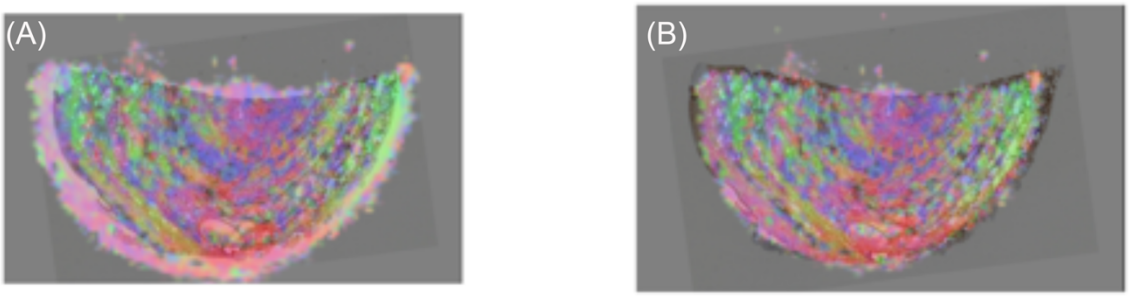

Figure 4.3 Manual alignment and two-dimensional in plane registration of histology section to corresponding plane in the DTI volumetric dataset.

Volumetric data were superimposed onto corresponding histological section. Manual alignment was achieved by inputting location of the histological section in the z direction. A. Histological section is smaller compared to corresponding DTI section due to the fixative processes associated with histological tissue processing. B. Two-dimensional in-plane registration was performed to correct for fixative processes.

4.2.5 Statistics

In all instances, quantitative diffusion data were not normally distributed, as assessed by the Kolmogorov-Smirnov test ($p < 0.05$). Kruskal-Wallis tests were therefore conducted to determine if there were intra-sample differences in FA and ADC between the proximal, middle and distal cervical regions. Distributions of diffusion measurements were not similar, based on visual inspections of boxplots, and so Ranked Sums tests were used. Subsequent pairwise comparisons were performed using Dunn's procedure when appropriate (Dunn, 1964).

Eta squared (η^2) was used to calculate effect size. The output of η^2 indicated the percentage variance in the dependent variable that was explained by the independent variable. η^2 was calculated as follows:

Equation 4.4 Calculation of η^2

$$\eta^2 = \left[\left(\frac{x^2}{N-1}\right)\right] \times 100$$

where X^2 is the Chi-square value of the Kruskal-Wallis test and N is the total number of cases.

Relationships between quantitative measurements of diffusion and ROI were determined by Spearman's rank order correlation when a monotonic relationship was observed (i.e. as the value of one variable increases, so does the value of the other variable, or vice-versa).

Total tract volume measurements were not normally distributed as assessed using the Shapiro-Wilk test. Distributions of diffusion measurements were not similar based on visual inspections of boxplots and so Kruskal-Wallis Ranked Sums tests were used. Subsequent pairwise comparisons were performed using Dunn's procedure when appropriate (Dunn, 1964)

Data were presented as mean ± standard deviation with a statistical significance accepted at $p < 0.05$. All statistical analyses were performed using SPSS software v.23.0 (SPSS, Inc., Chicago, IL).

4.3 Results

4.3.1 Vector maps

Analysis of colour-coded vector maps demonstrated a microarchitecture common to each cervix sample. In slices orthogonal to the long axis, an inner longitudinal layer and an outer circular layer were consistently identified at the proximal and middle portions of the cervix (Fig. 4.4 A and B), though both were less evident towards the distal cervix (Fig. 4.4 C and D).

4.3.2 Vector maps

The randomised fibre-tracking reconstruction of approximately 5,000 fibres further confirmed inner longitudinal tracts extending from the proximal to the middle cervix parallel to the cervical canal, and outer encircling tracts (Fig. 4.5 A and E). Segmentation of the encircling tracts in the proximal, middle and distal cervix showed that this system of fibres became more prominent towards the proximal cervix (proximal = 176 ± 145 mm^3, middle = 106 ± 120 mm^3, distal = 9 ± 20 mm^3; Fig.4.5 & 4.6).

Measurements in the three regions were found to be significantly different (χ^2 (3) = 12.118, $p < 0.02$). *Post hoc* analysis demonstrated a significant increase in tract volume (mm^3) from the distal (5.88) to proximal (18.00; $p = 0.002$) regions. No significant differences were observed for the remaining regions.

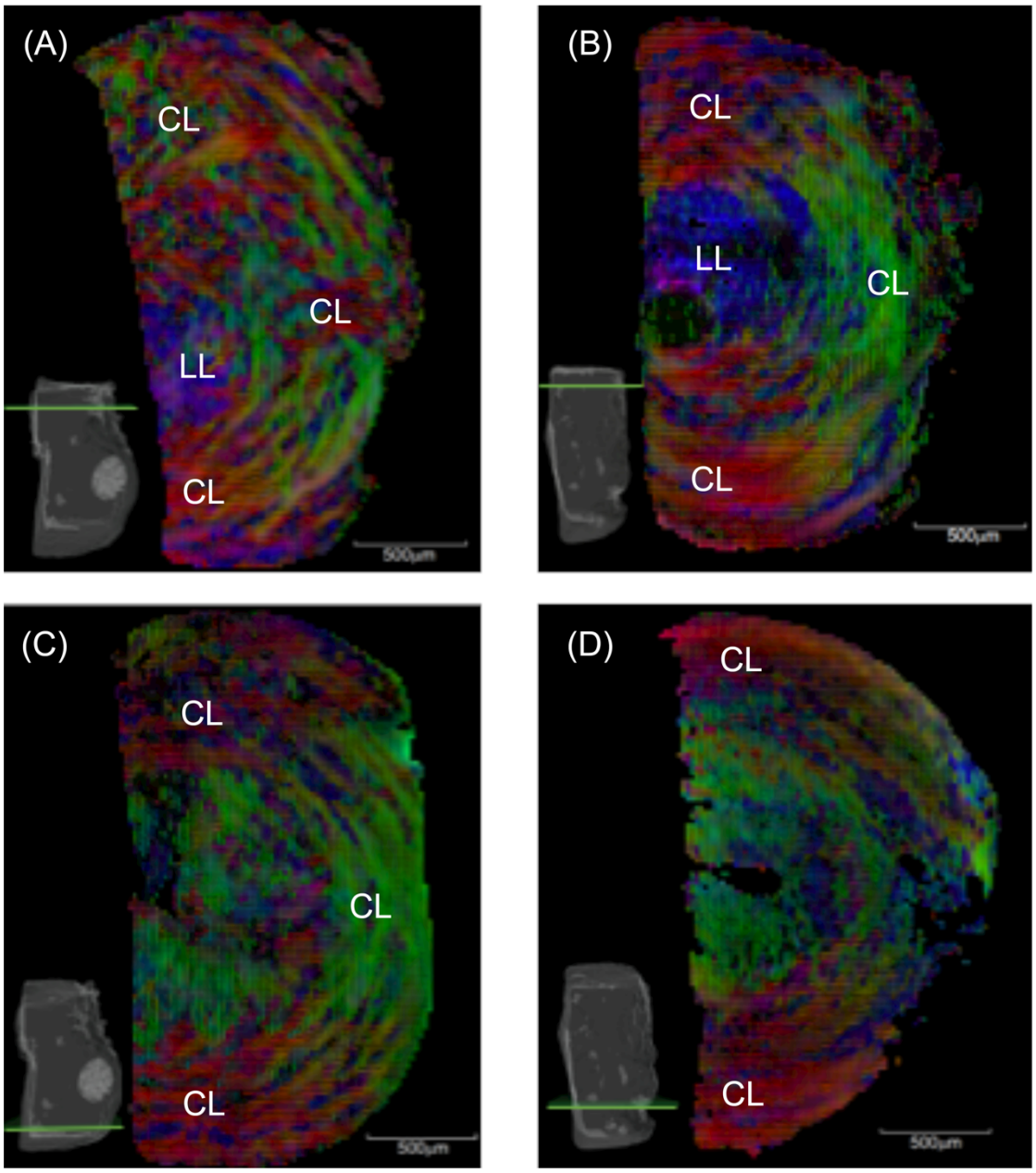

Figure 4.4 Colour vector maps depicting principle diffusion directions on slices orthogonal to the long axis at proximal (A, B,) and corresponding distal (D, E,) regions.

Colours reflect the orientation of the principle diffusion vector with respect to Cartesian axes system (x=red, y=green, z=blue). Slice positions are indicated in bottom corners by the green cut plane. A longitudinal layer (LL) and circular layer (CL) are identifiable in the proximal region of both samples (A, B). The outer CL extends towards the distal region in both samples, yet the LL is less evident in the distal region (C, D).

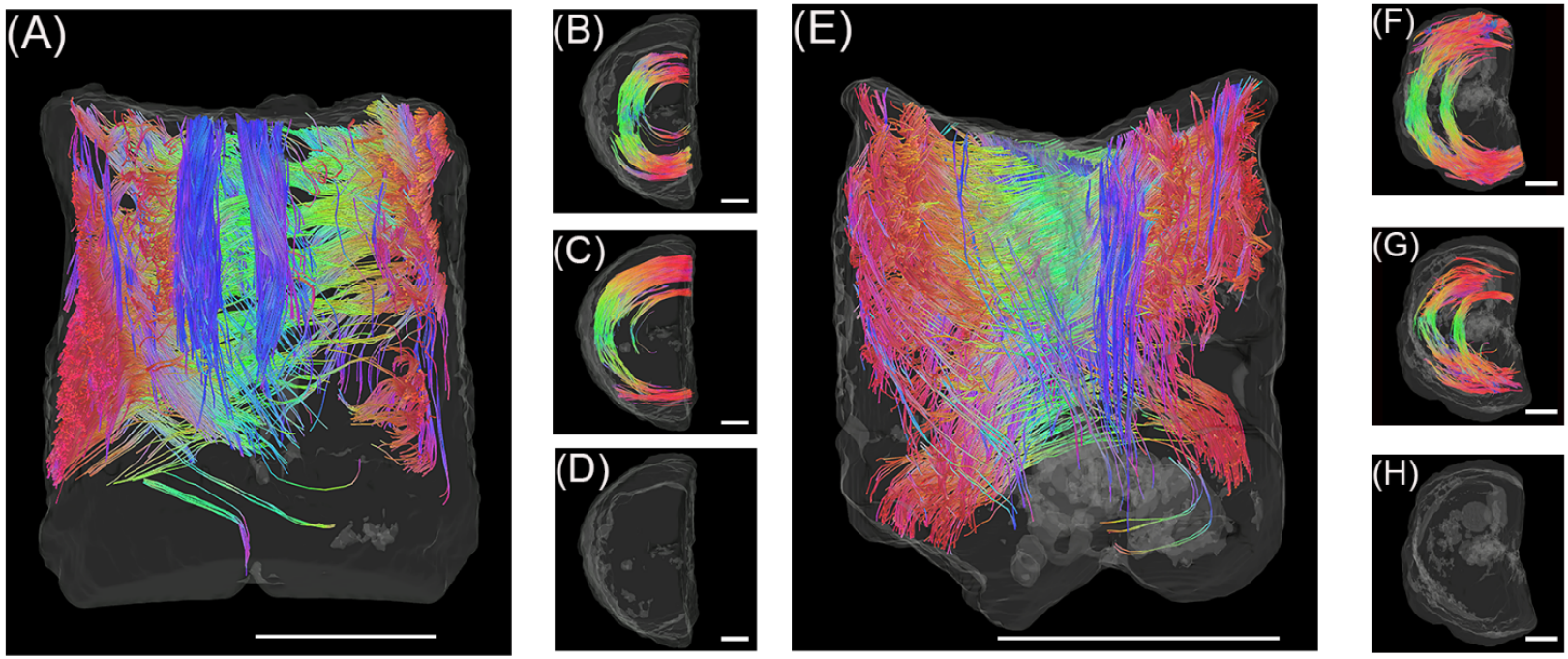

Figure 4.5 Three-dimensional tractography computed using a deterministic fibre-tracking algorithm.

The surface of the cervix is indicated by the grey scale border. Colours reflect orientation of fibres (x=red, y=green, z=blue). A, E: Images display midline surfaces of hemisected samples four (A) and five (E; scale bar = 1 cm). Both samples demonstrate two ROIs: inner longitudinal (blue) and outer circumferential (red, green). Corresponding transverse cross-sections depict encircling fibres at the respective proximal (B, F) middle (C, G) and distal (D, H) regions of each sample (scale bar = 500 μm).

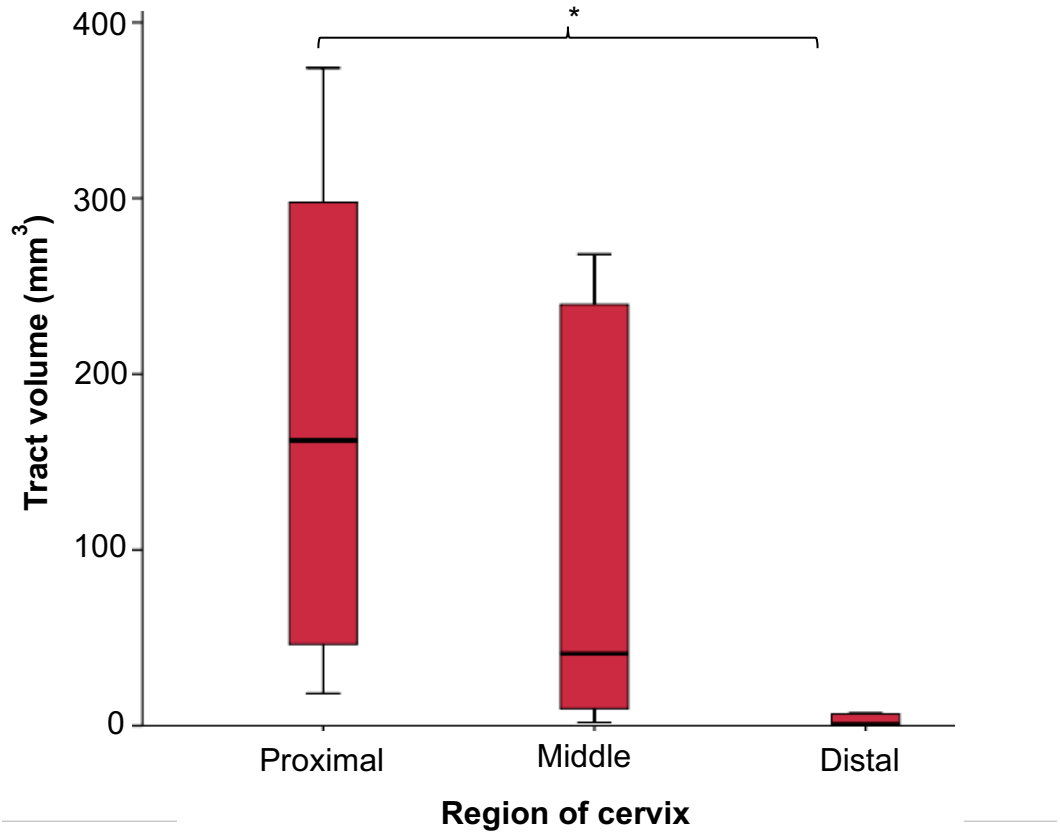

Figure 4.6 Volume of circumferential fibres increased towards the proximal region of the cervix.

*Indicates significant difference relative to distal region of cervix, $P < 0.05$ (Kruskall-Wallis)

4.3.3 Analysis of tissue structure

Intra-sample comparisons of FA demonstrated that regional measurements were significantly different ($p < 0.0005$) following Kruskal-Wallis analysis (Table 4.2; Fig. 4.7). The proportion of variability in FA accounted for by region ranged from 4% – 29%. In all instances, pairwise comparisons demonstrated significant differences ($p < 0.0005$) between regions. Mean FA values were largest in the proximal region in all samples and values progressively decreased towards the distal region in seven samples, indicating that tract organisation increased towards the proximal cervix. Similarly, Kruskal-Wallis analysis demonstrated ADC measurements were significantly different between regions ($p < 0.0005$), with the proportion of variability in ADC accounted for by region ranging 4% - 30% (Table 4.3; Fig. 4.8). Pairwise comparisons demonstrated significant differences ($p < 0.0005$) between all regions. Measurements of ADC were found to be lower in the proximal portion and progressively increased towards the distal region in seven of the samples, indicating that tract density increased towards the proximal cervix. In the remaining sample, the ADC value was lowest in the middle region, followed by the proximal and distal regions.

Table 4.2 Intra-sample comparisons of FA

Sample	Region	No. of Voxels	Mean (±SD)	X^2	η^2
1	Proximal	566981	0.28 (.09)	86028.161	0.12
	Middle		0.21 (.10)		
	Distal		0.18 (.07)		
2	Proximal	172420	0.27 (.12)	22615.848	0.13
	Middle		0.19 (.10)		
	Distal		0.20 (.10)		
3	Proximal	890184	0.48 (.18)	83976.474	0.09
	Middle		0.38 (.17)		
	Distal		0.34 (.15)		
4	Proximal	621712	0.26 (.11)	17818.661	0.02
	Midde		0.25 (.10)		
	Distal		0.22 (.11)		
5	Proximal	928268	0.39 (.16)	150754.068	0.39
	Middle		0.31 (.14)		
	Distal		0.21 (.14)		
6	Proximal	12958	0.34 (.19)	2303.936	0.002
	Middle		0.21 (.15)		
	Distal		0.19 (.13)		
7	Proximal	14597	0.20 (.10)	2008.283	0.15
	Middle		0.15 (.09)		
	Distal		0.12 (.05)		
8	Proximal	652997	0.32 (.16)	43055.686	0.07
	Middle		0.26 (.16)		
	Distal		0.21 (.12)		

Table 4.3 3 Intra-sample comparisons of ADC (x10-3 mm2/s)

Sample	Region	Total no. of Voxels	Mean (±SD)	X^2	η^2
1	Proximal	566981	0.77 (0.12)	50882.938	0.08
	Middle		0.87 (0.23)		
	Distal		0.88 (0.16)		
2	Proximal	172420	0.72 (0.22)	18528.390	0.11
	Middle		0.81 (0.22)		
	Distal		0.89 (0.21)		
3	Proximal	890184	0.56 (0.20)	93450.008	0.1
	Middle		0.59 (0.20)		
	Distal		0.70 (0.20)		
4	Proximal	621712	0.77 (0.23)	58766.115	0.09
	Middle		0.75 (0.20)		
	Distal		0.87 (0.20)		
5	Proximal	928268	0.57 (0.18)	195267.162	0.21
	Middle		0.64 (0.24)		
	Distal		0.92 (0.34)		
6	Proximal	12958	0.81 (0.38)	3557.017	0.27
	Middle		1.07 (0.38)		
	Distal		1.43 (0.44)		
7	Proximal	14597	1.01 (0.23)	4350.022	0.30
	Middle		1.26 (0.31)		
	Distal		1.38 (0.20)		
8	Proximal	652177	0.80 (.03)	44083.842	0.07
	Middle		0.73 (.24)		
	Distal		0.92 (.33)		

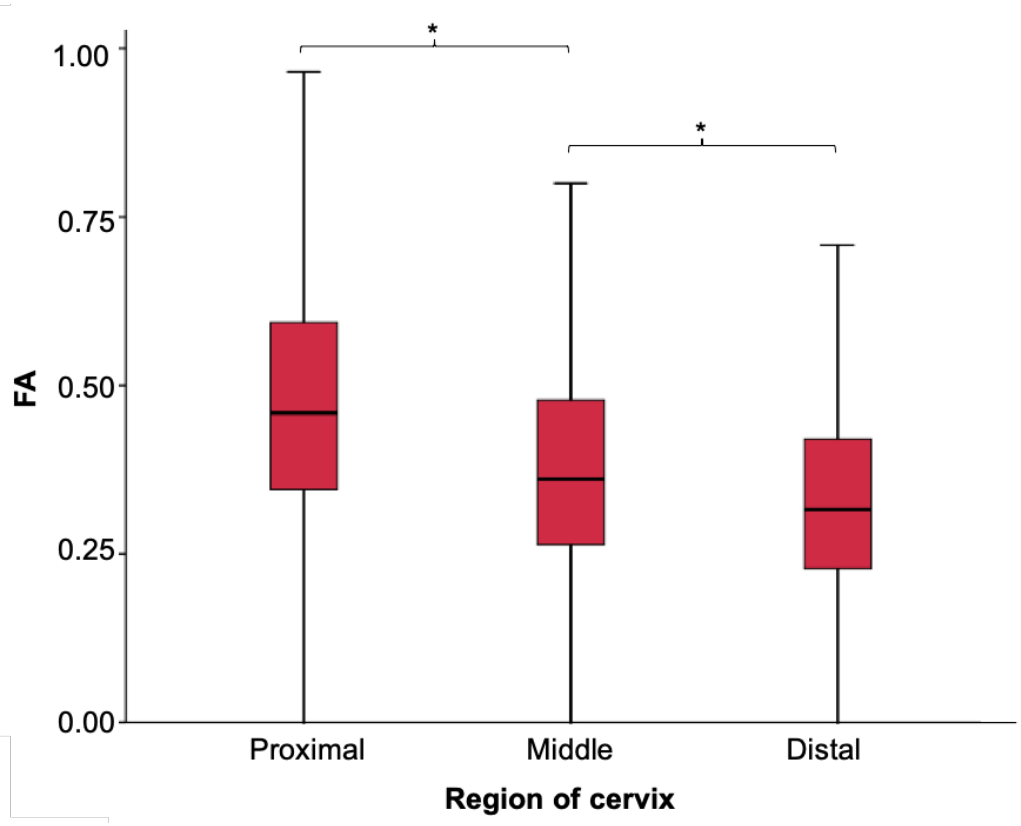

Figure 4.7 Regional FA values recorded in a representative sample.

FA increased towards proximal region of cervix, indicating that tract alignment increased towards the internal os. The trend observed was observed in seven samples. * *p<0.0005.*

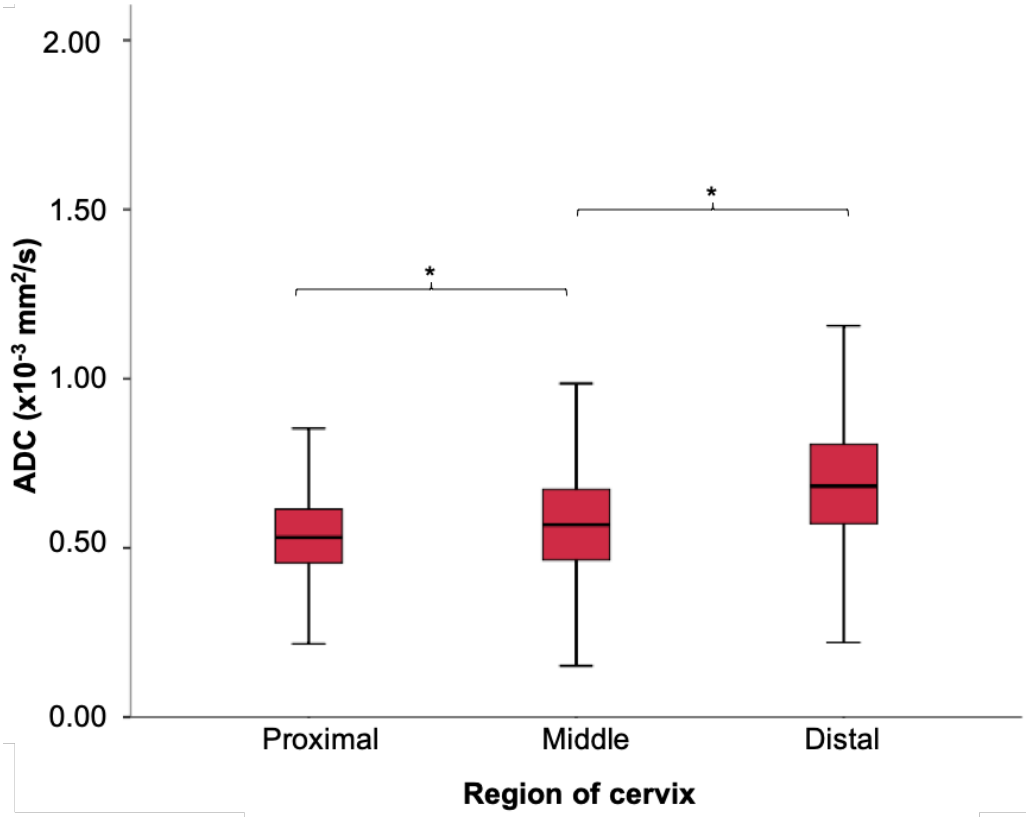

Figure 4.8 Regional ADC values recorded in a representative sample.

ADC decreased towards proximal region of cervix, indicating that tract density increased towards the internal os. The trend was observed in seven samples. * *p<0.0005.*

4.3.4 Changes in fractional anisotropy

Axial and radial diffusion measurements were extracted to determine what was driving the changes in FA throughout the cervix. Statistical analysis was appropriate in 4 and 6 samples for AD and RD respectively, with each relationship being significant (Table 4.4; $p < 0.0005$). Analysis of coefficient values demonstrated weak to fairly strong positive correlations in all analyses, with RD demonstrating a stronger correlation in all comparable examples. Consequently, the progressive increase in FA towards the proximal cervix is being predominantly driven by diffusion restriction in the radial directions. This suggests that fibre density and/or diameter is increasing towards the internal os.

Table 4.4 Rho (r_s) values for ROI and AD or RD

Sample	AD	RD
1	-	0.384
2	0.219	0.367
3	-	0.352
4	-	-
5	0.29	0.475
6	0.473	0.536
7	0.513	0.543
8	-	-

4.3.5 Histological validation

DTI volumes and corresponding histological slides were examined both separately and as superimposed overlays (Figs 4.9 and 4.10). Diffusion volumes were presented as a colour vector map in MIM. In general, diffusion patterns were similar to colour vector map descriptions, with outer encircling

and inner longitudinal layers observed. Analysis of immunohistochemical-stained sections demonstrated positive staining for both α-SMA and collagen in all regions of the cervix. There was a consistent general morphology observed. In the proximal and middle regions of the cervix, encircling fibres were observed primarily in the radial regions, whereas longitudinal fibres were observed towards the canal. This pattern was similar for both markers. At the distal cervix, positive α-SMA staining was reserved for vessels, whereas there was a high volume of collagen fibres observed. Collagen fibres were arranged similarly to the proximal and middle regions, though random scattering of fibres was also observed.

A detailed comparison was performed by selecting rectangular ROIs on the DTI volume and directly comparing them to the equivalent region on the corresponding histological section. Three ROI were selected at the periphery in the anterior, radial and posterior regions, and one selected towards the canal (Fig. 4.10). Further examination at a greater magnification was performed, although appreciation of fibre direction was lost at magnifications greater than x5.

In general, DTI volumes correlated well with corresponding histological tissue. Examination of ROIs demonstrated diffusion patterns similar to general fibre direction on antibody stained sections in the proximal and middle regions (Figs 4.9 & 4.10). At the distal cervix, histological sections did not correlate well with DTI volumes at the periphery. Examination of the volumetric data demonstrated encircling diffusion, with a random scattering of collagen fibres observed in the corresponding section.

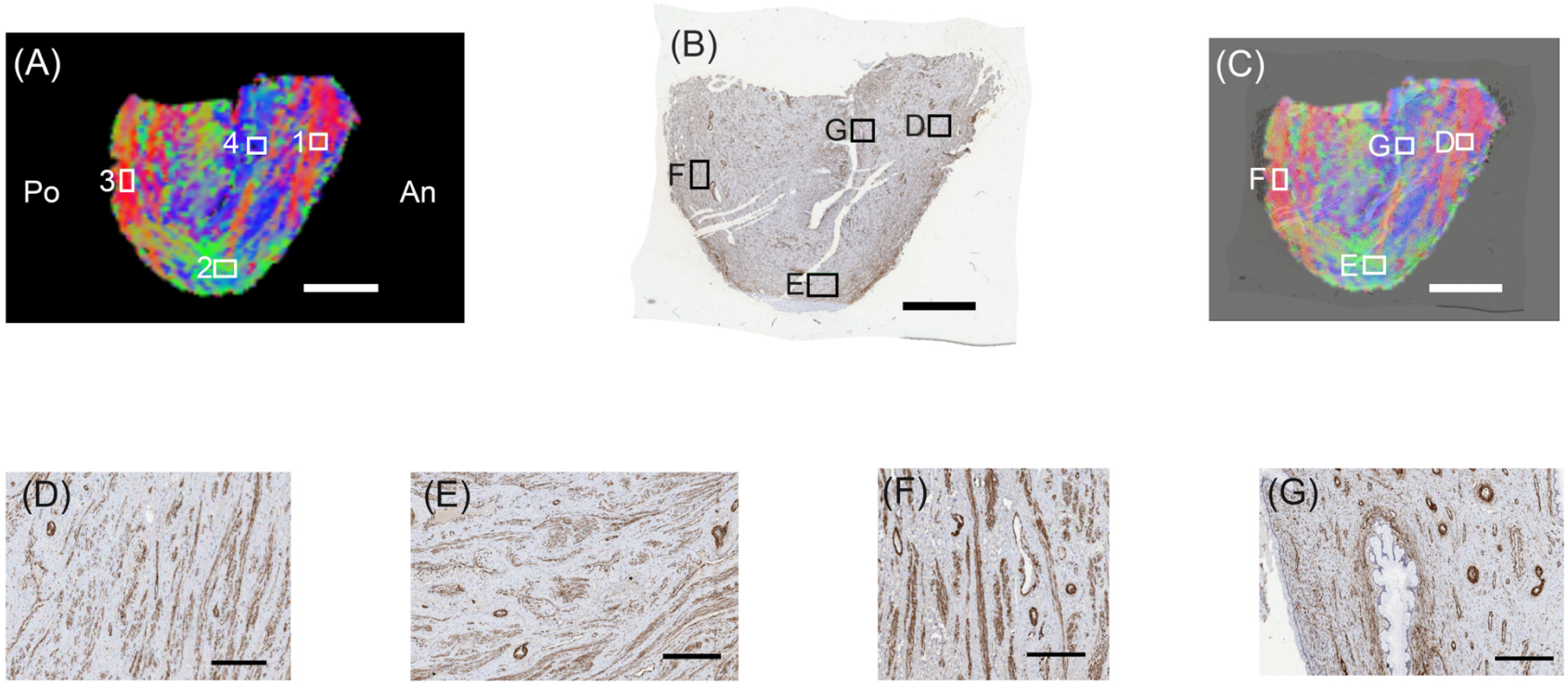

Figure 4.9 Comparison of DTI volumetric data to corresponding α-SMA stained histological section in proximal cervix.

A, B, C. Transverse sections of DTI volume, tissue section and superimposed overlay respectively. ROIs are indicated on each image and labelled on the DTI volume. D-G. α-SMA stained sections of ROI 1-4 respectively. D, E, F. Encircling transverse CSMCs are observed at the peripheral ROIs and correlate well with corresponding with DTI volume. G. Longitudinal CSMCs correspond to diffusion in the longitudinal axis in the diffusion image. Anterior (An), posterior (Po).

Colours in diffusion image reflect the orientation of the principle diffusion vector with respect to Cartesian axes system (x=red, y=green, z=blue).

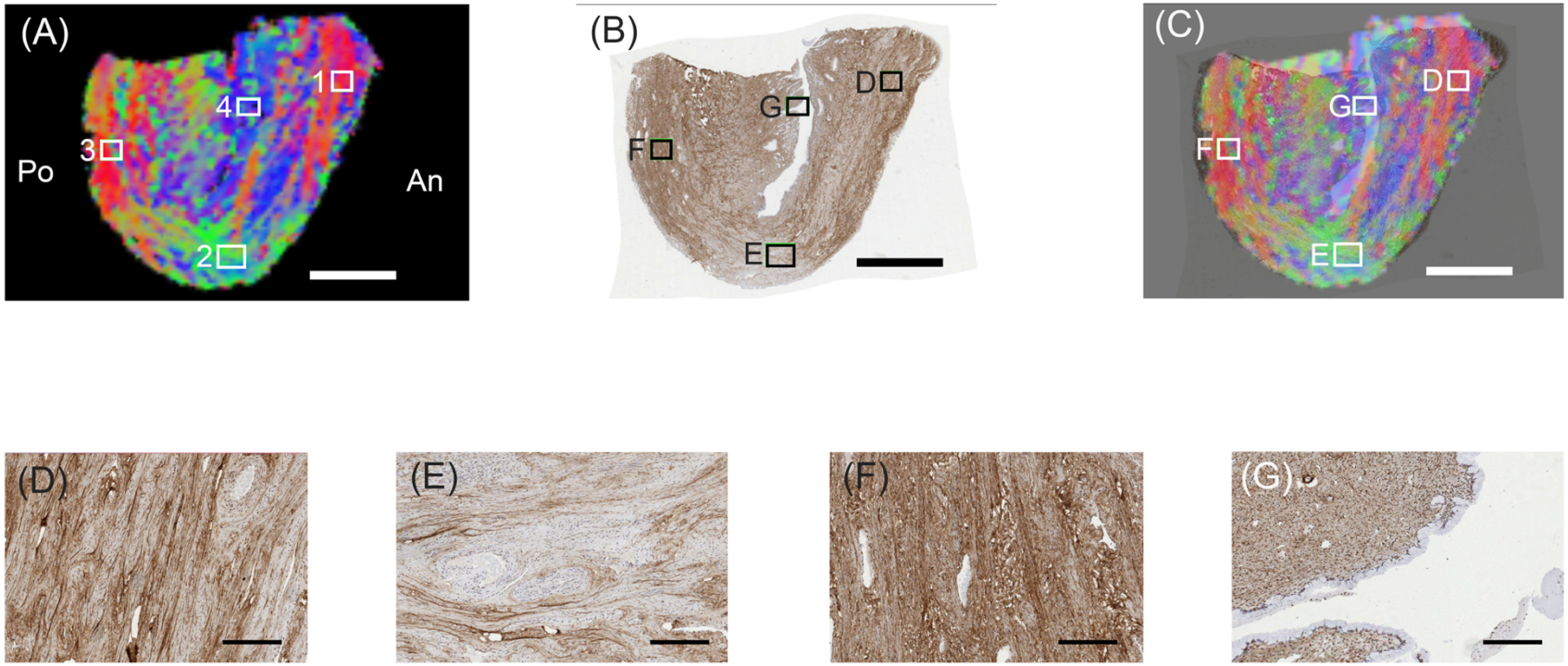

Figure 4.10 Comparison of DTI volumetric data to corresponding Col1α-1 stained histological section in proximal cervix.

A, B, C. Transverse sections of DTI volume, tissue section and superimposed overlay respectively. ROIs are indicated on each image and labelled on the DTI volume. D-G. Col1α-1 stained sections of ROI 1-4 respectively. D, E, F. Encircling transverse collagen fibres are observed at the peripheral ROIs and correlate well with corresponding with DTI volume. G. Longitudinal collagen fibres correspond to diffusion in the longitudinal axis in the diffusion image. Anterior (An), posterior (Po). Colours in diffusion image reflect the orientation of the principle diffusion vector with respect to Cartesian axes system (x=red, y=green, z=blue).

4.4 Discussion

4.4.1 Main findings

This study used a high-resolution 3D imaging technique that allowed for analysis throughout the length of the cervix. This allowed for the determination of regional differences in tissue properties as measured by quantitative measurements of diffusion.

The inference of encircling fibres within the cervix correlates well with previous ultrastructural studies (Aspden, 1988; Gan et al., 2015). Furthermore, the two distinct fibre zones observed were in accordance with previous *ex vivo* and *in vivo* DT-MRI observations (Weiss et al., 2006; Fujimoto et al., 2013). The prominence of the encircling fibres at the internal os may provide evidence of a specific microarchitecture that resists forces associated with pregnancy and encourages the possibility of an occlusive structure corresponding to this region of the cervix. Such an observation is consistent with previous biomechanical modelling (House et al., 2013). It could be inferred that mid-trimester funnelling of the internal os, as observed on ultrasound, may be due to an absence of or damage to these prominent encircling fibres.

Quantitative measurements of diffusion demonstrate that the cervix is not a uniform structure, supporting previous histological and radiographic observations (Rorie and Newton, 1967; Leppert et al., 1986; DeSouza et al., 1994; Chapter 3). Significant differences were observed in each identified region with regards to measurements of FA and ADC. However, this should be interpreted with caution, as the effect size ranged from weak to fairly strong across the sample for each quantitative measurement and therefore significance may have been achieved due to the volume of data being studied.

Nonetheless, findings indicate that tract uniformity and density differ throughout the cervix at an intravoxel level, as 86% of the observations in the present study demonstrated that tract uniformity and density progressively increase towards the internal os. The increased tract uniformity towards the proximal cervix was predominantly driven by increased diffusion restriction in the radial direction, which may reflect a progressive increase in fibre diameter and/or density. The proximal cervix possesses a higher proportion of collagen I/III ratio (Chapter 3). The restriction in radial diffusion could therefore be due to a higher proportion of large diameter collagen I fibres in this region.

4.4.2 Correlation with histological investigations

Examination of histological slides demonstrated a common fibre architecture in the proximal and middle regions of the cervix, which correlated well with diffusion patterns observed on corresponding volumetric data. Histological validation was necessary as diffusion studies cannot determine the fibre composition of tissue. Nevertheless, comparisons are challenging. Firstly, it is difficult to predict tissue deformation as a consequence of routine histological procedures, which makes slide registration challenging. Secondly, the spatial resolution of current DTI methods is not high enough to expose the fine details that are demonstrated in microscopic sections. Furthermore, as the in-plane resolution in the z-axis of the DTI dataset ranges from 0.2 – 0.25mm and in the histology sections it is 5μm, manual registration of the volumes can only be approximated. This may have accounted for the differences observed in the distal cervix of one of the samples. Nevertheless, the inspected regions in the diffusion volume correlated well with most of the corresponding histological sections and results obtained in Chapter 3.

4.4.3 Application of DT MRI to assess cervical structure

The application of *in vivo* DTI is contingent on the trade-off between spatial resolution, scan time and signal-to-noise ratio. With advances in DT-MRI schemes, imaging at a sub-millimetre scale *in vivo* using a 3T clinical scanner is achievable (Chang et al., 2015). However, the feasibility and acceptability of high-resolution DT-MRI use in the clinical setting, while technically possible, is yet to be ascertained.

However, if advanced DT-MRI schemes became commonplace, it may serve as biomarker to identify those who may have a weak cervix. RD is thought to be a sensitive marker to axonal degeneration, as a consequence of demyelination. RD is the average diffusion that occurs perpendicular to the long axis of the neurone/fibre (second and tertiary directions). Experimental models of demyelination have demonstrated a correlation between myelin loss and RD, which was further supported in human post-mortem studies (Song et al., 2005; Schmierer et al., 2007; Janve et al., 2013). Progressive demyelination causes the overall thickness of neurones to decrease, causing the space between neurones to increase and therefore RD to increase. A similar application may be possible in the cervix. RD progressively increased towards the proximal cervix where there was an increased collagen I/III ratio (Chapter 3). Alterations in RD at the proximal cervix may indicate an increase in smaller collagen III fibres and therefore greater weakness at the internal os. If this relationship is confirmed, DTI could be used to identify those with CIn.

Secondly, there is growing evidence to suggest that prior emergency CD increases the risk of PTB in subsequent pregnancies, especially if performed after a prolonged second stage of labour (Koyama et al., 2010; Levine et al.,

2015; Levine and Srinivas, 2016; Zhang et al., 2019). Caesarean sections performed at this stage may result in a transverse incision through the fully dilated cervix, rather than the lower uterine segment (Berghella et al., 2017). This has the potential to disrupt the encircling collagen and muscle, particularly at the internal cervical os, which may increase the risk of a subsequent PTB. Research using *in vivo* 3T DT-MRI has detected damage to the anteroinferior uterus in women with a prior caesarean delivery (Fiocchi et al., 2012, 2015). Previous *ex vivo* imaging at 3T could not accurately depict the fibres at the level of the cervix, yet advances in protocols may allow for high-resolution DT-MRI to become a practical and effective tool in identifying these patients (Weiss et al., 2006).

Nevertheless, DTI is not able to discern collagen and smooth muscle fibres. The relative proportions of CSMCs and collagen at the proximal cervix likely contribute to cervical competence during pregnancy. Recently, authors proposed that a muscular sphincter analogous to other pelvic sphincters is present at the internal cervical os, (Vink et al., 2016; Vink and Myers, 2018) Although clinical and physiological evidence provides support, histological evidence presented in this thesis has not confirmed this (Chapter 3).

4.4.4 Limitations

There were several limitations associated with the study. Firstly, the data were obtained from a small sample of women that had already received conservative management and then a subsequent hysterectomy for benign gynaecologic pathology, and therefore may not be representative of a larger population of healthy women. For example, it is possible that treatment with GnRH analogues may influence fibre density and thereby MR imaging. Secondly, *ex vivo* imaging

of fixed samples may be considered artificial and not comparable to *in vivo* DT-MRI measurements. However, imaging of fixed tissues provides the opportunity for longer scan times and images of greater resolution (Guilfoyle et al., 2003). A general consensus must still be reached on whether tissue fixation alters the quantitative measurements that are yielded by diffusion imaging, yet regional differences observed in *in vivo* and fresh tissue imaging are observed in formalin fixed samples (Sun et al., 2003; Bourne et al., 2016). Furthermore, comparisons with fresh tissue imaging show that although tissue shrinkage is observed following fixation, no obvious changes were seen in the orientation of the primary eigenvector (Bourne et al., 2016). Consequently, *ex vivo* DT-MRI is becoming common place in laboratory imaging studies.

4.4.5 Conclusion

The purpose of this Chapter was to identify an imaging strategy capable of assessing the microanatomy identified in Chapter 3. DT imaging did indeed identify a system of dense, well defined, encircling fibres that corresponded to the location of the internal os. Furthermore, analysis of quantitative diffusion measurements demonstrated increased tract uniformity, diameter and density towards the proximal region of the cervix. This technique could serve as biomarker to identify women with decreased volume of collagen I or scarring at the proximal cervix. However, as discussed, it is not possible to discern fibre types. The next chapter will address endocervical ultrasound, which has the potential to overcome this limitation.

Chapter 5 Endoscopic Microprobe Ultrasound of the Cervix

5.1 Introduction

The proximal cervix possesses a relatively high concentration of encircling smooth muscle and collagen I fibres that likely provide structural integrity (Chapters 3 & 4). Specifically, the encircling CSMCs are thought to form a sphincter that resists forces associated with pregnancy. Cervical funnelling, as observed on TVUS, may be a consequence of inherited and/or acquired weakness to the specific microarchitecture at the internal cervical os (Iams and Goldenberg, 1996). However, TVUS does not provide a detailed account of the internal os and therefore fails to explain why cervical change presents in this way. This may be due to the frequency at which endovaginal probes operate, as image resolution is exchanged for deeper tissue penetration (5 – 7.5 MHz; Kaur and Kaur, 2011). If a muscular sphincter exists at the internal cervical os, it may be possible to evaluate using high-resolution endocervical ultrasound.

Previous studies investigating the presence of a muscular sphincter complex have used ultrasound, with Kondo *et al.* assessing the urethra (Kondo et al., 2001). Researchers used TVUS to image the external urethral sphincter in continent and incontinent women, as well as cadaveric specimens. The external urethral sphincter was demonstrated to be a hypoechoic ring that surrounded the urethra, which correlated with a muscular region on corresponding histological images. Further analysis of sphincter thickness noted differences between continent and incontinent women, and analysis following 3D ultrasound established a relationship between sphincter volume and the degree of urinary incontinence (Athanasiou et al., 1999; Kondo et al., 2001).

The utility of endoscopic ultrasound was also demonstrated when imaging the anal sphincter complex. Transrectal ultrasound is an established method to rapidly assess the integrity of the internal and external anal sphincters (Bartram, 2005). Original *ex vivo* imaging of fresh and fixed anal resections were correlated with corresponding histological sections to determine the nature of echogenic regions (Sultan et al., 1993). Further *in vivo* imaging of the anal sphincter complex confirmed observations obtained in previous *ex vivo* studies (Sultan et al., 1994; Sultan, 2003; Thakar and Sultan, 2004). These original observations inform current interpretations of the anal sphincter complex on 360° axial ultrasound.

Assessing the cervix using endoscopic ultrasound would have implications for better identifying women at risk of delivering early. Current routine and novel methods of assessing the cervix primarily measure its biomechanical properties, yet as dilation and effacement is the final common pathway in cases of PTB, it is not clear whether these techniques distinguish between cervical weakness from other causes of prematurity (section 1.10). Proposed preconceptual tests are similarly limited, as these also fail to account for the effects of the menstrual cycle on the cervix (Asplund, 1952; Youssef, 1958; Anthony et al., 1982). Endocervical ultrasound could overcome these limitations as it may allow for direct qualitative and quantitative assessment of the microarchitecture at the internal os.

Despite detailed histological investigation, researchers have been unable to identify an anatomical muscular sphincter at the internal cervical os. Therefore, this chapter had two aims. Firstly, to provide an account of normal cervical anatomy on *ex vivo* endoscopic ultrasound. Secondly, to determine whether the encircling smooth muscle at the proximal cervix corresponds to a

discrete hypoechoic ring and therefore an anatomical muscular sphincter such as those seen in the urethra and distal gastrointestinal tract (Oelrich, 1980; Sultan et al., 1993; Kondo et al., 2001).

5.2 Methods

Ethical approval was granted by the Yorkshire and Humber Regional Ethical Committee (reference number 17/YH/0383). Five non-pregnant, premenopausal women undergoing TAH or VH for benign pathology were consented. No participants had a history of CIn or cervical excisional surgery (Table 5.1).

5.2.1 Tissue Preparation

Following hysterectomy, cervical dilators of increasing size from 3mm were inserted into the cervical canal until resistance was met at the internal os. This procedure was repeated three times and a mean distance from the external os was recorded. The cervical dilator was then placed in the cervical canal so that the canal remained patent during the fixative process. A longitudinal incision was made in the uterine corpus, which extended from the fundus to the isthmus, to facilitate the fixative process (Fig. 5.1). The uterus was immersed in a formal-saline solution (10% formalin, 0.9% sodium chloride, 4% formaldehyde) for 72 hours. This time frame was chosen so not to interfere with protocols established by the histopathology department within the Leeds Teaching Hospitals Trust.

Table 5.1 Patient demographics for cervical samples

Participant no.	Age (years)	Parity	Obstetric History	Diagnosis	Pre-hysterectomy investigation/ interventions
1	44	0	N/A	Fibroid Uterus Endometriosis	Esmya Diagnostic laparoscopy
2	44	2	2 CD	Fibroid Uterus	CT Ultrasound
3	47	2	2 NVD 1 miscarriage	Fibroid Uterus	Hysteroscopy Mirena coil Esmya Norethisterone Tranexamic acid
4	44	1	1 CD 2 miscarriages	Menorrhagia	Hysteroscopy Prostap
5	46	3	3 NVD	Menorrhagia	Hysteroscopy

NVD- Normal vaginal delivery N/A – Not applicable CD- Caesarian delivery

Figure 5.1 Preparation of uterine tissue

Image demonstrates longitudinal incision within the uterine corpus.

5.2.2 Imaging protocols

5.2.2.1 Endoscopic ultrasound

The location of the internal os was estimated following fixation with the reinsertion of a cervical dilator until a resistance was met. This procedure was performed three times to obtain a mean value. *Ex vivo* scanning was performed on a lab bench with ultrasound gel and within a phosphate buffered saline (PBS) filled water bath to facilitate acoustic coupling. 360° axial ultrasound images were obtained using a 40 MHz Intravascular Ultrasound probe (IVUS; 3mm diameter; Boston Scientific, US) and a 9 MHz Ultra Intracardiac Echo probe (Ultra ICE™; 3mm diameter; Boston Scientific, US) catheters in conjunction with the iLab™ Ultrasound Imaging System (Boston Scientific, US). The sonographic beam was angled forward at 45° perpendicular to the long axis of the catheters, which displayed 360° tomographic images with the catheter in the centre (Figs 5.4 & 5.5). The catheters were fitted with an integrated sonolucent window that was filled with 10 cc of sterile water via a flushing port at the distal end of the catheter, to improve acoustic coupling (Fig. 5.2). Ultrasound gel was inserted into the cervical canal to further improve coupling. Videos and still images of the uterine cavity and proximal, middle and distal cervix were obtained.

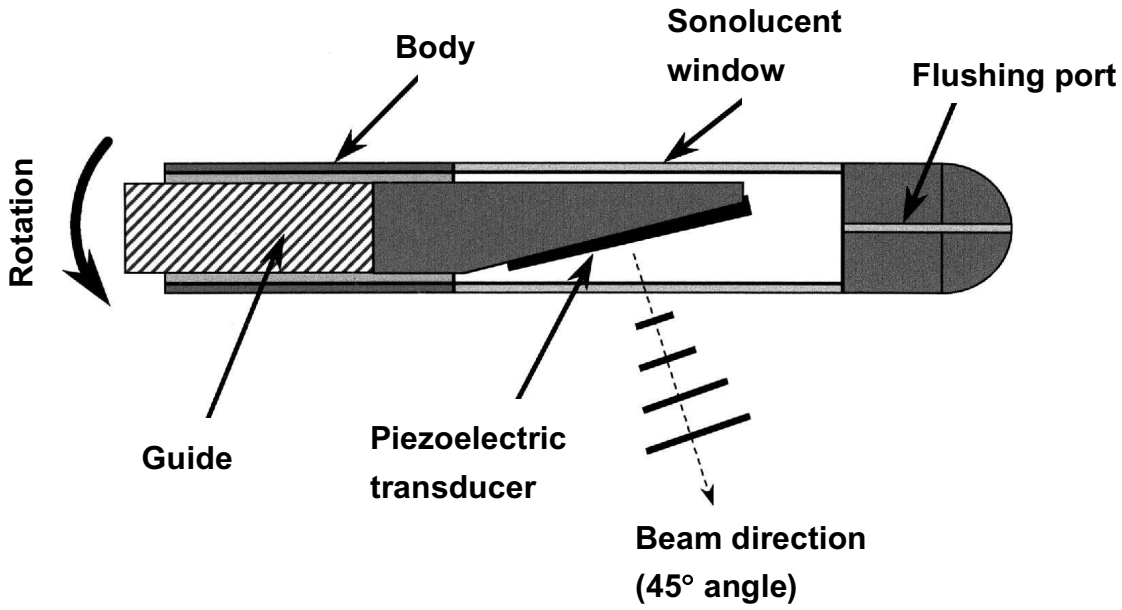

Figure 5.2 Schematic of the distal portion of the Ultra ICE catheter

The piezoelectric ultrasound transducer is visible through the sonolucent window. Rotation of the crystal is generated by a drive-shaft, which was powered by a motor drive (1800 rpm) at the proximal end of the catheter. The crystal moved within the probe in response to manual rotation of the catheter.

Adapted with permission from Zanchetta *et al.* (2002)

5.2.2.2 Linear ultrasound

In one sample, further ultrasound images were obtained using a SonoSite M-Turbo portable ultrasound device (Fujifilm Sonosite, Inc., Bothell, USA) with a SLAx 13 MHz 25mm hockey stick linear array transducer (Fig. 5.3). Ultrasound was performed with the transducer inserted in a sterile cover and placed on the periphery of the cervix and on the cervical canal once the sample had been hemisected (Chapter 2). Ultrasound gel was used as a coupling agent. Still images of the proximal, middle and distal cervix were obtained.

Figure 5.3 25 mm hockey stick transducer

Image reused with permission from Davies *et al.* (2012)

5.2.3 Image analysis

All endoscopic ultrasound videos and images were exported with an imaging viewer (McKesson, Sheffield) and analysed on a desktop computer. The diameter of the probe was used as a calibration measurement. The diameter of the tissue was estimated through analysis of echogenic areas and confirmed with previously recorded measurements. Linear ultrasound images were obtained using a digital single-lens reflex camera (Canon, Tokyo). Medium-frequency sonographic images were compared to corresponding histological sections stained with MT and α-SMA using methods described in Chapter 2. All slides were scanned and digitized with an Aperio AT2 scanner using a x20 objective (Leica, UK) and analysed using MIM. Gross morphology was examined and recorded.

5.3 Results

Cervical ultrasound images were obtained from five non-pregnant women. Of these women, one was nulliparous and four were multiparous. The mean age of the group was 45 ± 1.4 years.

5.3.1 High-frequency axial ultrasound

High-frequency endoscopic ultrasound was performed on one cervical sample (Participant 1). Images demonstrated homogenous hyperechoic areas adjacent to the probe (Fig. 5.4). When compared to non-tissue images, no differences were observed, which is likely a consequence of the limited tissue penetration with ultrasound at 40 MHz. No further tissue samples were scanned using the IVUS catheter.

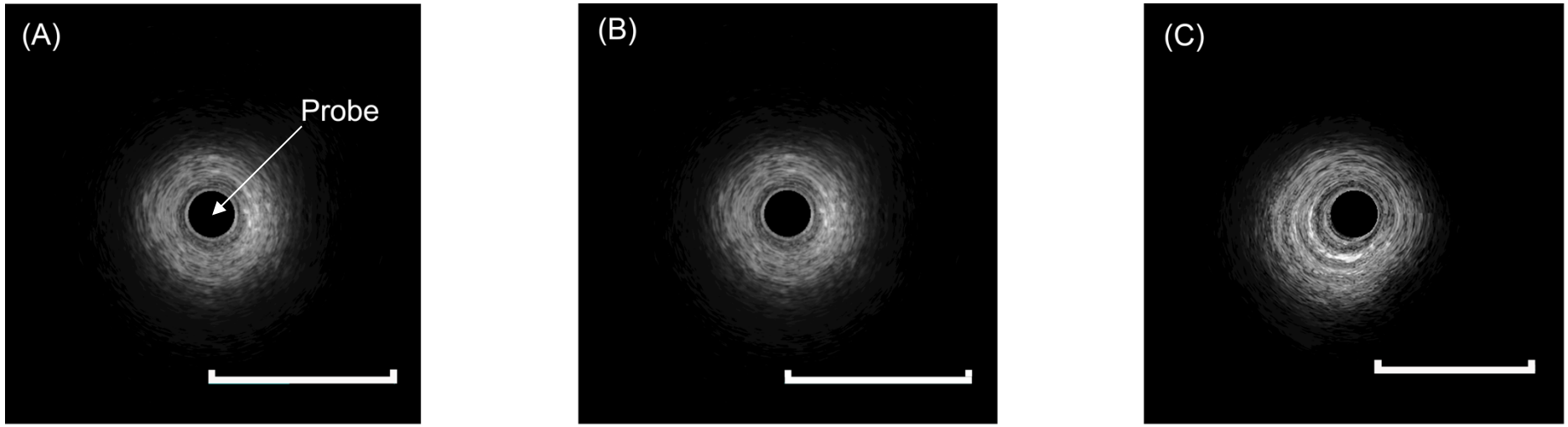

Figure 5.4 High-frequency endoscopic ultrasound images of the cervix

Endoscopic ultrasound images of air (A), cervical tissue (B) and cervical tissue within a PBS water bath (C) obtained from participant 1. No identifiable landmarks were observed in images. Probe diameter 3 mm, Scale bar 1 cm.

5.3.2 Medium-frequency axial Ultrasound

Medium-frequency endoscopic ultrasound was performed on four uterine samples. Images at the uterine corpus demonstrated no gross structures. However, in one sample, the incision made during tissue preparation was observed (Fig. 5.5E). Images of the cervix demonstrated 3 regions: an inner hyperechoic (high signal) region, a middle hypoechoic (low signal) region and an outer hyperechoic ring. This outer hyperechoic ring was confirmed as the edge of the cervical samples by previously recorded measurements (Fig 5.5). Nabothian follicles were observed as oval anechoic (no signal) regions in the proximal and distal regions of the cervix in 2 of the cervical samples (Fig. 5.5 D, F).

Figure 5.5 B and D demonstrated an artefact created by the probe. Manual rotation of the probe caused the crystal to extend and retract (Fig. 5.2). This produced an encircling hyperechoic artefact on the ultrasound image.

5.3.2.1 Comparison with histology

Figure 5.6 shows corresponding cross-sectional images of the proximal cervix on ultrasound and MT and α-SMA stained tissue. Corresponding sections were confirmed due to the presence of Nabothian follicles within the glandular region of the cervical sample. Analysis of α-SMA demonstrated regions of encircling CSMCs, which were most prominent towards the periphery of the tissue. The encircling CSMCs were interspersed within a dense collagen network. No distinct muscle or collagenous regions were identified on sonographic images.

5.3.3 Medium-frequency linear Ultrasound

Figure 5.7 shows images of the cervix in the sagittal and transverse planes using linear ultrasound. The mucus lining the cervical canal is hyperechoic in

the sagittal plane. A signal void (acoustic shadow) was demonstrated in the portion of tissue furthest from the ultrasound probe, as cervical mucus strongly reflected the ultrasonic waves. Scanning of the proximal cervix in the transverse plane demonstrated a hypoechoic canal. Similar gross structures were observed in the hemisected samples. No distinct microarchitectural differences were observed along the length of the cervix.

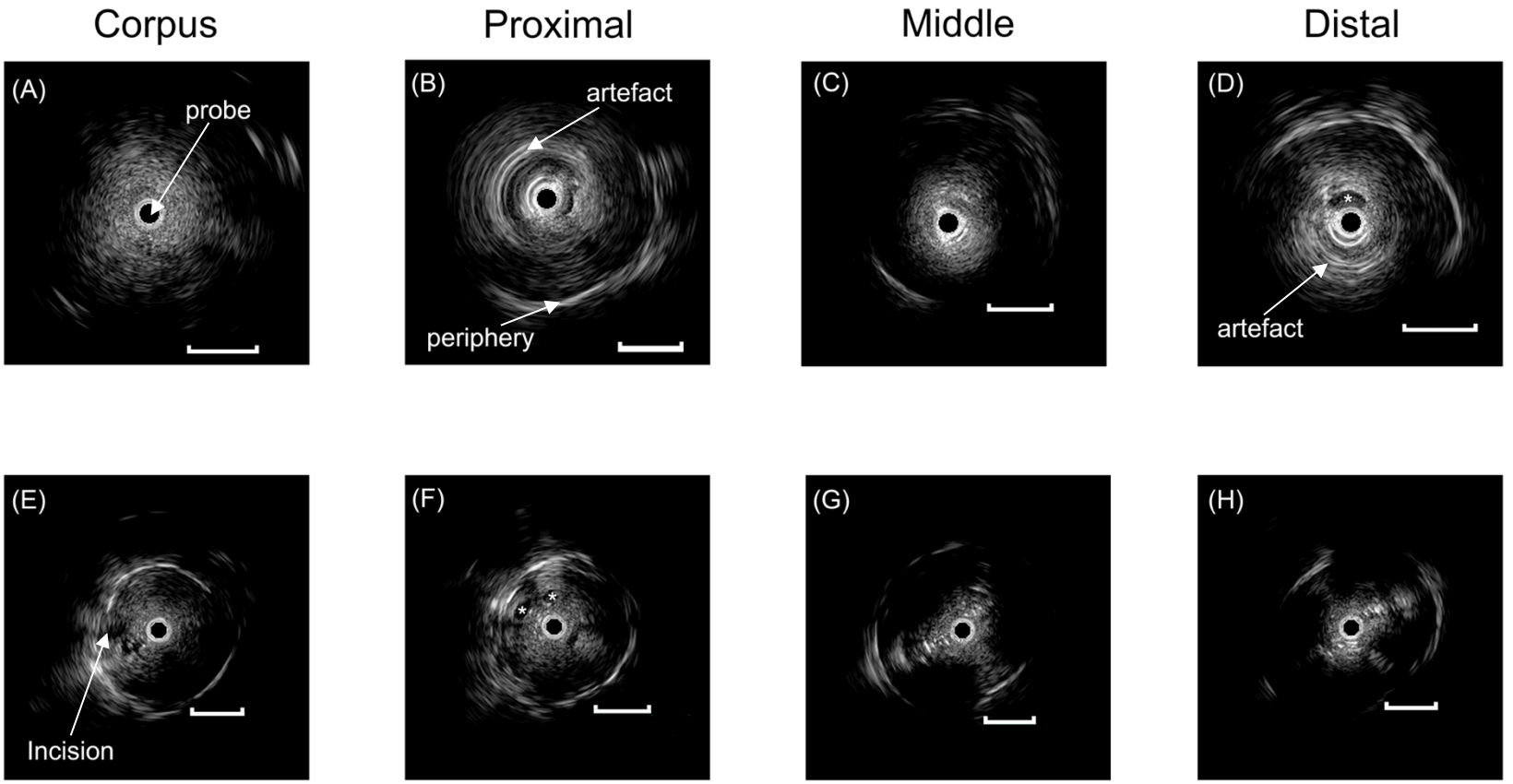

Figure 5.5 Medium-frequency endoscopic ultrasound of the uterus

Medium-frequency endoscopic ultrasound of the uterine corpus (A, E) and proximal (B, F), middle (C, G) and distal (D, H) in samples 2 and 4 respectively. Hyperechoic regions at the periphery of images indicated the edge of the tissue sample A No distinctive features observed in uterine image. E. Anechoic region extending from the periphery towards the probe is the longitudinal incision made during tissue preparation. B Demonstrates an artefact produced from the ultrasound probe. F Two Nabothian follicles demonstrated by two circular anechoic regions*. C, G No identifiable landmarks observed in middle region of cervix. D Nabothian follicle at the distal cervix. H No identifiable features identified. Scale bar 1 cm.

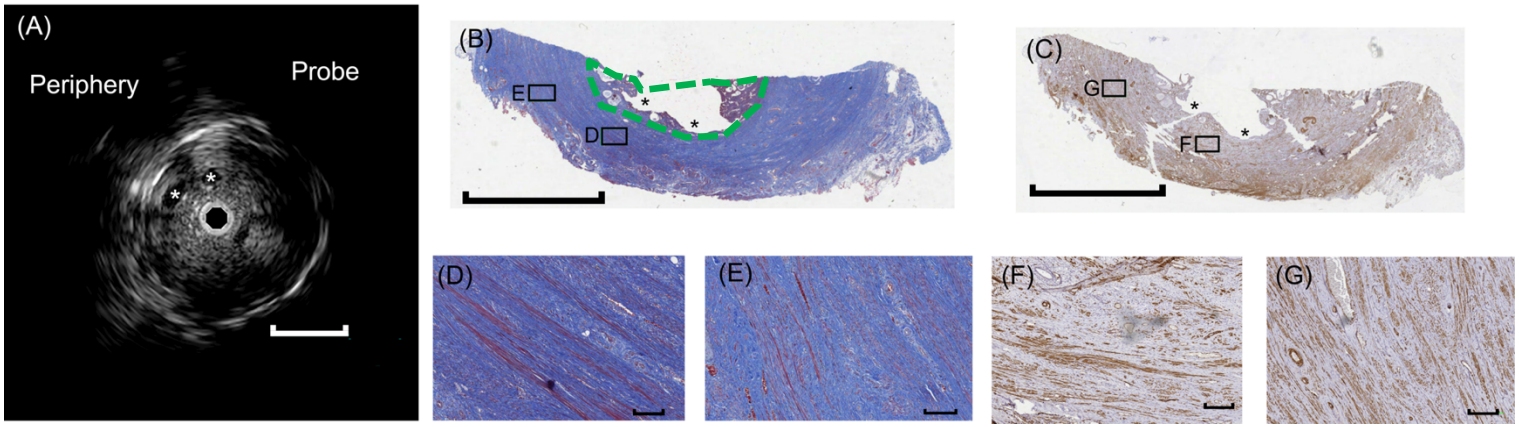

Figure 5.6 Histological comparison with medium-frequency ultrasound

Medium-frequency endoscopic ultrasound of the proximal cervix and corresponding histological sections. A Nabothian follicles demonstrated by circular anechoic regions*. Scale bar 1 cm. B, C Transverse sections of the proximal cervix stained with MT and α-SMA respectively. Nabothian follicles are located within the glandular region of the cervix (green dashed area on MT-stained slide). Boxes represent regions of interest that were inspected at greater magnification. Scale bar 5mm. D-G Selected regions of interest at x5 magnification, scale bar 2mm. D, E MT stained sections: Red = smooth muscle, blue = collagen. Encircling smooth muscle cells are visible within dense regions of collagen. F, G Encircling smooth muscle cells (brown) cells observed.

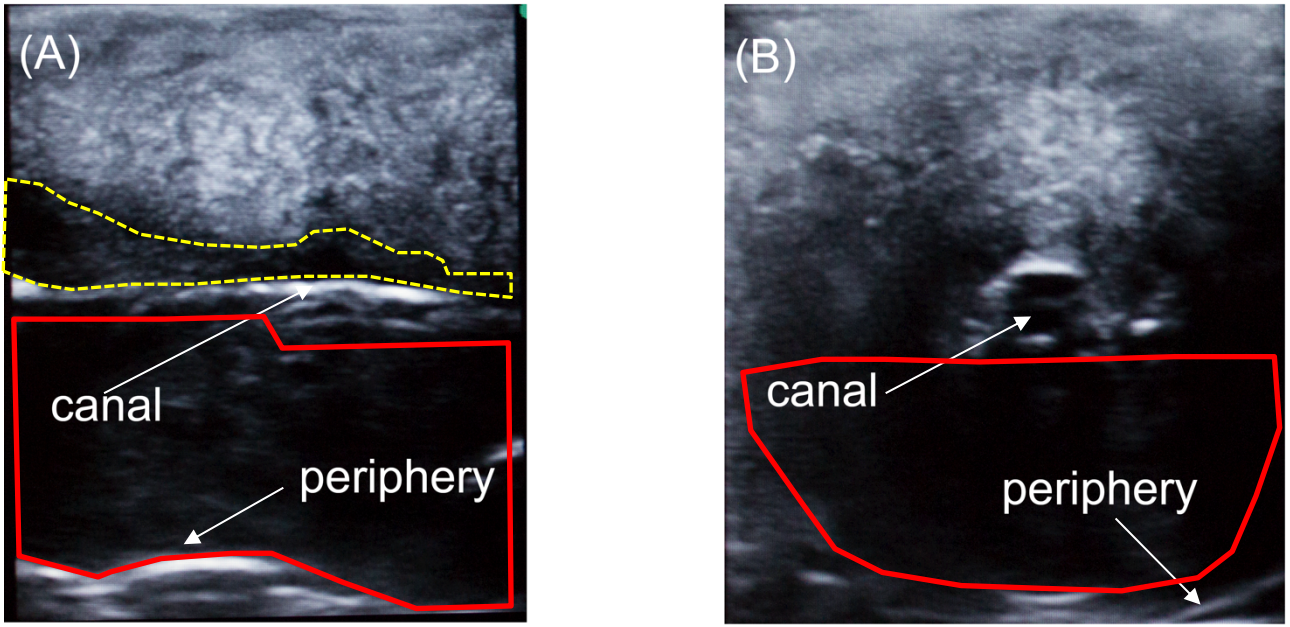

Figure 5.7 Linear ultrasound of the whole cervix

Medium-frequency linear ultrasound of the cervix in the sagittal (A) and transverse (B) planes. Gross structures such as the canal and the radial edges are observed in both images. A. Hypoechoic region located lateral to the canal corresponds to the glandular region of the cervix (yellow dashed line) A, B Acoustic shadowing (signal void) is present in the lower portion of each image due to reflection of sound waves by the cervical canal/mucus (red solid line).

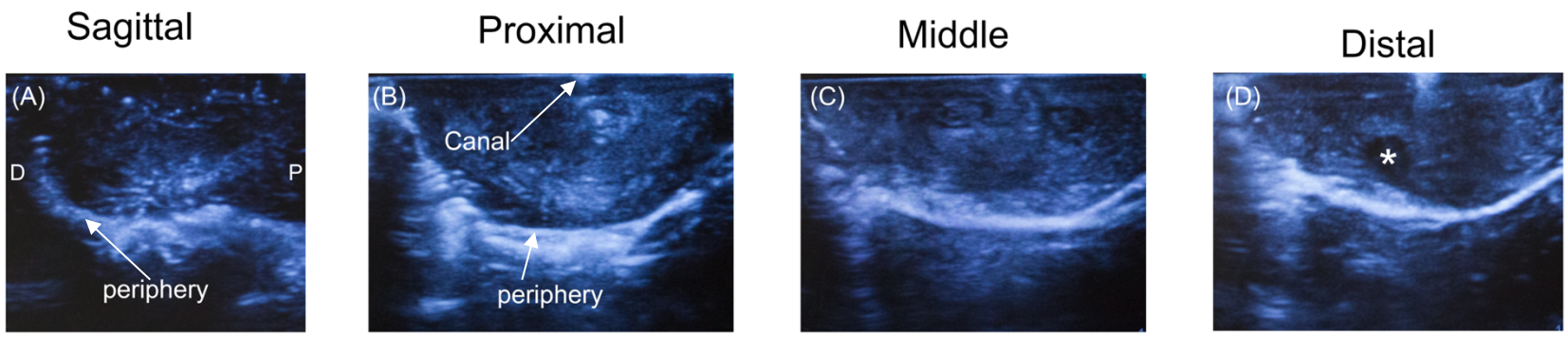

Figure 5.8 Linear ultrasound of the hemisected cervix

Medium-frequency linear ultrasound in the sagittal (A) and transverse planes (B-D). Gross structures such as the canal and the radial edge are observed. A Nabothian follicle* is present in the distal cervix. No other distinguishable features are observed.

5.4 Discussion

Cervical competence is thought to be determined by the structural integrity of the internal cervical os. Prominent encircling smooth muscle fibres towards the proximal cervix are thought to contribute to cervical competency during pregnancy. Current routine and experimental methods of assessing the cervix are unable to discern microstructural anatomical differences that have been demonstrated on histological investigation. This chapter aimed to assess normal cervical anatomy on *ex vivo* endoscopic ultrasound and to determine whether an anatomical muscular sphincter is located at the internal cervical os.

High frequency ultrasound was an unsuitable method to visualise cervical anatomy. The 40Mhz IVUS probe produced images at a resolution of 0.05mm, yet only yielded a maximum imaging depth of 0.5cm (Stainback, 2007), and so ultrasonic waves did not penetrate beyond the canal or inner stroma. In contrast, sonography using 9Mhz penetrated up to 5cm with a resolution of 0.3 mm (Zanchetta et al., 2002). Three regions of interest were observed: an inner hyperechoic, middle hypoechoic and outer hyperechoic region. Echogenicity is determined by a mismatch in tissue density and the orientation of underlying fibres (Chan and Perlas, 2011). In this instance, the inner and middle hyper- and hypoechoic regions could be a reflection of the orientation of the fibres within the cervix i.e. inner longitudinal and outer circular (Chapters 3 & 4). The peripheral hyperechoic region is likely due to the interface between tissue and air, causing greater reflection of sound waves. Gross structures, such as Nabothian follicles and incisions through uterine tissue were observed, which appeared anechoic on sonography. Regions of encircling smooth muscle were observed on α-SMA and MT stained tissue sections,

which were entangled within a dense collagen network. Comparison with sonographic images demonstrated no distinct regions of smooth muscle that may correspond to an anatomical muscular sphincter. Although images were obtained at a resolution of 0.3mm, no microstructural differences were observed along the length of the cervix on endocervical sonography. This is likely due to the staining methodologies and image magnification needed to observe these structural differences. Despite significant differences in smooth muscle content between the proximal and distal cervix (Chapter 3), it required advanced digitised histological practices that operate at an image resolution (0.5 μm^2) and magnification (> x5) that clinical imaging is not yet capable of.

Further analysis of whole and hemisected samples using a linear probe did not highlight echogenic regions that could correspond to differences in fibre orientation. Images demonstrated homogenous echogenicity along the length of the cervix, with only gross structures such as Nabothian follicles and the cervical canal discerned. Hypoechogenic regions were identified adjacent to the cervical canal in sagittal sections, which is the opposite of what may be expected if these fibres are longitudinally orientated. It is likely that this hypoechoic region corresponded to the glandular region of the cervix.

5.4.1 Smooth muscle and cervical competence

Both axial and linear ultrasound images were unable to identify an encircling structure that could correspond to a sphincteric mechanism at the internal os. Analysis of stained tissue sections demonstrated interweaving collagen and smooth muscle fibres, instead of a discrete band of smooth muscle, unlike that seen in the anal sphincter complex or the external urethral sphincter (Oelrich, 1980; Athanasiou et al., 1999; Kondo et al., 2001). This observation, as well as

those from Chapter three, likely confirm that a distinct and discrete anatomical muscular sphincter is not present in the non-gravid condition.

CSMCs in the proximal cervix may proliferate during pregnancy to create an anatomical sphincter, as seen in other primate species (Ivy et al., 1931). This, however, has not been observed in early histological investigations following peripartum hysterectomy (Danforth, 1947, 1954). This author noted smooth muscle cell hypertrophy and hyperplasia in the first trimester, but these cells were scattered within a dense collagen network. Though these studies were technically limited, similar practices were used to identify other pelvic sphincters (Sultan et al., 1993; Kondo et al., 2001).

Encircling smooth muscle cells may form a physiological sphincter (i.e. smooth muscle that blends into surrounding tissue with no localised muscle thickening), which increases in volume/strength during pregnancy. Electromyography (EMG) investigations of the cervix during labour demonstrate that the cervix actively contracts, rather than being just a passive dilator. Most contractions are thought to be synchronous with contractions of the corpus when the cervix is fully dilated and effaced, to allow for expulsion of the foetus (Pajntar and Verdenik, 1995; Pajntar et al., 1998, 2001; Rudel and Pajntar, 1999). Recent evidence suggests that connexin 43 (a gap junction protein found on uterine smooth muscle cells) is present on cervical smooth muscle cells, which could propagate contractions from the uterine fundus (Smith et al., 2015; Vink *et al.*, 2016). Asynchronous cervical contractions were categorised as delayed or independent (Rudel and Pajntar, 1999). Delayed contractions were thought to occur in response to stretching of the cervix caused by uterine contractions, yet were not related to EMG activity of the corpus (Kao, 1989; Rudel and Pajntar, 1999). Independent cervical contractions occur in the

absence of uterine contractions. Authors noted that this type of contraction most commonly occurred in the unripened cervix and the strength of these contractions correlated with the length of the latent phase of labour, which they hypothesised prevented injury to the unripened cervix (Pajntar and Verdenik, 1995; Pajntar et al., 1998, 2001; Rudel and Pajntar, 1999). As pregnancy progresses, increasing pressure is centred at the proximal cervix. As cervical collagen remodels, the internal os must have a mechanism that resists this increasing pressure. Cervical weakness is defined as spontaneous and painless dilation, in the absence of uterine contractions. It is possible that cervical funning occurs in the absence of cervical muscle contraction.

Yet, this is likely to be complicated further. Evidence suggests that smooth muscle orchestrates the extracellular remodelling of collagen throughout gestation (Watari et al., 1999; Mourad et al., 2017). In the circulatory and pulmonary systems there is a balanced relationship between smooth muscle cells and the components of the extracellular matrix, each of which can stimulate or inhibit proliferation and/or modification of the other (Koyama et al., 1996; Li et al., 2003; Pak et al., 2007; Schuliga et al., 2010). Could the relationship between these two components within the cervix partly determine competence during pregnancy? To date, cervical smooth muscle and collagen have been thought of as two separate entities, with much of the attention focused on collagen content/maturity as the determinant of competence. Yet, CSMCs can produce enzymes and chemokines/cytokines that facilitate cervical remodelling (Watari et al., 1999, 2000; Mourad et al., 2017). Smooth muscle cells in other regions polymerize collagen fibrils into longer/larger supramolecular collagen assemblies (Schuliga, 2015). This results in collagen fibres with an increased tensile strength and greater resistance to

collagenolysis. Therefore, cervical smooth muscle could influence both the formation and degradation of collagen assemblies.

5.4.2 Applications of endoscopic ultrasound

Endocervical ultrasound will serve no clinical value in assessing the degree of smooth muscle hyperplasia/hypertrophy during pregnancy, as this would require direct instrumentation of the cervical canal and risk the integrity of the CMP. However, as endocervical ultrasound is capable of identifying gross structures, such as Nabothian follicles and incisions within tissue, it may identify cervical scarring due to previous trauma. Therefore, this method may serve as a biomarker to identify those at risk of miscarriage due to a previous second stage caesarean section, similar to DTI. Moreover, ultrasound is more suitable in the this regard, as it is fast, portable and routinely used in obstetric medicine.

5.4.3 Limitations

The technology used in this study was limited, as imaging artefacts were common due to manual rotation of the probe by the user. Furthermore, it was not possible to discern the orientation of *ex vivo* images. However, if endoscopic ultrasound was used to identify cervical scarring *in vivo*, orientation would be gained from adjacent structures (e.g. bladder). Secondly, it was noted in Chapter three that smooth muscle content slightly decreased with each successive pregnancy. Multiparous cervical samples were imaged using medium-frequency ultrasound and so this may have affected the identification of a muscular region. However, as previously described in this thesis and by previous authors, the interspersed nature of smooth muscle and collagen would likely prevent the user from identifying a muscular region. Even if this was not

the case, it is not routine to screen for cervical weakness in nulliparous women, so this imaging technique would not serve a clinical purpose in this instance.

5.4.4 Conclusion

The cervix demonstrates sphincteric behaviour both in the non-pregnant and pregnant condition (Chapter 1). The results presented in this chapter (and thesis) indicate that there is no discrete anatomical sphincter located at the proximal cervix, or at least not one that can be directly observed using current investigative practices. Encircling smooth muscle cells within the cervix may still serve as a physiological sphincter that proliferates during pregnancy to resist increasing forces. However, histological confirmation of this is challenging, as samples of the proximal cervix would either need to be taken post-delivery or following peripartum hysterectomy. These methods of sampling are not feasible as the first is invasive/destructive and the second is rare (approximately 4.1 per 10,000 births per year in the UK; Knight et al., 2008) Electromyography is comparatively less invasive. Measurements in non-pregnant and pregnant women may indirectly confirm proliferation of CSMCs during pregnancy. Yet, this method of assessing cervical contractility, and possibly cervical competence, would be impractical in routine clinical practice because measurements would need to be taken over an extended period of time. Furthermore, measurements obtained out with pregnancy are unlikely to be a suitable predictor of cervical contraction during pregnancy, as the degree of smooth muscle proliferation during pregnancy is likely to be variable. Therefore, suitable methods of assessing cervical competence at present are those that measure the mechanical properties of the cervix, or possibly the influence of smooth muscle and other variables on the ECM.

Chapter 6 Discussion and Future Directions

6.1 Final discussion

Cervical insufficiency is caused by several mechanisms at a structural and molecular level. One mechanism is thought to be a deficient internal os, whereby a weakness that corresponds to this region results in early cervical funnelling. The goal of this thesis was to re-examine the anatomy of the cervix using novel imaging strategies to identify anatomy that both determines competence and the ability to progressively open to allow for childbirth. This is significant, as identification of 'normal' anatomy will allow for the development of clinical tools to accurately diagnose CIn earlier in pregnancy, or even prior to conception.

The results from this thesis clearly identify a microarchitecture at the proximal cervix that could provide structural integrity to this region during pregnancy. The increase in smooth muscle content and the collagen I/III ratio towards the proximal cervix may provide evidence of separate, yet cooperative, mechanisms to resist intrauterine forces. The progressive change in anatomy towards the distal cervix (i.e. decrease in smooth muscle, increase in collagen III and progressive disorganisation of encircling fibres) may facilitate cervical dilation and effacement in the latter stages of pregnancy, following collapse of the internal os. Consequently, the anatomy described may partly explain how the cervix fulfils its two principle functions during pregnancy: 1) to remain closed to maintain the

fetus *in utero* (microarchitecture at proximal cervix), 2) to shorten and dilate in preparation for labour (microarchitecture towards distal cervix).

DT imaging was successful in qualitatively and quantitatively detecting the subtle differences in cervical anatomy. Consequently, diffusion measurements that indirectly measure fibre organisation and/or thickness could be used as a criterion for cervical management, if a 'normal' threshold or range is established. High-quality, submillimetre *in vivo* imaging is achievable, and so efforts should be made to use similar DTI schemes in *in vivo* cervical imaging studies, to assess whether this technology can better detect cervical change compared to current accepted/experimental methods (Chang et al., 2015).

Finally, and perhaps most importantly, the results obtained further emphasise the heterogenous anatomy within the cervix, and consequently the inherent limitations of studies that just analyse the distal cervix to provide insight into cervical function. Moving forward, research must analyse multiple regions of the cervix, particularly the proximal region, to ascertain how this organ functions during pregnancy.

6.2 Comparison with previous descriptions of cervix

Due to the complexity and heterogeneity of cervical anatomy and the complicated nature of remodelling during pregnancy, results obtained from non-pregnant tissue must be treated with caution. Nevertheless, inferences can be drawn that can go some way to further our understanding of cervical function during pregnancy. The proximal cervix undoubtedly possesses multiple anatomical structures that provide

a mechanical integrity to this region. This is novel, as research to date has focused on the fibrous nature of the whole cervix, with little attention on the internal os and other components of the stroma. Even so, the recent descriptions of CSMCs using computer-assisted quantification histological analysis indicated that an occlusive muscular structure was likely the primary determinant of competence at the proximal cervix (Vink et al., 2016). Perhaps this is true of some women, as studies to date have consistently reported individual differences in anatomy within samples, especially with regards to muscle content (Danforth, 1947, 1954; Rorie and Newton, 1967). However, the primary determinant of cervical competence is an anatomy at the proximal cervix that can achieve a minimum occlusive force during pregnancy, which is likely achieved by variations in the anatomy described in this thesis (i.e. ratios of encircling smooth muscle and collagen I and III).

DT imaging further confirmed systems of longitudinal and encircling fibres within the cervix observed in previous imaging studies, which provides evidence to the validity of this method (Aspden, 1988; Weiss et al., 2006; Fujimoto et al., 2013; Reusch et al., 2013; Gan et al., 2015; Yao et al., 2016). However, this method improves on previous descriptions, as DTI is capable of providing a detailed anatomical account of large tissue volumes. Principally, this method provided evidence of a system of dense, well-defined, encircling fibres which corresponded to the location of the internal os. Disruption to these prominent, encircling fibres will affect the ability of the cervix to remain closed, increasing the risk of CIn and subsequent PTB. This, alongside variations in the fibre and cellular composition at the proximal cervix, may partially support and provide an explanation for CIn being

an extended biological continuum with degrees of cervical competence (Iams et al., 1995).

6.3 Cervical competence

The process of cervical remodelling involves complex molecular and structural alterations that allows for expulsion of the fetus. The proximal cervix possesses a relatively high concentration of encircling CSMCs and collagen I fibres that will provide this region with a structural integrity to resist gestational forces (Chapter 3). This anatomy is of importance, as intrauterine forces are centred at the internal os, which makes this region susceptible to early cervical funnelling (House et al., 2013). Despite a high collagen turnover, competence throughout pregnancy is maintained, in part, by the upregulation of collagen I and possibly the proliferation of CSMCs (Danforth, 1947, 1954; Akins et al., 2011). The accelerated phases of remodelling (i.e. dilation and effacement) may be influenced by a progressive decrease in the collagen I/III ratio (Iwahashi et al., 2003), the balance between mature and immature collagen fibres (Read et al., 2007; Akins et al., 2010), the limits of CSMC contraction (Pajntar and Verdenik, 1995; Pajntar et al., 1998, 2001; Rudel and Pajntar, 1999), and increasing gestational forces. This ‘tipping point’ may result in the stretching of CSMCs, as immature collagen fibres possess less tensile strength, leading to the release of cytokines from CSMCs that further increase the activity of enzymes that facilitate collagenolysis (Mourad et al., 2017). In addition, increasing progesterone levels may also lead to a decrease in CSMC contractility, which may influence stretching of CSMCs (Szekeres-Bartho, 1992; Vink et al., 2019). The increased activation of enzymes associated with

collagenolysis leads to a perpetually accelerating phase of collagen remodelling, due to the progressive decrease in prominent, organised encircling smooth muscle and collagen I fibres towards the distal cervix (Chapter 3 and 4). This could lead to a positive feedback loop and consequently dilation and effacement of the cervix at term.

A reduced smooth muscle or collagen I content, a decrease in the collagen I/III ratio, or a disruption to the encircling fibres at the proximal cervix may result in deviation from a minimum occlusive force, and therefore an increased susceptibility to the early onset of cervical remodelling and funnelling. The accelerated phases of remodelling may occur even sooner in multigravida/parous women, as described in Chapter 3. Although this chapter was limited by a small sample size, it did identify a decrease in smooth muscle content and an increased proportion of collagen III at the proximal cervix in subsequent pregnancies, regardless of previous methods of delivery.

6.4 Limitations and solutions

Although the results obtained in this thesis provide an updated account of cervical anatomy, a number of additional questions have arisen as a consequence. Firstly, and most importantly, cervical remodelling during pregnancy is a dynamic process that involves complex biochemical and anatomical interplay (Parisi, 1988; Read et al., 2007). Consequently, it is not possible to accurately predict cervical change during pregnancy from the anatomy described in this thesis. Current, anatomical descriptions of remodelling are derived from *ex vivo* histological investigations following punch biopsy of the distal cervix, which is invasive, or caesarean

hysterectomy. DTI is a non-invasive method capable of imaging large tissue volumes, and is sensitive to the complex anatomy of the cervix. Therefore, this method is a safe and accurate method to investigate cervical remodelling *in vivo*, and may allow researchers to build upon descriptions derived from non-pregnant tissue.

An area that must be investigated further is the possible high collagen I/III ratio at the proximal cervix. Although a lower ratio has been associated with lower tensile strength within other structures in the pelvis, this does not confirm it has an influence on cervical competence. (Keene et al., 1987; Liu et al., 1997; Ewies et al., 2003; Moalli et al., 2004). Second harmonic generation (SHG) is a non-invasive optical imaging technique that can discriminate between collagen I and III fibres, and therefore could be used to determine a link between this ratio and cervical competence (Chen et al., 2012; Suzuki et al., 2012; Tilbury et al., 2014). The technology is limited by poor depth penetration (50 -100μm), as evidenced in previous cervical investigations, yet is sensitive to collagen structural changes during pregnancy (Akins et al., 2010; Zhang et al., 2012; Lau et al., 2013; Reusch et al., 2013; Narice et al., 2016). Zhang et al., (2012) developed a two-millimetre diameter endoscopic probe, which would allow for direct instrumentation of the cervical canal, and therefore measurement of the proximal cervix (Zhang et al., 2012). Accordingly, a 'normal' non-pregnant collagen I/III ratio at the internal os could be determined and correlated to time to delivery in the subsequent pregnancy.

Although descriptions from this thesis confirm the progressive increase of CSMCs towards the weight-bearing region of the cervix, this does not provide

evidence that smooth muscle influences cervical competence. The uterine corpus and cervix are derivatives of the paramesonephric ducts, so CSMCs could just be an extension from the corpus that progressively diminish towards the distal cervix (Standring, 2004; Weiss et al., 2006). This may explain why previous histological investigation noted CSMC hypertrophy and hyperplasia during pregnancy (i.e. a consequence of corporal muscle cell growth; Danforth, 1947, 1954) However, these observations do not account for why the encircling smooth muscle contracts independently of corporal contraction during labour, as observed in EMG investigations (Pajntar and Verdenik, 1995; Pajntar et al., 1998, 2001; Rudel and Pajntar, 1999). Further EMG studies should investigate encircling smooth muscle activity throughout pregnancy to determine if 1) encircling smooth muscle is active, 2) contractility increases throughout pregnancy and 3) it is a determinant of cervical competence.

The significance of smooth muscle is unlikely to be limited to contractility. Histological, immunohistochemical and sonographic investigation demonstrates that there is no distinct muscular or collagenous region in the proximal and middle cervix (Chapters 3 & 5). This may provide further evidence of close interplay between these two components of the cervical stroma. This interplay has been demonstrated in *ex vivo* studies, where CSMCs produced enzymes and cytokines that facilitate collagenolysis (Watari et al., 1999, 2000), particularly following stretching (Mourad et al., 2017). However, this relationship could extend to collagen fibrillogenesis and cross-linking processes, as demonstrated in arterial and pulmonary smooth muscle cells (Li et al., 2003; Schuliga et al., 2010).

Therefore, primary CSMCs could be obtained at hysterectomy and cultured on collagen I to determine whether these cells remodel the extracellular environment.

6.5 Conclusions and future work

Descriptions of the cervix have changed little since the seminal work conducted by Danforth and colleagues sixty years ago. Although this had a profound and positive effect on our understanding of the cervix, these descriptions fall short, as they do not provide an explanation for why CIn presents with weakness at the internal os. The series of experiments presented here not only provide an account for why the proximal cervix may behave in this way, it demonstrates that further information can still be obtained using novel histological and radiological practices. Therefore, it is paramount that researchers continue to examine the cervix using innovative methods.

Secondly, results demonstrated that accurate anatomical descriptions of the human cervix can be achieved using DTI *ex vivo*, and therefore potentially *in vivo*. This is significant, as this would provide an opportunity to accurately investigate the anatomical changes that occur in response to cervical remodelling *in vivo*, something of which has not been achieved, or reported in the literature at the very least.

Finally, further study of the interplay between CSMCs and the associated ECM is clearly necessary, as results may challenge the traditional view of cervical collagen being the primary/sole determinant of cervical competence. If altered anatomy at the proximal cervix is a cause of CIn, this would provide support for

interventions that aim to increase strength or distribute forces at the internal os, such as cerclage or cervical pessaries, and may potentially improve the efficacy of these methods. Therefore, researchers and clinicians must work cooperatively to identify screening tools to better identify this subset of women.

Chapter 7 References

Aggarwal, M., Zhang, J., Pletnikova, O., Crain, B., Troncoso, J., and Mori, S. 2013. Feasibility of creating a high-resolution 3D diffusion tensor imaging based atlas of the human brainstem: a case study at 11.7 T. *NeuroImage*. **74**, pp. 117–127.

Akins, M.L., Luby-Phelps, K., Bank, R.A., and Mahendroo, M. 2011. Cervical Softening During Pregnancy: Regulated Changes in Collagen Cross-Linking and Composition of Matricellular Proteins in the Mouse. *Biology of Reproduction*. **84**(5), pp. 1053–1062.

Akins, M.L., Luby-Phelps, K. and Mahendroo, M. 2010. Second harmonic generation imaging as a potential tool for staging pregnancy and predicting preterm birth. *Journal of biomedical optics*. **15**(2), p. 026020.

Alfirevic, Z., Stampalija, T., and Medley, N. 2012. Cervical stitch (cerclage) for preventing preterm birth in singleton pregnancy. *Cochrane Database of Systematic Reviews*. [Online]. Issue 6. Art. No. CD008991 [Accessed 23 May 2017].

Alfirevic, Z., Owen, J., Carreras, M.E, Sharp, A.N., Sazchoqski, J.M., and Goya, M. 2013. Vaginal progesterone, cerclage or cervical pessary for preventing preterm birth in asymptomatic singleton pregnant women with a history of preterm birth and a sonographic short cervix. *Ultrasound in Obstetrics & Gynecology*. **41**(2), pp. 146–151.

Anthony, G.S., Fisher, J., Coutts, J.R., Calder, A.A. 1982. Forces required for surgical dilatation of the pregnant and non-pregnant human cervix. *British Journal of Obstetrics and Gynaecology*. **89**(11), pp. 913–916.

Aspden, R. M. 1988. Collagen Organisation in the Cervix and its Relation to Mechanical Function. *Collagen and Related Research*. **8**(2), pp. 103–112.

Asplund, J. 1952. The uterine cervix and isthmus under normal and pathological conditions; a clinical and roentgenological study. *Acta radiologica. Supplementum*. **37**(91), pp. 1–76.

Athanasiou, S., Khullar, V., Boos, K., Salvatore, S., and Cardoza, L. 1999. Imaging the urethral sphincter with three-dimensional ultrasound. *Obstetrics & Gynecology*. **94**(2), pp. 295–301.

Bammer, R., Acar, B. and Moseley, M.E. 2003. In vivo MR tractography using diffusion imaging. *European journal of radiology*, **45**(3), pp. 223–234.

Bartram, C. I. 2005.. Functional anorectal imaging. *Abdominal Imaging*. **30**(2), pp. 195–203.

Basser, P.J., Mattiello, J. and LeBihan, D. 1994. MR diffusion tensor spectroscopy and imaging. *Biophysical Journal*. **66**(1), pp. 259–267.

Becher, N., Adams Waldorf, K., Hein, M., and Uldberg, N. 2009. The cervical mucus plug: structured review of the literature. *Acta Obstetricia et Gynecologica Scandinavica*. **88**(5), pp. 502–513.

Beckmann, C. R. B., Ling, F.W., Barzansky, B.M., Herbert, W.N.P., Laube, D.W., and Smith, R.P. 2010. *Obstetrics and Gynecology*. 6th edn. Baltimore: Lippincott Williams & Wilkins.

Bereza, T., Tomaszerwski, K.A., Balajewicz-Nowak, M., Mizia, E., Pasternak, A., and Walocha, J. 2012. The vascular architecture of the supravaginal and vaginal

parts of the human uterine cervix: a study using corrosion casting and scanning electron microscopy. *Journal of Anatomy*. **221**(4), pp. 352–357.

Bergelin, I. and Valentin, L. 2001. Patterns of normal change in cervical length and width during pregnancy in nulliparous women: a prospective, longitudinal ultrasound study. *Ultrasound in Obstetrics and Gynecology*. **18**(3), pp. 217–222.

Berghella, V., Rafael, T.J., Szychowski, J.M., Rust, O.A., Owen, J. 2011. Cerclage for short cervix on ultrasonography in women with singleton gestations and previous preterm birth: a meta-analysis. *Obstetrics and Gynecology*. **117**(3), pp. 663–671.

Berghella, V., Gimovsky, A.C., Levine, L.D., and Vink, J. 2017. Cesarean in the second stage: a possible risk factor for subsequent spontaneous preterm birth. *American Journal of Obstetrics and Gynecology*. **217**(1), pp. 1-3.

Bergsjø, P., Bakketeig, L. and Eikhom, S.N. 1979. Duration of labour with spontaneous onset. *Acta Obstetricia et Gynecologica Scandinavica*. **58**(2), pp. 129–134.

Le Bihan, D., Mangin, J.F., Poupon, C., Clark, C.A., Pappata, S., Molko, N., and Chabriat. 2001. Diffusion tensor imaging: Concepts and applications. *Journal of Magnetic Resonance Imaging*. **13**(4), pp. 534–546.

Blaisdell, F. E. 1917. The anatomy of the sacro-uterine ligaments. *The Anatomical Record*. **12**(1), pp. 1–42.

Bourne, R.M., Bongers, A., Chatterjee, A., Sved, P., and Watson, G. 2016. Diffusion anisotropy in fresh and fixed prostate tissue ex vivo. *Magnetic Resonance*

in Medicine. **76**(2), pp. 626–634.

Buckingham, J.C., Buethe, R.A., and Danforth, D. N. 1965. Collagen-muscle ration in clinically normal and clinically incompetent cervices. *American Journal of Obstetrics and Gynecology*. **91**(2), pp. 232–237.

Butler-Manuel, S.A., Buttery, L.D, A'Hern, R.P., Polak, J.M., and Barton, D.P. 2000. Pelvic nerve plexus trauma at radical hysterectomy and simple hysterectomy: the nerve content of the uterine supporting ligaments. *Cancer*. **89**(4), pp. 834–841.

Butler-Manuel, S. A., Buttery, L.D., Polak, J.M., A'Hernm R., Barton, D.P. 2008. Autonomic Nerve Trauma at Radical Hysterectomy: The Nerve Content and Subtypes Within the Superficial and Deep Uterosacral Ligaments. *Reproductive Sciences*. **15**(1), pp. 91–96.

Cabrol, D., Carbonne, B., Jannet, D., Baton, C., Bonoris, E., Dudzik, W., and Lehouezec, R. 1991. Prognostic Value of Cervical Distensibility Index Measurement in the Outcome of Pregnancies with Threatened Premature Labor. *Gynecologic and Obstetric Investigation*. **32**(1), pp. 28–32.

Callahan, T. and Caughey, A. B. 2013. *Blueprints Obstetrics and Gynecology*. 6th ed. Baltimore: Lippincott Williams & Wilkins.

Campbell, R. M. 1950. The anatomy and histology of the sacrouterine ligaments. *American Journal of Obstetrics and Gynecology*. **59**(1), pp. 1–12.

Cappelletti, M., Della Bella, S., Ferrazzi, E., Mavilio, D., and Divanovic, S. 2016. Inflammation and preterm birth. *Journal of Leukocyte Biology*. **99**(1), pp. 67–78.

Chan, V. and Perlas, A. 2011. Basics of ultrasound imaging. In: Narouze, S. ed. *Atlas of ultrasound-guided procedures in interventional pain management*. New York: Springer, pp. 13–19.

Chan, Y.L., Lam, W.W., Lau, T.K., Wong, S.P., Li, C.Y., and Metreweli, C. 1998. Cervical assessment by magnetic resonance imaging--its relationship to gestational age and interval to delivery. *The British Journal of Radiology*. **71**(842), pp. 155–159.

Chan, Y.Y., Jayaprakasan, K., Tan, A., Thorton, J.G., Coomarasamy, A., and Raine-Fenning, N.J. 2011. Reproductive outcomes in women with congenital uterine anomalies: a systematic review. *Ultrasound in Obstetrics & Gynecology*. **38**(4), pp. 371–382.

Chang, H, Sundman, M., Petit, L., Guhaniyogi, S., Chu, M., Petty, C., Song, A.W., and Chen, N. 2015. Human brain diffusion tensor imaging at submillimeter isotropic resolution on a 3 Tesla clinical MRI scanner. *NeuroImage*. **118**, pp. 667–675.

Chen, X., Nadiarynkh, O., Plotnikov, S., and Campagnola, P.J. 2012. Second harmonic generation microscopy for quantitative analysis of collagen fibrillar structure. *Nature protocols*. **7**(4), pp. 654–669.

Cole, E.E., Leu, P.B., Gomelsky, A., Revelo, P., Shappell, H., Scarpero, H.M., and Dmochowski, R.R. 2006. Histopathological evaluation of the uterosacral ligament: is this a dependable structure for pelvic reconstruction?. *BJU International*, **97**(2), pp. 345–348.

Csapo, A.I. and Pulkkinen, M. 1978. Indispensability of the human corpus luteum in the maintenance of early pregnancy. Luteectomy evidence. *Obstetrical &*

Gynecological survey. **33**(2), pp. 69–81.

Cunningham, F.G., Kenneth, J.L., Bloom, S.L., Hauth, J.C., Rouse, D.J., and Song, C.Y. 2010. *Williams Obstetrics*. 23rd ed. New York: McGraw-Hill.

Curlin, M. and Bursac, D. 2013. Cervical mucus: from biochemical structure to clinical implications. *Frontiers in Bioscience (Scholar edition)*. **5**, pp. 507–515.

Danforth, D. 1954. The distribution and functional activity of the cervical musculature. *American Journal of Obstetrics and Gynecology*. **68**(5), pp. 1261–1271.

Danforth, D. 1947. The Fibrous Nature of the Human Cervix, and its relation to the isthmic segment in gravid and nongravid uteri. *American journal of obstetrics and gynecology*. **53**(4), pp. 541–560.

Danforth, D., Veis, A., Breen, M., Weinstein, H.G., Buckingham, J.C., Manalo, P. 1974. The effect of pregnancy and labor on the human cervix: Changes in collagen, glycoproteins, and glycosaminoglycans. *American Journal of Obstetrics and Gynecology*. **120**(5), pp. 641–651.

Danforth, D. 1983. The morphology of the human cervix. *Clinical Obstetrics and Gynecology*. **26**(1), pp. 7–13.

Danforth, D., Buckingham, J.C., and Roddick, J.W. 1960. Connective tissue changes incident to cervical effacement. *American Journal of Obstetrics and Gynecology*. **80**, pp. 939–945.

Danielson, K.G., Baribault, H., Holmes, D.F., Graham, H., Kadler, K.E., and Lozzo, R.V. 1997. Targeted disruption of decorin leads to abnormal collagen fibril

morphology and skin fragility.*The Journal of Cell Biology*. **136**(3), pp. 729–743.

DeSouza, N.M., Hawley, I.C., Schwieso, J.E., Gilderdale, D.J., and Soutter, W.P. 1994. The uterine cervix on *in vitro* and *in vivo* MR images: a study of zonal anatomy and vascularity using an enveloping cervical coil. *AJR. American Journal of Roentgenology*. **163**(3), pp. 607–612.

Drake, R., Vogl, W. and Mitchell, A. 2010. *Gray's Anatomy for Students*. 2nd edn. Philadelphia, PA: Churchill Livingston.

Dunn, O. 1964. Multiple comparisons using rank sums. *Technometrics*. 6, pp. 241–252.

Durnwald, C.P., Lynch, C.D., Walker, H., and Iams, J.D. 2009. The effect of treatment with 17 alpha-hydroxyprogesterone caproate on changes in cervical length over time Background and Objective. *American Journal of Obstetrics and Gynecology*. **201**(4), p. 410.

Ekman, G. Malmström, A., Uldbjerg, N., and Ulmsten, U. 1986. Cervical collagen: an important regulator of cervical function in term labor. *Obstetrics and Gynecology*. **67**(5), pp. 633–636.

Eriksen, H.A., Pajala, A., Leppilahti, J., and Risteli, J. 2002. Increased content of type III collagen at the rupture site of human Achilles tendon. *Journal of Orthopaedic Research*. **20**(6), pp. 1352–1357.

Esko, J. D., Kimata., K. and Lindahl, U. 2009. Proteoglycans and Sulfated Glycosaminoglycans Essentials of Glycobiology. In: Varki, A., Cummings, R.D., and Esko, J.D. ed. *Essentials of Glycobiology.* New York: Cold Spring Harbor

Laboratory Press, pp. 2015-2017.

Ewies, A.A.A., Al-Azzawi, F. and Thompson, J. 2003. Changes in extracellular matrix proteins in the cardinal ligaments of post-menopausal women with or without prolapse: a computerized immunohistomorphometric analysis. *Human Reproduction*. **18**(10), pp. 2189–2195.

Farquharson, R. 2006. The incompetent cervix. In: Jordan, J. and Singer, A. ed. *The Cervix* (2nd ed). Malden, Massachusetts: Blackwell, pp. 194–205.

Ferin, M., Jewelewicz, R., and Warren, M. P. 1993. *The menstrual cycle : physiology, reproductive disorders, and infertility*. Oxford: Oxford University Press.

Fiocchi, F., Nocetti, L., Siopis, E., Curra, S., Costi, T., Ligabue, G., and Torricelli, P. 2012. In vivo 3 T MR diffusion tensor imaging for detection of the fibre architecture of the human uterus: a feasibility and quantitative study. *The British Journal of Radiology*. **85**(1019), pp. e1009-e1017.

Fiocchi, F., Petrella, E., Nocetti, L., Curra, S., Ligabue, G., Costi, T., Torricelli, P., and Facchinetti, F. 2015. Transvaginal ultrasound assessment of uterine scar after previous caesarean section: comparison with 3T-magnetic resonance diffusion tensor imaging. *La Radiologia Medica*. **120**(2), pp. 228–238.

FitzGerald, T.B. 1949. The obstetric capacity of the undilated cervix. *BJOG: An International Journal of Obstetrics and Gynaecology*. **56**(2), pp. 229–236.

Fluhmann, C.F. 1957. The nature and development of the so-called glands of the cervix uteri. *American Journal of Obstetrics and Gynecology*, **74**(4), pp. 753–766.

Fonseca, E.B., Celik, E., Parra, M., Singh, M., Nicolaides, K.H. 2007. Progesterone

and the Risk of Preterm Birth among Women with a Short Cervix. *New England Journal of Medicine*. **357**(5), pp. 462–469.

De Franco, E.A., O'Brien, J.M., Adair, C.D., Lewis, D.F., Hall, D.R., Fuse, S., Soma-Pillay, P., Porter, K., How, H., Schakis, R., Eller, D., Trivedi, Y., Vanburen, G., Khandelwal, M., Trofatter, K., Vidyadhari, D., Vijayaraghaven, J., Weeks, J., Dattel, B., Newton, E., Chazotte, C., Valezuela, G., Calda, P., Bsharat, M., and Creasy, G.W. 2007. Vaginal progesterone is associated with a decrease in risk for early preterm birth and improved neonatal outcome in women with a short cervix: a secondary analysis from a randomized, double-blind, placebo-controlled trial. *Ultrasound in Obstetrics and Gynecology*. **30**(5), pp. 697–705.

Fuchs, T. Woyton, R., Pormorski, M., Wiatrowski, A., Slejman, N., Tomialowicz, M., Florianski, J., Milnerowicz-Nabzdyk, E., and Zimmer, M. 2013. Sonoelastography of the uterine cervix as a new diagnostic tool of cervical assessment in pregnant women – preliminary report. *Polish Gynaecology*. **84**(1), pp. 12-16.

Fujimoto, K., Kido, A., Okada, T., Uchikoshi, M., and Togashi, K. 2013. Diffusion tensor imaging (DTI) of the normal human uterus in vivo at 3 tesla: comparison of DTI parameters in the different uterine layers. *Journal of magnetic resonance imaging : JMRI*. **38**(6), pp. 1494–1500.

Gan, Y., Yao, W., Myers, K.M., Vink, J.Y., Wapner, R.J., and Hendon, C.P. 2015. Analyzing three-dimensional ultrastructure of human cervical tissue using optical coherence tomography. *Biomedical optics express*. **6**(4), pp. 1090–1108.

Gandhi, S. V., Walker, D., Milnes, P., Mukherjee, S., Brown, B.H., Anumba, D.O.C. 2006. Electrical impedance spectroscopy of the cervix in non-pregnant and

pregnant women. *European Journal of Obstetrics & Gynecology and Reproductive Biology*. **129**(2), pp. 145–149.

Goya, M., Pratcorona, L., Merced, C., Rodo, C., Valle, L., Romero, A., Juan, M., Rodriguez, A., Munoz, B., Santacruz, B., Bello-Munoz, J.C., Llurba, E., Higueras, T., Cabero, L., and Carreras, E. 2012. Cervical pessary in pregnant women with a short cervix (PECEP): an open-label randomised controlled trial. *Lancet*. **379**(9828), pp. 1800–1806.

Granström, L, Ekman, G., Ulmsten, and Malmström, A. 1989. Changes in the connective tissue of corpus and cervix uteri during ripening and labour in term pregnancy. *British Journal of Obstetrics and Gynaecology*. **96**(10), pp. 1198–1202.

Granström, L., Ekman, G. and Malmström, A. 1991. Insufficient remodelling of the uterine connective tissue in women with protracted labour. *British Journal of Obstetrics and Gynaecology.* **98**(12), pp. 1212–1216.

Gravett, M. G., Rubens, C. E. and Nunes, T. M. 2010. Global report on preterm birth and stillbirth (2 of 7): discovery science. *BMC Pregnancy and Childbirth*. **10**(Suppl 1), p. S2.

Grobman, W.A., Thom, E.A., Spong, C.Y., Iams, J.D., Saade, G.R., Mercer, B.M., Tita, A.T., Rouse, D.J., Sorokin, Y., Wapner, R.J., Leveno, K.J., Blackwell, S., Esplin, M.S., Tolosa, J.E., Thorp, J.M., Caritis, S.N., and Van Drosten, J.P. 2012. 17 alpha-hydroxyprogesterone caproate to prevent prematurity in nulliparas with cervical length less than 30 mm. *American Journal of Obstetrics and Gynecology*. **207**(5), pp. 390.e1–8.

Guilfoyle, D.N., Helpern, J.A. and Lim, K.O. 2003. Diffusion tensor imaging in fixed

brain tissue at 7.0 T. *NMR in biomedicine*. **16**(2), pp. 77–81.

Gurcan, M.N., Boucheron, L.E., Can, A., Madabhushi, A., Rajpoot, N.M., and Yener, B. 2009. Histopathological image analysis: a review. *IEEE reviews in Biomedical Engineering*. **2**, pp. 147–171.

Guzman, ER., Mellon, R., Vintzileos, A.M., Ananth, C.V., Walters, C., and Gipson, K. 1998. Relationship between endocervical canal length between 15-24 weeks gestation and obstetric history. *The Journal of Maternal-Fetal medicine*. **7**(6), pp. 269–272.

Hansen, L.K., Becher, N., Bastholm, S., Glavid, J., Ramsing, M., Kim, C.J., Romero, R., Jensen, J.S., and Uldbjerg, N. 2014. The cervical mucus plug inhibits, but does not block, the passage of ascending bacteria from the vagina during pregnancy. *Acta Obstetricia et Gynecologica Scandinavica*. **93**(1), pp. 102–108.

Hassan, S.S., Romero, R., Beryy, S.M., Dang, K., Blackwell, S.C., Treadwell, M.C., and Wolfe, H.M. 2000. Patients with an ultrasonographic cervical length ≤15 mm have nearly a 50% risk of early spontaneous preterm delivery. *American Journal of Obstetrics and Gynecology*. **182**(6), pp. 1458–1467.

Hassan, S.S., Romero, R., Gotsch, F., Nikita, R.N., and Chaiworapongsa, T. 2011. Cervical Insufficiency. In: Winn, H., Chervenak, F., and Romero, R. eds. *Clinical Maternal-Fetal Medicine Online*. Informa healthcare.

Hassan, S.S., Romero, R., Vidyadhari, D., Fusey, S., Baxter, J.K., Khandelwal, M., Vijayaraghavan, J., Trivedi, Y., Soma-Pillay, P., Sambarey, P., Dayal, A., Potapov, V., O'Brien, J., Astakhov, V., Yuzko, O., Kinzler, W., Dattel, B., Sehdev, H., Mazheika, L., Manchilenko, D., Gervasi, M.T., Sullican, L., Conde-Agudelo, A.,

Phillips, J.A., and Creasy, G.W. 2011. Vaginal progesterone reduces the rate of preterm birth in women with a sonographic short cervix: a multicenter, randomized, double-blind, placebo-controlled trial. *Ultrasound in Obstetrics & Gynecology*. **38**(1), pp. 18–31.

Hee, L., Sandager, P., Petersen, O., and Uldbjerg, N. 2013. Quantitative sonoelastography of the uterine cervix by interposition of a synthetic reference material. *Acta Obstetricia et Gynecologica Scandinavica*. **92**(11), pp. 1244–1249.

Hee, L., Liao, D., Sandager, P., Gregersen, H., and Uldbjerg, N. 2014. Cervical Stiffness Evaluated In Vivo by Endoflip in Pregnant Women. *PLoS ONE*. **9**(3), p. e91121.

House, M., O'Callaghan, M., Bahrami, S., Chelmow, D., Kini, J., Wu, D., Patz, S., and Bhadelia, R.A. 2005. Magnetic resonance imaging of the cervix during pregnancy: effect of gestational age and prior vaginal birth. *American Journal of Obstetrics and Gynecology*. **193**(4), pp. 1554–1560.

House, M., Bhadelia, R.A., Myers, K.M., and Socrate, S. 2009. Magnetic resonance imaging of three-dimensional cervical anatomy in the second and third trimester. *European Journal of Obstetrics, Gynecology, and Reproductive Biology*. **144**(Suppl 1), pp. S65-69.

House, M., Kaplan, D.L., and Socrate, S. 2009. Relationships between mechanical properties and extracellular matrix constituents of the cervical stroma during pregnancy. *Seminars in Perinatology*. **33**(5), pp. 300–307.

House, M., McCabe, R., and Socrate, S. 2013. Using imaging-based, three-dimensional models of the cervix and uterus for studies of cervical changes during

pregnancy. *Clinical anatomy.* **26**(1), pp. 97–104.

House, M., and Socrate, S. 2006. The cervix as a biomechanical structure. *Ultrasound in Obstetrics & Gynecology : the official journal of the International Society of Ultrasound in Obstetrics and Gynecology*. **28**(6), pp. 745–749.

Hricak, H., Chang, Y.C., Cann, C.E., and Parer, J.T. 1990. Cervical incompetence: preliminary evaluation with MR imaging. *Radiology*. **174**(3), pp. 821–826.

Hughesdon, P.E. 1952. The fibromuscular structure of the cervix and its changes during pregnancy and labour. *BJOG: An International Journal of Obstetrics and Gynaecology*. **59**(6), pp. 763–776.

Hurton, T., Morrill, H., Mascola, M., York, C., and Bromley, B. 1998. Cervical varices: an unusual etiology for third-trimester bleeding. *Journal of Clinical Ultrasound: JCU*. **26**(6), pp. 317–319.

Iams, J.D., Johnson, F.F., Sonek, J., Sachs, L., Gebauer, C., and Samuels, P. 1995. Cervical competence as a continuum: a study of ultrasonographic cervical length and obstetric performance. *American Journal of Obstetrics and Gynecology*. **172**(4 Pt 1), pp. 1097–1103

Iams, J.D., Goldenburg, R.L., Meis, P.J., Mercer, B.M., Moawad, A., Das, A., Thom, E., McNellis, D., Copper, R.L., Johnson, F., and Roberts, J.M. 1996. The length of the cervix and the risk of spontaneous premature delivery. National Institute of Child Health and Human Development Maternal Fetal Medicine Unit Network. *The New England Journal of Medicine.* **334**(9), pp. 567–572.

Iams, J.D. 2009. Cervical Insufficiency. In: Creasy, R.K., Lockwood, C.J., Moore,

T.R., Greene, M.E., Copel, J.A., and Silver, R.M. eds. *Creasy and Resnick's Maternal-Fetal Medicine- Principles and Practice*. 6th edn. Philadelphia, PA.

Iams, J. and Goldenberg, R. 1996. The length of the cervix and the risk of spontaneous premature delivery. *The New England Jounal of Medicine*. **334**(9), pp. 567–572.

Ivy, A.C., Hartman, C.G. and Koff, A. 1931. The contractions of the monkey uterus at term. *American Journal of Obstetrics and Gynecology*. **22**(3), pp. 388–399.

Iwahashi, M., Muragaki, Y., Ooshima, A., and Umesaki, N. 2003. Decreased Type I Collagen Expression in Human Uterine Cervix during Pregnancy. *The Journal of Clinical Endocrinology & Metabolism*. **88**(5), pp. 2231–2235.

Janve, V.A. Zu, Z., Yao, S.Y., Li, K., Zhang, F.L., Wilson, K.J., Ou, X., Does, M.D., Subramaniam, S., Gochberg, D.F. 2013. The radial diffusivity and magnetization transfer pool size ratio are sensitive markers for demyelination in a rat model of type III multiple sclerosis (MS) lesions. *NeuroImage*. **74**, pp. 298–305.

Jokhi, R.P. Ghule, V.Q., Brown, B.H., and Anumba, D.O.C. 2009. Reproducibility and repeatability of measuring the electrical impedance of the pregnant human cervix-the effect of probe size and applied pressure. *Biomedical Engineering online*. **8**(10), p. 10.

Jokhi, R.P., Brown, B.H., and Anumba, D.O.C. 2009. The role of cervical Electrical Impedance Spectroscopy in the prediction of the course and outcome of induced labour. *BMC Pregnancy and Childbirth*. **9**, p. 40.

Junge, K., Klinge, U., Rosch, R., Mertens, P.R., Kirch, J., Klosterhalfen, B., Lynen,

P., and Schumpelik, V. 2004. Decreased collagen type I/III ratio in patients with recurring hernia after implantation of alloplastic prostheses. *Langenbeck's Archives of Surgery*. **389**(1), pp. 17–22.

Kao, C. 1989. Electrophysiological properties of uterine smooth muscle. In: Wynn, R., and Jollie, W. eds. *Physiology of the uterus*. New York: Plenum Medical Book Company, pp. 403–454.

Kao, K.Y. and Leslie, J.G. 1977. Polymorphism in human uterine collagen. *Connective Tissue Research*. **5**(2), pp. 127–129.

Kato, T., Murakami, G. and Yabuki, Y. 2002. Does the cardinal ligament of the uterus contain a nerve that should be preserved in radical hysterectomy?. *Anatomical Science International*. **77**(3), pp. 161–168.

Kaur, A., and Kaur, A. 2011. Transvaginal ultrasonography in first trimester of pregnancy and its comparison with transabdominal ultrasonography. *Journal of Pharmacy and Bioallied Sciences*. **3**(3), pp. 329-338.

Keene, D.R., Sakai, L.Y., Bachinger, H.P., and Burgeson, R.E. 1987. Type III collagen can be present on banded collagen fibrils regardless of fibril diameter. *The Journal of Cell Biology*. **105**(5), pp. 2393–2402.

Keirse, M. J. 1990. Progestogen administration in pregnancy may prevent preterm delivery. *British Journal of Obstetrics and Gynaecology*. **97**(2), pp. 149–154.

Kiwi, R., Neuman, M.R., Merkatz, I.R., Selim, M.A., and Lysikiewicz, A. 1988. Determination of the elastic properties of the cervix. *Obstetrics and Gynecology*. **71**(4), pp. 568–574.

Klinge, U., Si, Z.Y., Zheng, H., Schumpelick, V., Bhardwaj, R.S., and Klosterhalfen, B. 2001. Collagen I/III and Matrix Metalloproteinases (MMP) 1 and 13 in the Fascia of Patients With Incisional Hernias. *Journal of Investigative Surgery*. **14**(1), pp. 47–54.

Knight, M., Kurinczuk, J.J., Spark, P., and Brocklehurst, P. 2008. Cesarean Delivery and Peripartum Hysterectomy. *Obstetrics & Gynecology*. **111**(1), pp. 97–105.

Komisaruk, B. R., Whipple, B., Crawford, A., Liu, W.C., Kalnin, A., and Mosier, K. 2004. Brain activation during vaginocervical self-stimulation and orgasm in women with complete spinal cord injury: fMRI evidence of mediation by the vagus nerves. *Brain research*. **1024**(1–2), pp. 77–88.

Komisaruk, B.R., Gerdes, C.A. and Whipple, B. 1997. “Complete” spinal cord injury does not block perceptual responses to genital self-stimulation in women. *Archives of Neurology*. **54**(12), pp. 1513–1520.

Kondo, Y., Homma, Y., Takahashi, S., Kitamura, T., and Kawabe, K. 2001. Transvaginal ultrsound of urethral sphincter at the mid urethrea in continent and incontinent women. *The Journal of Urology*. **165**(1), pp. 149–152.

Koyama, H., Raines, E.W., Bornfeldt, K.E., Roberts, J.M., and Ross, R. 1996. Fibrillar collagen inhibits arterial smooth muscle proliferation through regulation of Cdk2 inhibitors. *Cell*. **87**(6), pp. 1069–1078.

Koyama, S., Tomimatsu, T., Kanagawa, T., Sawada, K., Tsutsui, T., and Kimura, T. 2010. Cervical insufficiency following cesarean delivery after prolonged second stage of labor: Experiences of two cases. *Journal of Obstetrics and Gynaecology*

Research. **36**(2), pp. 411–413.

Kuwata, T., Matsubara, S., Taniguchi, N., Ohkuchi, A., Ohkusa, T., and Suzuki, M. 2010. A novel method for evaluating uterine cervical consistency using vaginal ultrasound gray-level histogram. *Journal of Perinatal Medicine*. **38**(5), pp. 491-494

Lang, C.T., Iams, J.D., Tangchitnob, E., Socrate, S., and House, M. 2010. A method to visualize 3-dimensional anatomical changes in the cervix during pregnancy: a preliminary observational study. *Journal of Ultrasound in Medicine : official journal of the American Institute of Ultrasound in Medicine*. **29**(2), pp. 255–260.

Lash, A.F. and Lash, S.R. 1950. Habitual abortion; the incompetent internal os of the cervix. *American Journal of Obstetrics and Gynecology*. **59**(1), pp. 68–76.

Lau, T.Y., Sangha, H.K., Chien, E.K., McFarlin, B.L., Wagoner Johnson, A.J., and Toussaint, K.C. 2013. Application of Fourier transform-second-harmonic generation imaging to the rat cervix. *Journal of Microscopy*. **251**(1), pp. 77–83.

Lazar, P., Gueguen, S., Dreyfus, J., Renaud, R., Pontonnier, G., and Papiernik, E. 1984. Multicentred controlled trial of cervical cerclage in women at moderate risk of preterm delivery. *BJOG: An International Journal of Obstetrics and Gynaecology*. **91**(8), pp. 731–735.

Leppert, P.C., Keller, S., Cerreta, J., Hosannah, Y., and Mandl, I. 1983. The content of elastin in the uterine cervix. *Archives of Biochemistry and Biophysics*. **222**(1), pp. 53–58.

Leppert, P., Cerreta, J. and Mandl, I. 1986. Orientation of elastic fibers in the

human cervix. *American Journal of Obstetrics and Gynecology*. **155**(1), pp. 219–224.

Leppert, P. and Keller, S. 1982. Conclusive evidence for the presence of elastin in human and monkey cervix. *American Journal of Obstetrics and Gynecology*. **142**(2), pp. 179–182.

Levine, L.D., Sammel, M.D., Hirshberg, A., Elovitz, M.A., and Srinivas, S.K. 2015. Does stage of labor at time of cesarean delivery affect risk of subsequent preterm birth?. *American Journal of Obstetrics and Gynecology*. **212**(3), pp. 360.e1-360.e7.

Levine, L.D. and Srinivas, S.K. 2016. Length of second stage of labor and preterm birth in a subsequent pregnancy. *American Journal of Obstetrics and Gynecology*. 214(4), pp. 535.e1-535.e4.

Li, S., Van Den Diepstraten, C., D'Souza, S.J., Chan, B.M., and Pickering, J.G. 2003. Vascular smooth muscle cells orchestrate the assembly of type I collagen via alpha2beta1 integrin, RhoA, and fibronectin polymerization. *The American Journal of Pathology*. **163**(3), pp. 1045–1056.

Liem, S.M., van Pampus, M.G., Mol, B.W., and Bekedam, D.J. 2013. Cervical Pessaries for the Prevention of Preterm Birth: A Systematic Review. *Obstetrics and Gynecology International*, 2013, pp. 1–10.

Liu, X., Wu, H., Byrne, M., Krane, S., and Jaenisch, R. 1997. Type III collagen is crucial for collagen I fibrillogenesis and for normal cardiovascular development. *Proceedings of the National Academy of Sciences of the United States of America*. **94**(5), pp. 1852–1856.

Loudon, J.A.Z., Elliot, C.L., Hills, F., and Bennett,P.R. 2003. Progesterone Represses Interleukin-8 and Cyclo-Oxygenase-2 in Human Lower Segment Fibroblast Cells and Amnion Epithelial Cells1. *Biology of Reproduction*. **69**(1), pp. 331–337.

Ludmir, J. and Sehdev, H.M. 2000. Anatomy and physiology of the uterine cervix. *Clinical Obstetrics and Gynecology*. **43**(3), pp. 433–439.

Lui, P.P., Chan, L.S., Lee, Y.W., Du, S.C., and Chan, K.M. 2010. Sustained expression of proteoglycans and collagen type III/type I ratio in a calcified tendinopathy model. *Rheumatology*. **49**(2), pp. 231–239.

Maillot, K.V and Zimmermann, B.K. 1976. The solubility of collagen of the uterine cervix during pregnancy and labour. *Archiv fur Gynakologie*. **220**(4), pp. 275–280.

El Maradny, E., Kanayama, N., Kobayashi, H., Hossain, B., Khatun, S., Liping, S., Kobayashi., and Terao, T. 1997. The role of hyaluronic acid as a mediator and regulator of cervical ripening. *Human Reproduction.* **12**(5), pp. 1080–1088.

March of Dimes. 2012 *WHO | Born Too Soon: The Global Action Report on Preterm Birth*. In: C.P. Howson, M. Kinney, and J.E. Lawn. Geneva: World Health Organization.

Marieb, E. 2004 *Human Anatomy and Physiology*. 6th ed . San Francisco: Pearson Education.

Martyn, F., McAuliffe, F.M. and Wingfield, M. 2014. The role of the cervix in fertility: is it time for a reappraisal?. *Human Reproduction*. **29**(10), pp. 2092–2098.

McCarthy, S., Tauber, C. and Gore, J. 1986. Female pelvic anatomy: MR

assessment of variations during the menstrual cycle and with use of oral contraceptives. *Radiology*, **160**(1), pp. 119–123.

McFarlin, B.L. Bigelow, T.A., Laybed, Y., O'Brien, W.D., Oelze, M.L., and Abramowicz, J.S. 2010. Ultrasonic attenuation estimation of the pregnant cervix: a preliminary report. *Ultrasound in Obstetrics & Gynecology : the official journal of the International Society of Ultrasound in Obstetrics and Gynecology*. **36**(2), pp. 218–225.

Meis, P.J., Klebanoff, M., Thom, E., Dombrowski, M.P., Sibai, B., Moawad, A.H., Spong, C.Y., Hauth, J.C., Miodovnik, M., Varner, M.W., Leveno, K.J., and Caritis, S.N. 2003. Prevention of Recurrent Preterm Delivery by 17 Alpha-Hydroxyprogesterone Caproate. *New England Journal of Medicine*. **348**(24), pp. 2379–2385.

Mekkaoui, C., Porayette, P., Jackowski, M.P., Kostis, W.J., Dai, G., Sanders, S., and Sosnovik, D.E. 2013. Diffusion MRI Tractography of the Developing Human Fetal Heart. *PLoS ONE*. **8**(8), p. e72795.

Moalli, P.A., Talarico, L.C., Sung, V.W., Klingensmith, W.L., Shand, S.H., Meyn, L.A., and Watkins, S.C. 2004. Impact of menopause on collagen subtypes in the arcus tendineous fasciae pelvis. *American Journal of Obstetrics and Gynecology*. **190**(3), pp. 620–627.

Mori, S. 2007. *Introduction to Diffusion Tensor Imaging*. London: Elsevier.

Mourad, M., Qin, S., Ananth, C.V., Fu, A., Yoshida, K., Myers, K.M., Kitajewski, J., Shawber, C., Wapner, R., Sheetz, M., and Vink, J. .2017. 109: Human cervical smooth muscle stretch increases pro-inflammatory cytokine secretion. *American*

Journal of Obstetrics and Gynecology. **216**(1), pp. S77–S78.

MRC/RCOG. 1993. Final report of the Medical Research Council/Royal College of Obstetricians and Gynaecologists multicentre randomised trial of cervical cerclage. MRC/RCOG Working Party on Cervical Cerclage. *British Journal of Obstetrics and Gynaecology*. **100**(6), pp. 516–523.

Myers, K.M., Hendon, C.P., Gan, Y., Yao, W., Fernandez, M, Vink, J., and Wapner. 2015. A continuous fiber distribution material model for human cervical tissue. *Journal of Biomechanics*. **48**(9), pp. 1533–1540.

Myers, K.M., Feltovich, H., Mazza, E., Vink, J., Bajka, M., Wapner, R.J., Hall, T.J., and House, M. 2015. The mechanical role of the cervix in pregnancy. *Journal of Biomechanics*. **48**(9), pp. 1511–1523.

Narice, B.F., Green, N.H., MacNeil, S., and Anumba, D.O.C. 2016. Second Harmonic Generation microscopy reveals collagen fibres are more organised in the cervix of postmenopausal women. *Reproductive Biology and Endocrinology*. **14**(1), p. 70.

Norman, J.E., Marlow, N., Messow, C.M., Shennan, A., Bennett, P., Thornton, S., Robson, S.C., McConnachie, A., Petrou, S., Sebire, N.J., Lavender, T., Whyte, S., and Norrie, J.N. 2016. Vaginal progesterone prophylaxis for preterm birth (the OPPTIMUM study): a multicentre, randomised, double-blind trial. *The Lancet*. **387**(10033), pp. 2106–2116.

Norman, M., Ekman, G., UlmSten, U., Barchan, K., and Malmstrom, A. 1991. Proteoglycan metabolism in the connective tissue of pregnant and non-pregnant human cervix. An in vitro study. *The Biochemical Journal*. **275,** pp. 515–520.

Norwitz, E.R. and Caughey, A.B. 2011. Progesterone supplementation and the prevention of preterm birth. *Reviews in Obstetrics & Gynecology*. **4**(2), pp. 60–72.

O'Brien, J.M., Adair, C.D., Lewis, D.F., Hall, D.R., Defranco, E.A., Fusey, S., Soma-Pillay, P., Porter, K., How, H., Schackis, R., Eller, D., Trivedi, Y., Vanburen, G., Khandelwal, M., Trofatter, K., Vidyadhari, J., Weeks, J., Dattel, B., Newton, E., Chazotte, C., Valenzuela, G., Calda, P., Bsharat, M., and Creasy, G.W. 2007. Progesterone vaginal gel for the reduction of recurrent preterm birth: primary results from a randomized, double-blind, placebo-controlled trial. *Ultrasound in Obstetrics and Gynecology*. **30**(5), pp. 687–696.

Oelrich, T.M. 1980. The urethral sphincter muscle in the male. *American Journal of Anatomy*. **158**(2), pp. 229–246.

ONS., 2011. Gestation-specific Infant Mortatility in England and Wales 2011. *ONS.* [Online] [Accessed 21 November 2014] Available from: http://www.ons.gov.uk/ons/publications/re-reference-tables.html?edition=tcm:77-320891.

Osmers, R., Rath, W., Pflanz, M.A., Kuhn, W., Stuhlsatz, H.W., and Szeverenyi, M. 1993. Glycosaminoglycans in cervical connective tissue during pregnancy and parturition. *Obstetrics and Gynecology*. **81**(1), pp. 88–92.

Owen, J., Hankins, G., Iams, J.D., Berghella, V., Sheffield, J.S., Perez-Delboy, A., Egerman, R.S., Wing, D.A., Tomlinson, M., Silver, R., Ramin, S.M., Guzman, E.R., Gordon, M., How, H.Y., Knudtson, E.J., Szychowski, J.M., Cliver, S., and Hauth, J.C. 2009. Multicenter randomized trial of cerclage for preterm birth prevention in high-risk women with shortened midtrimester cervical length. *American Journal of*

Obstetrics and Gynecology. **201**(4), pp. 375.e1–8.

Oxlund, B.S., Ørtoft, G., Brüel, A., Danielsen, C.C., Oxlund, H., and Uldbjerg, N. 2010. Cervical collagen and biomechanical strength in non-pregnant women with a history of cervical insufficiency. *Reproductive Biology and Endocrinology.* **8**, p. 92.

Oxlund, B. S., Ørtoft, G., Brüel, A., Danielsen, C. C., Bor, P., Oxlund, H., and Uldbjerg, N. 2010. Collagen concentration and biomechanical properties of samples from the lower uterine cervix in relation to age and parity in non-pregnant women. *Reproductive Biology and Endocrinology.* **8**, p. 82.

Pajntar, M., Verdenik, I., Pusenjak, S., Rudel, D., and Leskosek, B. 1998. Activity of smooth muscles in human cervix and uterus. *European Journal of Obstetrics & Gynecology and Reproductive Biology*. **79**, pp. 199–204.

Pajntar, M., Leskosek, B., Rudel, D., and Verdenik, I. 2001. Contribution of cervical smooth muscle activity to the duration of latent and active phases of labour. *BJOG : an international journal of Obstetrics and Gynaecology*. **108**(5), pp. 533–538.

Pajntar, M. and Verdenik, I. 1995. Electromyographic activity in cervices with very low Bishop score during labor. *International Journal of Gynecology & Obstetrics*. **49**(3), pp. 277–281.

Pak, O., Aldasev, A., Welsh, D., and Peacock, A. 2007. The effects of hypoxia on the cells of the pulmonary vasculature. *European Respiratory Journal*. **30**(2), pp. 364–372.

Palacios Jaraquemada, J.M., Garcia, Monaco, R., Barbosa, N.E., Ferle, L., Iriarte,

H., and Conesa, H.A. 2007. Lower uterine blood supply: extrauterine anastomotic system and its application in surgical devascularization techniques. *Acta Obstetricia et Gynecologica Scandinavica*. **86**(2), pp. 228–234.

Parikh, M., Rasmussen, M., Brubaker, L., Salomon, C., Sakamoto, K., Evenhouse, R., Ai, Z., and Damaser, M.S. 2004. Three dimensional virtual reality model of the normal female pelvic floor. *Annals of Biomedical Engineering*. **32**(2), pp. 292–296.

Parikh, R., Patel, A., Stack, T., Socrate, S., and House, M. 2011. How the cervix shortens: an anatomical study using 3-dimensional transperineal sonography and image registration in singletons and twins. *Journal of Ultrasound in Medicine: official journal of the American Institute of Ultrasound in Medicine*. **30**(9), pp. 1197–1204.

Parisi, V. 1988. Cervical Incompetence and Preterm Labor. *Clinical Obstetrics and Gynecology*. **31**(3), pp. 585–598.

Parra-Saavedra, M., Gomez, L., Barrero, A., Parra, G., Vergara, F., and Navarro, E. 2011. Prediction of preterm birth using the cervical consistency index. *Ultrasound in Obstetrics & Gynecology*. **38**(1), pp. 44–51.

Pervolaraki, E., Anderson, R.A., Benson, A.P., Hayes-Gill, B., Holden, A.V., Moore, B.J., Paley, M.N., and Zhang, H. 2013. Antenatal architecture and activity of the human heart. *Interface Focus*. **3**(2), pp. 20120065–20120065.

Pervolaraki, E., Dachtler, J., Anderson, R.A., and Holden, A.V. 2017. Ventricular myocardium development and the role of connexins in the human fetal heart. *Scientific Reports.* **7**(1), p. 12272.

Pessel, C., Moni, S., Zork, N., Brubaker, S., Vink, J., Fuchs, K., Nhan-Chang, C.L., Ananth, C.V., and Gyamfi-Bannerman, C. 2013. The effect of intramuscular progesterone on the rate of cervical shortening. *American Journal of Obstetrics and Gynecology*. **209**(3), pp. 269.e1-269.e7.

Petersen, L.K. and Uldbjerg, N. 1996. Cervical collagen in non-pregnant women with previous cervical incompetence. *European Journal of Obstetrics, Gynecology, and Reproductive Biology*. **67**(1), pp. 41–45.

Peyron, R., Aubeny, E., Targosz, V., Silvestre, L., Renault, M., Elkik, F., Leclerc, P., Ulmann, A., and Baulieu, E.E. 1993. Early Termination of Pregnancy with Mifepristone (RU 486) and the Orally Active Prostaglandin Misoprostol. *New England Journal of Medicine*. **328**(21), pp. 1509–1513.

Pfefferbaum, A., Sullivan, E.V., Hedehus, M., Lim, K.O., Adalsteinsson, E., and Moseley, M. 2000. Age-related decline in brain white matter anisotropy measured with spatially corrected echo-planar diffusion tensor imaging. *Magnetic Resonance in Medicine*. **44**(2), pp. 259–268.

Ramanah, R., Parratte, B., Arbez-Gindre, F., Maillet, R., and Riethmuller, D. 2008. The uterosacral complex: ligament or neurovascular pathway? Anatomical and histological study of fetuses and adults. *International Urogynecology Journal*. **19**(11), pp. 1565–1570.

Ramanah, R., Berger, M.B., Parratte, B.M., and DeLancey, J.O. 2012. Anatomy and histology of apical support: a literature review concerning cardinal and uterosacral ligaments. *International Urogynecology Journal*. **23**(11), pp. 1483–1494.

Range, R.L. and Woodburne, R.T. 1964. The gross and microscopic anatomy of the transverse cervical ligament. *American Journal of Obstetrics and Gynecology*. **90**(4), pp. 460–467.

Read, C.P., Word, R.A., Ruscheinsky, M.A., Timmons, B.C., and Mahendroo, M.S. 2007. Cervical remodeling during pregnancy and parturition: molecular characterization of the softening phase in mice. *Reproduction*, **134**(2), pp. 327–340.

Rechberger, T., Uldbjerg, N. and Oxlund, H. 1988. Connective tissue changes in the cervix during normal pregnancy and pregnancy complicated by cervical incompetence. *Obstetrics and Gynecology*. **71**(4), pp. 563–567.

Reusch, L.M., Feltovich, H., Carlson, L.C., Hall, G., Campagnola, P.J., Eliceiri, K.W., and Hall, T.J. 2013. Nonlinear optical microscopy and ultrasound imaging of human cervical structure. *Journal of biomedical optics*. **18**(3), p. 031110.

Roberts, A.D.G., Cordiner, J.W., Hart, D.M., Barlow, D.H., MacRae, D., and Leggate, I. 1988. The variation in cervical hydroxyproline and cervical water with age. *British Journal of Obstetrics and Gynaecology*. **95**(11), pp. 1159–1164.

Roberts, N., Magee, D., Song, Y., Brabazon, K., Shires, M., Crellin, D., Orsi, N.M., Quirke, R., Quirke, P, Treanor, D. 2012. Toward routine use of 3D histopathology as a research tool. *The American Journal of Pathology*. **180**(5), pp. 1835–1842.

Roddick, J., Buckingham, J. and Danforth, D. 1961. The Muscular Cervix-A Cause of Incomptency in Pregnancy. *Obstetrics & Gynecology*. **17**(5), pp. 562–565.

Rorie, D.K. and Newton, M. 1967. Histological and chemical studies of the smooth

muscle in the human cervix and uterus. *American Journal of Obstetrics and Gynecology*. **99**(4), pp. 466–469.

Royal College of Obstetricans and Gynaecologists. 2011. *Green-top Guideline No. 60: Cervical Cerclage*.

Rudel, D. and Pajntar, M. 1999. Active contractions of the cervix in the latent phase of labour. *BJOG: An International Journal of Obstetrics and Gynaecology*. **106**(5), pp. 446–452.

Ruifrok, A.C. and Johnston, D.A. 2001. Quantification of histochemical staining by color deconvolution. *Analytical and Quantitative Cytology and Histology*. **23**(4), pp. 291–299.

Rush, R.W., Isaacs, S., McPherson, K., Jones, L., Chalmers, I., and Grant, A. 1984. A randomized controlled trial of cervical cerclage in women at high risk of spontaneous preterm delivery. *British Journal of Obstetrics and Gynaecology*. **91**(8), pp. 724–730.

Sammour, R.N., Gonen, R., Ohel, G., and Leibovitz, Z. 2011. Cervical varices complicated by thrombosis in pregnancy. *Ultrasound in Obstetrics & Gynecology : the official journal of the International Society of Ultrasound in Obstetrics and Gynecology*. **37**(5), pp. 614–616.

Schlembach, D., Maul, H., Fittkow, C., Olson, G., Saade, G., and Garfield, R. 2003. Cross-linked collagen in the cervix of pregnant women with cervical insufficiency. *American Journal of Obstetrics and Gynecology*. **189**(6), p. S70.

Schmierer, K., Wheeler-Kingshott, C.A.M., Boulby, P.A., Scaravilli, F., Altmann,

D.R., Barker, G.J., Tofts, P.S., and Miller, D.H. 2007. Diffusion tensor imaging of post mortem multiple sclerosis brain. *NeuroImage*. **35**(2), pp. 467–477.

Schuliga, M., Ong, S.C., Soon, L., Zal, F., Harris, T., and Stewart, A.G. 2010. Airway smooth muscle remodels pericellular collagen fibrils: implications for proliferation. *American Journal of Physiology-Lung Cellular and Molecular Physiology*. **298**(4), pp. L584–L592.

Schuliga, M. 2015. Smooth Muscle and Extracellular Matrix Interactions in Health and Disease. In: Sakuma, K. ed. *Muscle Cell and Tissue*. London: IntechOpen, pp. 973–813.

Shimizu, T., Endo, M., and Yosizawa, Z. 1980. Glycoconjugates (Glycosaminoglycans and Glycoproteins) and Glycogen in the Human Cervix Uteri. *The Tohoku Journal of Experimental Medicine.* **131**, pp. 289–299.

Singer, A. and Jordan, J. 2006. The functional anatomy of the cervix, the cervical epithelium and the stroma. In: Jordan, J., Singer, A., Jones, H., and Shafi, M. eds *The Cervix*. 2nd ed. Malden, Massachusetts: Blackwell, pp. 13–37.

Smith, R., Imtiaz, M., Banney, D., Paul, J.W., and Young, R.C. 2015. Why the heart is like an orchestra and the uterus is like a soccer crowd. *American Journal of Obstetrics and Gynecology*. **213**(2), pp. 181–185.

Smith, S. B. and Ravel, J. 2017. The vaginal microbiota, host defence and reproductive physiology. *The Journal of Physiology*. **595**(2), pp. 451–463.

Sneider, K., Christiansen, O.B., Sundtoft, I.B., and Langhoff-Roos, J. 2016. Recurrence of second trimester miscarriage and extreme preterm delivery at 16-

27 weeks of gestation with a focus on cervical insufficiency and prophylactic cerclage. *Acta Obstetricia et Gynecologica Scandinavica*. **95**(12), pp. 1383–1390.

Song, S.K., Yoshino, J., Le, T.Q., Lin, S.J., Sun, S.W., Cross, A.H., and Armstrong, R.C. 2005. Demyelination increases radial diffusivity in corpus callosum of mouse brain. *NeuroImage*. **26**(1), pp. 132–140.

Stainback, R. 2007. Introduction to Echocardiography. In: Willerson, J., Cohn, J.N., Wellends, H.J.J., and Holmes, D.R. eds *Cardiovascular medicine*. London: Springer, p. 98.

Standring, S. 2004. *Gray's Anatomy: The Anatomical Basis of Clinical Practice*. 39th edn. Edinbrugh: Churchill Livingston.

Straach, K.J., Shelton, J.M., Richardson, J.A., Hascall, V.C., and Mahendroo, M.S. 2005. Regulation of hyaluronan expression during cervical ripening. *Glycobiology*. **15**(1), pp. 55–65.

Sultan, A.H., Nicholls, R.J., Kamm, M.A., Hudson, C.N., Beynon, J., and Bartram, C.I. 1993. Anal endosonography and correlation with in vitro and in vivo anatomy. *The British Journal of Surgery*. **80**(4), pp. 508–511.

Sultan, A.H., Kamm, M.A., Talbot, I.C., Nicholls, R.J., and Bartram, C.I. 1994. Anal endosonography for identifying external sphincter defects confirmed histologically. *The British Journal of Surgery*. **81**(3), pp. 463–465.

Sultan, A. H. 2003. The role of anal endosonography in obstetrics. *Ultrasound in Obstetrics and Gynecology*. **22**(6), pp. 559–560.

Sun, S.W., Neil, J.J. and Song, S.K. 2003. Relative indices of water diffusion

anisotropy are equivalent in live and formalin-fixed mouse brains. *Magnetic Resonance in Medicine*. **50**(4), pp. 743–748.

Sundtoft, I., Langhoff-Roos, J., Sandager, P., Sommer, S., and Uldbjerg, N. 2017. Cervical collagen is reduced in non-pregnant women with a history of cervical insufficiency and a short cervix. *Acta Obstetricia et Gynecologica Scandinavica*. **96**(8), pp. 984-990

Sundtoft, I., Sommer, S. and Uldbjerg, N. 2011. Cervical collagen concentration within 15 months after delivery. *American Journal of Obstetrics and Gynecology*. **205**(1), pp. 59.e1-59.e3.

Suzuki, M., Kayra, D., Elliot, W.M., Hogg, J.C., and Abraham, T. 2012. Second harmonic generation microscopy differentiates collagen type I and type III in COPD. *Multiphoton Microscopy in the Biomedical Sciences.*

Szekeres-Bartho, J. 1992. *Immunosuppression by Progesterone in Pregnancy*. Boca Raton, USA: CRC Press.

Tekesin, I., Hellmeyer, L., Heller, G., Romer, A., Kuhnert, M., and Schmidt, S. 2003. Evaluation of quantitative ultrasound tissue characterization of the cervix and cervical length in the prediction of premature delivery for patients with spontaneous preterm labor. *American Journal of Obstetrics and Gynecology*. **189**(2), pp. 532–539.

Thakar, R. and Sultan, A.H. 2004. Anal endosonography and its role in assessing the incontinent patient. *Best Practice & Research Clinical Obstetrics & Gynaecology*. **18**(1), pp. 157–173.

Tilbury, K., Lien, C.H., Chen, S.J., and Campagnola, P.J. 2014. Differentiation of Col I and Col III Isoforms in Stromal Models of Ovarian Cancer by Analysis of Second Harmonic Generation Polarization and Emission Directionality. *Journal of Biophysics.* **106**(2), pp. 354-365

Timmons, B., Akins, M. and Mahendroo, M. 2010. Cervical remodeling during pregnancy and parturition. *Trends in endocrinology and metabolism: TEM*. **21**(6), pp. 353–361.

Tommaso, S., Cavallotti, C., Malvasi, A., Vergara, D., Rizello, A., De Nuccio, F., and Tinelli, A. 2016. A Qualitative and Quantitative Study of the Innervation of the Human Non Pregnant Uterus. *Current Protein & Peptide Science*. **18**(2), pp. 140–148.

Uldbjerg, N., Ekman, G., Malmstrom, A., Olsson, K., and Ulmsten, U. 1983. Ripening of the human uterine cervix related to changes in collagen, glycosaminoglycans, and collagenolytic activity. *American Journal of Obstetrics and Gynecology*. **147**(6), pp. 662–666.

Vahanian, S.A., Lavery, J.A., Ananth, C.V., and Vintzileos, A. 2015. Placental implantation abnormalities and risk of preterm delivery: a systematic review and metaanalysis. *American Journal of Obstetrics and Gynecology*. **213**(4), pp. S78–S90.

Vink, J., Sudip, D., Hongyu, L., Mourad, M., Ndubisi, C., Myers, K.M., Kitajewski, J., Sheetz, M., Wapner, R., and Gallos, G. 2019. 557: Progesterone decreases human cervical smooth muscle cell contractility. *American Journal of Obstetrics and Gynecology*. **220**(1), p. S372.

Vink, J. and Myers, K. 2018. Cervical alterations in pregnancy. *Best Practice & Research Clinical Obstetrics & Gynaecology*. **52**, pp. 88–102.

Vink, J.Y., Qin, S., Brock, C.O., Zork, N.M., Feltovich, H.M., Chen, X., Urie, P., Myers, K.M., Hall, T.J., Wapner, R., Kitajewski, J.K., Shawber, C.J., and Gallos, G. 2016. A new paradigm for the role of smooth muscle cells in the human cervix. *American Journal of Obstetrics and Gynecology*. **215**(4), pp. 478.e1-478.e11.

Walocha, J.A., Litwin, J.A., Bereza, T., Klimek-Piotrowska, W., and Miodonski, A.J. 2012. Vascular architecture of human uterine cervix visualized by corrosion casting and scanning electron microscopy. *Human Reproduction.* **27**(3), pp. 727–732.

Wang, J.Y., Healey, T., Barker, A., Brown, B., Monk, C., and Anumba, D.O.C. 2017. Magnetic induction spectroscopy (MIS)—probe design for cervical tissue measurements. *Physiological Measurement*. **38**(5), pp. 729–744.

Warren, J.E., Silver, R.M., Dalton, J., Nelson, L.T., Branch, D.W., and Porter, T.F. 2007. Collagen 1α1 and Transforming Growth Factor-β Polymorphisms in Women With Cervical Insufficiency. *Obstetrics & Gynecology*. **110**(3), pp. 619–624.

Watari, M., Watari, H., DiSanto, M.E., Chacko, S., Shi, GP., and Strauss, J.F. 1999. Pro-Inflammatory Cytokines Induce Expression of Matrix-Metabolizing Enzymes in Human Cervical Smooth Muscle Cells. *The American Journal of Pathology*. **154**(6), pp. 1755–1762.

Watari, M., Watari, H., Nachamkin, I., and Strauss, J.F. 2000. Lipopolysaccharide induces expression of genes encoding pro-inflammatory cytokines and the elastin-degrading enzyme, cathepsin S, in human cervical smooth-muscle cells. *Journal of the Society for Gynecologic Investigation*. **7**(3), pp. 190–198.

Weiss, S., Jaermann, T., Schmid, P., Staempfli, P., Boesiger, P., Niederer, P., Caduff, R., and Bajka, M. 2006. Three-dimensional fiber architecture of the nonpregnant human uterus determined ex vivo using magnetic resonance diffusion tensor imaging. *The Anatomical Record. Part A, Discoveries in Molecular, Cellular, and Evolutionary Biology*. **288**(1), pp. 84–90.

Westergren-Thorsson, G., Norman, M., Bjornsson, S., Endresen, U., Stjernholm, Y., Ekman, G., and Malmstrom, A. 1998. Differential expressions of mRNA for proteoglycans, collagens and transforming growth factor-beta in the human cervix during pregnancy and involution. *Biochimica et biophysica acta*. **1406**(2), pp. 203–213.

Wilbanks, G.D. and Richart, R.M. 1966. Postpartum cervix and its relation to cervical neoplasia A Colposcopic Study. *Cancer*. **19**(2), pp. 273-276

Wilbanks, G.D. and Richart, R.M. 1967. The puerperal cervix, injuries and healing: A colposcopic study. *American Journal of Obstetrics and Gynecology*, **97**(8), pp. 1105–1110.

Williams, M. and Iams, J.D. 2004. Cervical length measurement and cervical cerclage to prevent preterm birth. *Clinical Obstetrics and Gynecology*. **47**(4), pp. 775–783.

Yao, W., Gan, Y., Myers, K.M., Vink, J., Wapner, R.J., and Hendon, C.P. 2016. Collagen Fiber Orientation and Dispersion in the Upper Cervix of Non-Pregnant and Pregnant Women. *PLOS ONE*. **11**(11), p. e0166709.

Yeh, F.C., Verstynen, T.D., Wang, Y., Fernandez-Miranda, J.C., and Tseng, W.Y. 2013. Deterministic diffusion fiber tracking improved by quantitative anisotropy.

PloS one. **8**(11), p. e80713.

Youssef, A.F. 1958. The uterine isthmus and its sphincter mechanism, a Radiographic study: The Uterine Isthmus under Normal Conditions. *American Journal of Obstetrics and Gynecology*. **75**(6), pp. 1305–1319.

Zanchetta, M., Rigatelli, G., Pedon, L., Zennaro, M., Onorato, E., and Maiolino, P. 2002. Intracardiac echocardiography during catheter-based procedures: ultrasound system, examination technique, and image presentation. *Echocardiography.* **19**(6), pp. 501–507.

Zhang, Y., Akins, M.L., Murari, K., Xi, J., Li, M.J., Luby-Phelps, K., Mahendroo, M. and Li, X. 2012. A compact fiber-optic SHG scanning endomicroscope and its application to visualize cervical remodeling during pregnancy. *Proceedings of the National Academy of Sciences of the United States of America*. **109**(32), pp. 12878–12883.

Zhang, Y., Zhou, J., Ma, Y., Liu, L., Xia, Q., Fan, D., and Ai, W. 2019. Mode of delivery and preterm birth in subsequent births: A systematic review and meta-analysis. *PLOS ONE*. **14**(3), p. e0213784.

Chapter 8 Appendices

8.1 Aminopropyltriethoxysilane (APEs) slide protocol

Reagents

- Aminopropyltriethoxysilane
- Acetone
- 2% Aminopropyltriethoxysilane (APEs) in acetone

Protocol

1) Immerse in acetone for 5 minutes
2) Drain off excess acetone
3) Immerse in 2% APEs in acetone for 5 minutes
4) Wash in water for 5 minutes
5) Drain off excess water and allow slides to air dry at room temperature overnight

8.2 Masson's Trichrome protocol

Reagents

- Weigert Haematoxylin solution A and B
- Ponceau Fuchsin
- Deionised water
- Phosphotungstric acid
- Methyl Blue

Protocol

1) Prepare Weigert Haematoxylin by mixing equal volumes of solution A & B
2) Dewax and dehydrate slides through xylene and alcohol series
3) Bring sections to water
4) Stain nuclei with Weigert's Iron Haematoxylin for 30 mintues
5) Stain with Ponceau Fuchsin for 5 minutes
6) Differentiate in Phosphotungstic acid for a total of 15 minutes. Change solution at 7.5 minutes
7) Transfer to Methyl Blue solution for 1 minute

8.3 Immunohistochemistry protocol

IHC-P SOP

EQUIPMENT

Pressure cooker

Timer

Staining tubs

Slide covers

REAGENTS

NovoLink Polymer Detection System (500 tests) (cat no. RE7150-CE)

TBS buffer, pH7.6

Antigen Unmasking Solution (AUS) – Citrate buffer (Vector Laboratories, cat. no. H-3300)

Casein (Vector)

Antibody diluent (Invitrogen, cat. no. # 00-3218, 500ml)

Primary antibody (as required)

Distilled water (dH_20) and running water

Ethanol at 100%

Mayers Haematoxylin

Scotts Tap Water

Xylene

DPX

METHODS

1. Cut and mount FFPE blocks on slides coated with a suitable tissue adhesive

2. Dry sections overnight in a 37°C incubator

3. Place sections onto hot block for ½ hour (or longer if necessary)

4. Prepare 50mM TBS buffer, pH7.6 and AUS (1.875ml concentrated AUS + 200ml dH_20)

TBS recipe 10x

For 1 lit: Tris 61gr

NaCl 90gr

Dissolve in 600ml dH_20. Adjust pH to 7.6 with concentrated HCl. Top up with dH_20 to 1 lit. Dilute for working solution (1x) when needed.

GO TO IHC-P STATION AT THE BACK OF LABORATORY

5. De-paraffinize sections in xylene **(MAKE SURE THE XYLENE IS CLEAN, OTHERWISE REPLACE WITH FRESH)**:

a. De-wax in xylene – 3min

b. De-wax in xylene – 3 min

c. De-wax in xylene – 3 min

d. De-wax in xylene – 3 min

6. Re-hydrate through absolute alcohol **(AGAIN MAKE SURE THAT THE ETHANOLS ARE CLEAR, OTHERWISE REPLACE)**:

a. Absolute ETOH: 3 min

b. Absolute ETOH: 3 min

c. Absolute ETOH: 3 min

d. Absolute ETOH: 3 min

7. Wash sections in running tap water (in rack in plastic container)

8. Perform heat mediated antigen retrieval:

a. Use **automated** pressure cooker

b. Add 500ml of dH_20 in the pressure cooker.

c. Transfer the slides in the plastic pot containing the AUS.

d. Place the rubber seal and top on the cooker.

e. Turn on and press start.

f. When it gets to 125^0C and hold for two minutes, it will beep. Press start/stop.

g. The temperature will gradually drop after that, and when it reaches 90^0C it will beep again to indicate that you can release the lid and remove your pot

9. Wash sections in distilled water **(make sure you keep your slides in liquid while they are hot to avoid drying)**

RETURN TO LABORATORY BENCH

10. Neutralize endogenous peroxidase. Use Sigma Hydrogen Peroxidase (1:10). Keep slides in their racks and fill a pot with peroxidase. Leave for 20 minutes.

11. Wash step: Rinse with running tap water for 5min. Then label sections appropriately mount on coverplates before situating in the sequenza and do a TBS wash for 5 minutes.

To place sections in the sequenza, use TBS to provide adhesion of sections to plastic holder before placing them in the container. Wash through some TBS buffer to ensure flow through of solution is not interrupted (e.g. bubbles)

12. Incubate with 100µl Casein, used as protein block, (1:10 in diluent) per section for 20-30min

13. No wash after Casein

14. Incubate with optimally diluted primary antibody for 1 hour Dilute using antibody diluent, 100µl required per section

15. Wash in TBS 2 x 5min

16. Incubate with 3 drops (roughly around 100 µl) of Post Primary Block (provided in kit) per section for 30 minutes.

17. Wash in TBS 2 x 5min

18. Incubate with 3 drops of NovoLink Polymer (provided in kit) per section for 30 minutes

19. Wash in TBS 2 x 5min

20. Prepare an appropriate volume of DAB working solution. Use ImmPact DAB from Vector. Add 1 drop of DAB Chromogen in 1ml of Substrate Buffer. Approximately 150µl required per section (use a paster pipette)

21. Remove sections from sequenza and put on a tray

22. Place sections flat in an appropriate plastic container and add DAB working solution

23. Develop peroxidase activity with DAB working solution (see above) for 5 minutes

24. Dispose of excess DAB working solution and all contaminated plastics in concentrated bleach and leave overnight to ensure safe disposal

25. Rinse sections in distilled water (sections in gray rack in plastic container)

GO TO IHC-P STATION AT THE BACK OF LABORATORY

26. Blot dry sections (use paper towel and wrap up sections in metal rack to get rid of excess moisture)

27. Counterstain with Hematoxylin for 1.5 minutes (**2.5 minutes**)

28. Rinse sections in tap water until clear

29. Blue in Scotts water for 2 minutes

30. Rinse sections in water for 1 minute

31. Blot dry sections (use paper towel and wrap up sections in metal rack to get rid of excess moisture)

32. Dehydrate in absolute alcohol:

a. Absolute ETOH: Dip 3 times

b. Absolute ETOH: 1 min

c. Absolute ETOH: 5 min

d. Absolute ETOH: 5 min

33. Clear sections in xylene:

a. Clear in xylene – 3min

b. Clear in xylene – 3 min

c. Clear in xylene – 3 min

d. Clear in xylene – 3 min (leave sections here until ready to mount)

34. Mount sections using DPX (place cover slips on paper towel, apply minimal amount of DPX then gently touch section to slide, ensuring there are no bubbles)

35. Leave sections to dry over night then analyse

8.4 C code to convert 2dseq binary DT-MRI data file

```
// Written by Dr. Al Benson
#include <stdio.h>
#include <stdlib.h>
#include <math.h>

// DEFINE THE NUMBER OF VOXELS IN THE DATASET.

#define     X     128    // number of voxels in x direction
#define     Y     160    // number of voxels in y direction
#define Z     192    // number of voxels in z direction

main () {

FILE *oldfile;
FILE *newfile1;
FILE *newfile2;

int x, y, z, d;
signed int ival;
double scale;
double oval;

oldfile = fopen("2dseq", "rb");

d=1;
```

```
while (d<=22) {


        if (d==1)  newfile1 = fopen("processed_files/01_fractional_anisotropy.txt",
"w");
        if (d==2)  newfile1 = fopen("processed_files/02_tensor_trace.txt", "w");
        if (d==3)  newfile1 = fopen("processed_files/03_intensity.txt", "w");
        if (d==4)  newfile1 =
fopen("processed_files/04_diffusion_weighted_image.txt", "w");
        if (d==5)  newfile1 = fopen("processed_files/05_tensor_component_xx.txt",
"w");
        if (d==6)  newfile1 = fopen("processed_files/06_tensor_component_yy.txt",
"w");
        if (d==7)  newfile1 = fopen("processed_files/07_tensor_component_zz.txt",
"w");
        if (d==8)  newfile1 = fopen("processed_files/08_tensor_component_xy.txt",
"w");
        if (d==9)  newfile1 = fopen("processed_files/09_tensor_component_xz.txt",
"w");
        if (d==10) newfile1 = fopen("processed_files/10_tensor_component_yz.txt",
"w");
        if (d==11) newfile1 = fopen("processed_files/11_eigenvalue_1.txt", "w");
        if (d==12) newfile1 = fopen("processed_files/12_eigenvalue_2.txt", "w");
        if (d==13) newfile1 = fopen("processed_files/13_eigenvalue_3.txt", "w");
        if (d==14) newfile1 =
fopen("processed_files/14_eigenvector_1_component_x.txt", "w");
        if (d==15) newfile1 =
fopen("processed_files/15_eigenvector_1_component_y.txt", "w");
        if (d==16) newfile1 =
fopen("processed_files/16_eigenvector_1_component_z.txt", "w");
```

```
        if (d==17) newfile1 =
fopen("processed_files/17_eigenvector_2_component_x.txt", "w");
        if (d==18) newfile1 =
fopen("processed_files/18_eigenvector_2_component_y.txt", "w");
        if (d==19) newfile1 =
fopen("processed_files/19_eigenvector_2_component_z.txt", "w");
        if (d==20) newfile1 =
fopen("processed_files/20_eigenvector_3_component_x.txt", "w");
        if (d==21) newfile1 =
fopen("processed_files/21_eigenvector_3_component_y.txt", "w");
        if (d==22) newfile1 =
fopen("processed_files/22_eigenvector_3_component_z.txt", "w");


        if (d==1)  newfile2 = fopen("processed_files/01_fractional_anisotropy.vtk",
"w");
        if (d==2)  newfile2 = fopen("processed_files/02_tensor_trace.vtk", "w");
        if (d==3)  newfile2 = fopen("processed_files/03_intensity.vtk", "w");
        if (d==4)  newfile2 =
fopen("processed_files/04_diffusion_weighted_image.vtk", "w");
        if (d==5)  newfile2 = fopen("processed_files/05_tensor_component_xx.vtk",
"w");
        if (d==6)  newfile2 = fopen("processed_files/06_tensor_component_yy.vtk",
"w");
        if (d==7)  newfile2 = fopen("processed_files/07_tensor_component_zz.vtk",
"w");
        if (d==8)  newfile2 = fopen("processed_files/08_tensor_component_xy.vtk",
"w");
        if (d==9)  newfile2 = fopen("processed_files/09_tensor_component_xz.vtk",
"w");
        if (d==10) newfile2 = fopen("processed_files/10_tensor_component_yz.vtk",
"w");
```

```
        if (d==11) newfile2 = fopen("processed_files/11_eigenvalue_1.vtk", "w");
        if (d==12) newfile2 = fopen("processed_files/12_eigenvalue_2.vtk", "w");
        if (d==13) newfile2 = fopen("processed_files/13_eigenvalue_3.vtk", "w");
        if (d==14) newfile2 =
fopen("processed_files/14_eigenvector_1_component_x.vtk", "w");
        if (d==15) newfile2 =
fopen("processed_files/15_eigenvector_1_component_y.vtk", "w");
        if (d==16) newfile2 =
fopen("processed_files/16_eigenvector_1_component_z.vtk", "w");
        if (d==17) newfile2 =
fopen("processed_files/17_eigenvector_2_component_x.vtk", "w");
        if (d==18) newfile2 =
fopen("processed_files/18_eigenvector_2_component_y.vtk", "w");
        if (d==19) newfile2 =
fopen("processed_files/19_eigenvector_2_component_z.vtk", "w");
        if (d==20) newfile2 =
fopen("processed_files/20_eigenvector_3_component_x.vtk", "w");
        if (d==21) newfile2 =
fopen("processed_files/21_eigenvector_3_component_y.vtk", "w");
        if (d==22) newfile2 =
fopen("processed_files/22_eigenvector_3_component_z.vtk", "w");


        fprintf(newfile2, "# vtk DataFile Version 3.0\n");
        fprintf(newfile2, "vtk output\n");
        fprintf(newfile2, "ASCII\n");
        fprintf(newfile2, "DATASET STRUCTURED_POINTS\n");
        fprintf(newfile2, "DIMENSIONS %d %d %d\n", X, Y, Z);
        fprintf(newfile2, "SPACING 1 1 1\n");
        fprintf(newfile2, "ORIGIN 0 0 0\n");
        fprintf(newfile2, "POINT_DATA %d\n", X*Y*Z);
```

```
fprintf(newfile2, "SCALARS ImageFile float 1\n");
fprintf(newfile2, "LOOKUP_TABLE default\n");
if (d==1)  scale = 1.0e-6;
if (d==2)  scale = 1.0e-9;
if (d==3)  scale = 1.0;
if (d==4)  scale = 1.0;
if (d==5)  scale = 1.0e-9;
if (d==6)  scale = 1.0e-9;
if (d==7)  scale = 1.0e-9;
if (d==8)  scale = 1.0e-9;
if (d==9)  scale = 1.0e-9;
if (d==10) scale = 1.0e-9;
if (d==11) scale = 1.0e-9;
if (d==12) scale = 1.0e-9;
if (d==13) scale = 1.0e-9;
if (d==14) scale = 1.0e-6;
if (d==15) scale = 1.0e-6;
if (d==16) scale = 1.0e-6;
if (d==17) scale = 1.0e-6;
if (d==18) scale = 1.0e-6;
if (d==19) scale = 1.0e-6;
if (d==20) scale = 1.0e-6;
if (d==21) scale = 1.0e-6;
if (d==22) scale = 1.0e-6;

for (z=1; z<=Z; z++)
for (y=1; y<=Y; y++) {
```

```
	for (x=1; x<=X; x++) {
		fread(&ival, 4, 1, oldfile);
		if (d==16 || d==19 || d==22) oval = -1.0*ival*scale;  // NOTE - for some reason, the z component of the vectors have the opposite sign in the 2dseq file. This corrects for that.
		else oval = ival*scale;
		fprintf(newfile1, "%lf ", oval);
		fprintf(newfile2, "%lf ", oval);
	}
	fprintf(newfile1, "\n");
	fprintf(newfile2, "\n");
	}

	printf("Finished file %d of 22\n", d);
	fclose(newfile1);
	fclose(newfile2);
	d++;
}

fclose (oldfile);

} // end of main
```

8.5 C code to convert primary separate primary eigenvector files to single file primary eigenvector RGB output file

```
// Generates new Primary eigenvector files in rastor scan order (x, y, z) with empty space delineated by a 0
// James Nott - February 2018

#include <stdio.h>
#include <stdlib.h>
#include <math.h>
#include <errno.h>

#define	X	128	// number of voxels in x direction
#define	Y	128	// number of voxels in y direction
#define Z	128	// number of voxels in z direction

#define	dx	0.25	// voxel size in x direction (mm)
#define	dy	0.2	// voxel size in y direction (mm)
#define dz	0.25	// voxel size in z direction (mm)

int main () {

	FILE *ev1xfile;
	FILE *ev1yfile;
	FILE *ev1zfile;
	FILE *PEVfile;
	FILE *PEVrawfile;
```

```
        FILE *PEVvtkfile;
        double e1x;                             // x component of the primary
eigenvector
        double e1y;                             // y component of the primary
eigenvector
        double e1z;                             // z component of the primary
eigenvector

        int x, y, z;                        // x, y and z locations of current voxel

        double EVx;                 // Primary Eigenvector x new file
        double EVy;       // Primary Eigenvector y new file
        double EVz;       // Primary Eigenvector z new file
    double EVxA;       //Absolute value of Primary Eigenvector x
    double EVyA;       //Absolute value of Primary Eigenvector y
    double EVzA;       //Absolute value of Primary Eigenvector z

        ev1xfile = fopen("processed_files/14_eigenvector_1_component_x.txt", "rt");
        ev1yfile = fopen("processed_files/15_eigenvector_1_component_y.txt", "rt");
        ev1zfile = fopen("processed_files/16_eigenvector_1_component_z.txt", "rt");
        PEVfile = fopen("PEV.txt", "w");
        PEVrawfile = fopen("PEV.raw", "w");
        PEVvtkfile = fopen("PEV.vtk", "w");

        // print VTK file headers
        printf("printing headers...\n");

        fprintf(PEVvtkfile, "# vtk DataFile Version 3.0\n");
```

```
fprintf(PEVvtkfile, "vtk output\n");
fprintf(PEVvtkfile, "ASCII\n");
fprintf(PEVvtkfile, "DATASET STRUCTURED_POINTS\n");
fprintf(PEVvtkfile, "DIMENSIONS %d %d %d\n", X, Y, Z);
fprintf(PEVvtkfile, "SPACING %f %f %f\n", 1.0*dx, 1.0*dy, 1.0*dz);
fprintf(PEVvtkfile, "ORIGIN 0 0 0\n");
fprintf(PEVvtkfile, "POINT_DATA %d\n", X*Y*Z);
fprintf(PEVvtkfile, "SCALARS ImageFile float 3\n");
fprintf(PEVvtkfile, "LOOKUP_TABLE default\n");

printf("printing headers complete...\n");

// idenfiers
for (z=1; z<=Z; z++) {
for (y=1; y<=Y; y++) {
for (x=1; x<=X; x++) {

        // read in eigenvector components and geometry

        fscanf(ev1xfile, "%lf ", &e1x);
        fscanf(ev1yfile, "%lf ", &e1y);
        fscanf(ev1zfile, "%lf ", &e1z);

        if (z<=Z, x<=X, y<=Y) {                    // this voxel is empty, so
print 0,0,0 to output files and move on

 EVx = (e1x * 1); //* 255;
                EVy = (e1y * 1); //* 255;
```

```
                    EVz = (e1z * 1); //* 255;

    //Retun absolute value

                    EVxA = abs(EVx);
                    EVyA = abs(EVy);
                    EVzA = abs(EVz);

    fprintf(PEVfile, "%.6f\ %.6f\ %.6f ", EVxA, EVyA, EVzA);
                    fprintf(PEVrawfile, "%.6f\ %.6f\ %.6f ", EVxA, EVyA, EVzA);
                    fprintf(PEVvtkfile, "%.6f\ %.6f\ %.6f ", EVxA, EVyA, EVzA);

            }

            else        // this voxel is tissue

            {

return 0;


            }

    }

    fscanf(ev1xfile, "\n");
    fscanf(ev1yfile, "\n");
```

```
            fscanf(ev1zfile, "\n");
            fprintf(PEVfile, "\n");
            fprintf(PEVrawfile, "\n");
            fprintf(PEVvtkfile, "\n");

            }
            printf("slice %d of %d finished...\n", z, Z);
            }

            printf("FINISHED\n");

            fclose (ev1xfile);
            fclose (ev1yfile);
            fclose (ev1zfile);
        fclose (PEVfile);
        fclose (PEVrawfile);
        fclose (PEVvtkfile);

     // end of main

}
```

8.6 REC favourable opinion for histology and DTI experiments

NHS
Health Research Authority

NRES Committee Yorkshire & The Humber - Leeds West

Room 001, Jarrow Business Centre

Rolling Mill Road

Jarrow Tyne and Wear

NE32 3DT

Telephone: 0191 428 3444

14 May 2015

Mr Nigel Simpson Room 9.88
Level 9, Worsley Building Clarendon Way
Leeds LS2 9JT

Dear Mr Simpson

Study title: The structure and function of the internal cervical os and its implications for cervical insufficiency

REC reference: **15/YH/0111**

IRAS project ID: **170319**

Thank you for your letter of 07 May 2015, responding to the Committee's request for further information on the above research and submitting revised documentation.

The further information was considered in correspondence by a Sub-Committee of the REC. A list of the Sub-Committee members is attached.

We plan to publish your research summary wording for the above study on the HRA website, together with your contact details. Publication will be no earlier than three months from the date of this favourable opinion letter. The expectation is that this information will be published for all studies that receive an ethical

opinion but should you wish to provide a substitute contact point, wish to make a request to defer, or require further information, please contact the REC Manager, Miss Christie Ord at nrescommittee.yorkandhumber-leedswest@nhs.net. Under very limited circumstances (e.g. for student research which has received an unfavourable opinion), it may be possible to grant an exemption to the publication of the study.

Confirmation of ethical opinion

On behalf of the Committee, I am pleased to confirm a **favourable** ethical opinion for the above research on the basis described in the application form, protocol and supporting documentation as revised, subject to the conditions specified below.

Management permission or approval must be obtained from each host organisation prior to the start of the study at the site concerned.

Management permission ('R&D approval) should be sought from all NHS organisations involved in the study in accordance with NHS research governance arrangements.

Guidance on applying for NHS permission for research is available in the Integrated Research Application System or at http://www.rdforum.nhs.uk.

Where a NHS organisation's role in the study is limited to identifying and referring potential participants to research sites ('participant identification centre'), guidance should be sought from the R&D office on the information it requires to give permission for this activity.

For non-NHS sites, site management permission should be obtained in accordance with the procedures of the relevant host organisation.

Sponsors are not required to notify the Committee of approvals from host organisations.

Registration of Clinical Trials

All clinical trials (defined as the first four categories on the IRAS filter page) must be registered on a publically accessible database. This should be before the first participant is recruited but no later than 6 weeks after recruitment of the first participant.

There is no requirement to separately notify the REC but you should do so at the earliest opportunity e.g. when submitting an amendment. We will audit the registration details as part of the annual progress reporting process.

To ensure transparency in research, we strongly recommend that all research is registered but for non-clinical trials this is not currently mandatory.

If a sponsor wishes to request a deferral for study registration within the required timeframe, they should contact hra.studyregistration@nhs.net. The expectation is that all clinical trials will be registered, however, in exceptional circumstances non-registration may be permissible with prior agreement from NRES. Guidance on where to register is provided on the HRA website.

It is the responsibility of the sponsor to ensure that all the conditions are complied with before the start of the study or its initiation at a particular site (as applicable).

Ethical review of research sites

NHS sites

The favourable opinion applies to all NHS sites taking part in the study, subject to management permission being obtained from the NHS/HSC R&D office prior to the start of the study (see 'Conditions of the favourable opinion' below).

Approved documents

The final list of documents reviewed and approved by the Committee is as follows:

Document	*Version*	*Date*
Evidence of Sponsor insurance or indemnity (non NHS Sponsors only) [Indemnity Certificate]	1	17 September 2014
IRAS Checklist XML [Checklist_07052015]		07 May 2015
Letter from funder [Grant letter]	1	14 March 2013
Letter from sponsor [Sponsorship email]	1	16 February 2015
Other [CV Dr Wilkinson]	1	23 February 2015
Other [CV Dr Benson]	1	23 February 2015
Other [CV Dr Pickering]	1	23 February 2015
Other [Patient review]	1	01 May 2015
Participant consent form [Consent form]	1	23 February

		2015
Participant information sheet (PIS) [PIS]	1	23 February 2015
Participant information sheet (PIS) [PIS]	1.1	20 April 2015
REC Application Form [REC_Form_06032015]		06 March 2015
Referee's report or other scientific critique report [External review]	1	11 February 2015
Research protocol or project proposal [Research Protocol]	1.0	23 February 2015
Summary CV for Chief Investigator (CI) [CI CV]	1	15 February 2015
Summary CV for student [Student CV]	1	23 February 2015

Statement of compliance

The Committee is constituted in accordance with the Governance Arrangements for Research Ethics Committees and complies fully with the Standard Operating Procedures for Research Ethics Committees in the UK.

After ethical review

Reporting requirements

The attached document *'After ethical review – guidance for researchers'* gives detailed guidance on reporting requirements for studies with a favourable opinion, including:

- Notifying substantial amendments
- Adding new sites and investigators
- Notification of serious breaches of the protocol
- Progress and safety reports
- Notifying the end of the study

The HRA website also provides guidance on these topics, which is updated in the

light of changes in reporting requirements or procedures.

User Feedback

The Health Research Authority is continually striving to provide a high quality service to all applicants and sponsors. You are invited to give your view of the service you have received and the application procedure. If you wish to make your views known please use the feedback form available on the HRA website: http://www.hra.nhs.uk/about-the-hra/governance/quality-assurance/

HRA Training

We are pleased to welcome researchers and R&D staff at our training days – see details at http://www.hra.nhs.uk/hra-training/

15/YH/0111	**Please quote this number on all**

With the Committee's best wishes for the success of this project.

Yours sincerely pp

Mr Anthony Warnock-Smith Alternate Vice-Chair

Email:nrescommittee.yorkandhumber-leedswest@nhs.net

Enclosures: *List of names and professions of members who were present at the meeting and those who submitted written comments*

"After ethical review – guidance for researchers" *[SL-AR2]*

Copy to: *Faculty Research Ethics and Governance and Administrator Anne Gowing, Leeds Teaching Hospitals NHS Trust*

NRES Committee Yorkshire & The Humber - Leeds West Attendance at Sub-Committee of the REC meeting held in correspondence

Committee Members:

Name	*Profession*	*Present*	*Notes*
Dr Diane Farrar	Research Programme Manager - Maternal and Child Health	Yes	
Dr Jan Geddes	Retired Senior Research Fellow	Yes	
Mr Anthony Warnock-Smith (Chair)	Retired solicitor	Yes	

Also in attendance:

Name	*Position (or reason for attending)*
Kirstie Penman	Amendments Coordinator

8.7 REC favourable opinion for endoscopic ultrasound experiment

Yorkshire & The Humber - Leeds East Research Ethics Committee

Health Research Authority

Jarrow Business Centre Rolling Mill Road

Jarrow NE32 3DT

Please note: This is the favourable opinion of the REC only and does not allow you to start your study at NHS sites in England until you receive HRA Approval

Telephone: 0207 104 8081

19 February 2018

Mr Nigel Simpson
Room 9.88 Worsley Building Clarendon Way
Leeds LS2 9JT

Dear Mr Simpson

Study title:	**Endocervical Microprobe Ultrasound of the human cervix**
REC reference:	**17/YH/0383**
IRAS project ID:	**201473**

Thank you for your letter of 19th February, responding to the Committee's request for further information on the above research and submitting revised documentation.

The further information has been considered on behalf of the Committee by the Chair.

We plan to publish your research summary wording for the above study on the HRA website, together with your contact details. Publication will be no earlier than three months from the date of this opinion letter. Should you wish to

provide a substitute contact point, require further information, or wish to make a request to postpone publication, please contact hra.studyregistration@nhs.net outlining the reasons for your request.

Confirmation of ethical opinion

On behalf of the Committee, I am pleased to confirm a favourable ethical opinion for the above research on the basi described in the application form, protocol and supporting documentation

as revised, subject to the conditions specified below.

Conditions of the favourable opinion

The REC favourable opinion is subject to the following conditions being met prior to the start of the study.

Management permission must be obtained from each host organisation prior to the start of the study at the site concerned.

Management permission should be sought from all NHS organisations involved in the study in accordance with NHS research governance arrangements. Each NHS organisation must confirm through the signing of agreements and/or other documents that it has given permission for the research to proceed (except where explicitly specified otherwise).

Guidance on applying for NHS permission for research is available in the Integrated Research Application System, www.hra.nhs.uk or at http://www.rdforum.nhs.uk.

Where a NHS organisation's role in the study is limited to identifying and referring potential participants to research sites ("participant identification centre"), guidance should be sought from the R&D office on the information it requires to give permission for this activity.

For non-NHS sites, site management permission should be obtained in accordance with the procedures of the relevant host organisation.

Sponsors are not required to notify the Committee of management permissions from host organisations

Registration of Clinical Trials

All clinical trials (defined as the first four categories on the IRAS filter page) must be registered on a publically accessible database within 6 weeks of recruitment of the first participant (for medical device studies, within the timeline determined by the current registration and publication trees).

There is no requirement to separately notify the REC but you should do so at the earliest opportunity e.g. when submitting an amendment. We will audit the registration details as part of the annual progress reporting process.

To ensure transparency in research, we strongly recommend that all research is registered but for non-clinical trials this is not currently mandatory.

If a sponsor wishes to request a deferral for study registration within the required timeframe, they should contact hra.studyregistration@nhs.net. The expectation is that all clinical trials will be registered, however, in exceptional circumstances non registration may be permissible with prior agreement from the HRA. Guidance on where to register is provided on the HRA website.

It is the responsibility of the sponsor to ensure that all the conditions are complied with before the start of the study or its initiation at a particular site (as applicable).

Ethical review of research sites

NHS sites

The favourable opinion applies to all NHS sites taking part in the study, subject to management permission being obtained from the NHS/HSC R&D office prior to the start of the study (see "Conditions of the favourable opinion" below).

Non-NHS sites

Approved documents

The final list of documents reviewed and approved by the Committee is as follows:

Document	*Version*	*Date*

Evidence of Sponsor insurance or indemnity (non NHS Sponsors only) [Indemnity]	1	21 July 2017
IRAS Application Form [IRAS_Form_18102017]		18 October 2017
IRAS Checklist XML [Checklist_15022018]		15 February 2018
Letter from sponsor [Sponsor letter]	1.0	10 October 2017
Other [EB CV]		29 September 2017
Other [JP CV]		29 September 2017
Other [John Dalton CV]		10 October 2017
Other [REC cover letter]	1.1	14 February 2018
Other [Revised protocol]	1.1	08 February 2018
Other [Transport_supporting_evidence]	1.1	07 February 2018
Other [HRA cover letter]	1.1	08 February 2018
Participant consent form [Consent form]	1.3	17 January 2018
Participant information sheet (PIS) [PIS form]	1.5	14 February 2018
Summary CV for Chief Investigator (CI) [NAB CV]		01 July 2017
Summary CV for student [JN CV]		04 October 2017
Summary CV for supervisor (student research) [CV NABS]		01 July 2017

Statement of compliance

The Committee is constituted in accordance with the Governance Arrangements for Research Ethics Committees and complies fully with the Standard Operating Procedures for Research Ethics Committees in the UK.

After ethical review

Reporting requirements

The attached document *"After ethical review – guidance for researchers"* gives detailed guidance on reporting requirements for studies with a favourable opinion, including:

- Notifying substantial amendments
- Adding new sites and investigators
- Notification of serious breaches of the protocol
- Progress and safety reports
- Notifying the end of the study

The HRA website also provides guidance on these topics, which is updated in the light of changes in reporting requirements or procedures.

User Feedback

The Health Research Authority is continually striving to provide a high quality service to all applicants and sponsors. You are invited to give your view of the service you have received and the application procedure. If you wish to make your views known please use the feedback form available on the HRA website: http://www.hra.nhs.uk/about-the-hra/governance/quality- assurance/

HRA Training

We are pleased to welcome researchers and R&D staff at our training days – see details at http://www.hra.nhs.uk/hra-training/

17/YH/0383	Please quote this number on all

With the Committee's best wishes for the success of this project.